TECHNISCHE UNIVERSITÄT MÜNCHEN
Fakultät für Chemie
Lehrstuhl I für Technische Chemie

Electrochemical Reduction of Carbon Dioxide and Carbon Monoxide towards Value-Added Chemicals

Nayra Sofia Romero Cuéllar

Vollständiger Abdruck der von der Fakultät für Chemie der Technischen Universität München zur Erlangung des akademischen Grades eines

Doktor-Ingenieurs (Dr.-Ing.)

genehmigten Dissertation.

Vorsitzender:	apl. Prof. Dr. Wolfgang Eisenreich
Prüfer der Dissertation:	1. Prof. Dr.-Ing. Kai-Olaf Martin Hinrichsen
	2. Prof. Dr.-Ing. Andreas Jossen
	3. Hon.-Prof. Dr. Maximilian Fleischer

Die Dissertation wurde am 24.09.2019 bei der Technischen Universität München eingereicht und durch die Fakultät für Chemie am 18.11.2019 angenommen.

para Lucerito, Romerin, la Tarula y Pedro

Acknowledgments

This period of my life will be for sure one of the most memorable chapters of my entire journey. It was a mixture of pain, hopelessness, failures but also companionship, happiness, satisfaction, achievements and after all an incredible personal growth. Therefore, I will always remember with deep gratitude all of the people that have supported and encouraged me in this overwhelming trip.

Firstly, I would like to express my sincere gratitude to my supervisor Dr. Kerstin Wiesner-Fleischer and Prof. Dr. Maximilian Fleischer, who offered me the opportunity to pursue my PhD at Siemens, granting me the freedom to investigate such an interesting topic and constantly supporting my ideas; secondly, to Prof. Dr.-Ing. Kai-Olaf Hinrichsen for his guidance, his academic and scientific suggestions and for thrusting my work as an external PhD student; thirdly, to the Siemens AG Corporate Technology and the TUM graduate school for financial support; and fourthly, I also would like to thank all the committee members for spending their precious time in reading and evaluating this thesis.

It was a great honour to be part of the CPS and the PXS teams at Siemens. I owe my sincere gratitude to all my former colleagues from both teams specially to the members of the CO_2^{to}*Value* Group, Dr. Philippe Jeanty, Christian Scherer, Dr. Erhard Magori, Dr. Remik Pastusiak, Dr. Angelika Tawil, and Dr. Van An Du for the valuable technical discussions, their ideas and support to improve my measurements and for the amazing time we spent working together. I have to thank Dr. Andreas Rucki for his support with the surface analysis of the electrodes. I am as well grateful to Romy, Robert, Anja, Phillip and all who shared or visited the "Kinderzimmer" for helping me to deal with frustration by playing "Kicker". Although it took me some time to feel integrated as a Colombian in this German environment, I learned that being a little different can become a strength once you embrace it. I am deeply grateful to all the members of the former CPS group and the current PXS team for sharing their knowledge with me. Thanks to the interns Mitchell Mackenzie, John Nielsen and Riley Mather for proofreading my papers and to the master's students Sina Smith and Berin Kackar for their support in the laboratory. Additionally, I would like to acknowledge my colleagues at Siemens Erlangen Dr. Günther Schmid, Dr. Ralf Krause, Dr. Christian Reller, Dr. Bernhard Schmid and Dr. Manfred Baldauf for their questions, suggestions, and for their scientific support. I also thank my Siemens mentor

in the last year Dr. Kerstin Haese for taking extra time to guide my professional development and for her support in the final steps to accomplish my PhD.

I am as well grateful to the TUM department of chemistry, specially to the former and current members of the chair of Chemical Technology I (TCI), who had a scientific impact on my career. I would like to express my gratitude to Prof. Eisenreich, Dr. Huber and M.Sc. Thomas Burger for being always ready to answer my questions and for their support with analytic measurements. Many thanks to the external collaborators Prof. Haenen and Dr. Shannon from the Hasselt University, as well as Prof. Rosiwal and Dr. Ghanem from the University Erlangen-Nürnberg for providing BDD samples and for the valuable discussions.

I would like to thank my friends, who can already be called Doctors: Carlos, Karla, Adrian, Diego, Maria Antonia, Jose, Natalia. Thanks for being like my group therapy, for understanding what I was going through, and for helping me to find motivation in all those moments of doubt I had. To Jairo, Carlos and Pedro thanks for proofreading some chapters of this thesis. I am also deeply thankful to my parents, Luz Helena Cuellar and Augusto Romero, for their support in the distance and for raising me to follow my dreams, to work hard, and to always look beyond the limits. Thanks to my sister, Yuly, for reminding me that working hard needs to be balanced and that life can be taken easy, even when you are working on your PhD. Very special thanks to my incredibly supportive boyfriend, Pedro, who had to deal with the roller coaster of emotions that came during my PhD and helped me to "keep pushing" till I found my own way to succeed with this project. To my parents, my sister and my boyfriend thanks for being by my side, without your relentless support I might have not being able to succeed. Finally, I am highly grateful to all, even those I might not name here, who have been having my back since I decided to come to Germany. You all made this document possible.

Agradecimientos

Mi época del doctorado es y será uno de los momentos más memorables de mi viaje por la vida. Ha sido una mezcla de momentos difíciles, de errores, de frustración, de desesperanza, pero también de alegrías, de triunfos y satisfacciones. En general, mas allá de los conocimientos científicos adquiridos, este ha sido un periodo acelerado e increíble de crecimiento personal. Por eso siempre les estaré muy agradecida a todas aquellas personas que me brindaron su apoyo y me motivaron a continuar por este camino que a veces parecía extremadamente difícil de recorrer, pero del que hoy me siento orgullosa.

Inicialmente me gustaría agradecer a quienes me abrieron las puertas de Siemens AG para investigar en un tema tan interesante y realizar mi doctorado, Dr. Kerstin Wiesner y Prof. Maximilan Fleischer. En segunda instancia, agradezco al Prof. Dr-Ing. Kai-Olaf Hinrichsen por guiarme académica y científicamente y por confiar en mi trabajo como candidata a doctorado externa. En tercer lugar, agradezco a Siemens AG Corporate Technology y a la Universidad Técnica de Múnich por el soporte financiero. En cuarto lugar, agradezco a los miembros del comite evaluador por dedicar parte de su valioso tiempo para leer y evaluar esta tesis.

Ha sido un honor para mí hacer parte de los equipos de Siemens, CPS y PXS. Les agradezco especialmente a los miembros del grupo CO_2^{to}*Value*: Philippe Jeanty, Christian Scherer, Dr. Erhard Magori, Dr. Remik Pastusiak, Dr. Van An Du, Dr. Angelika Tawil por su apoyo en la realización de mi doctorado, por todas sus enseñanzas y por la buena atmosfera de trabajo. Al Dr. Andreas Rucki le agradezco por todas sus enseñazas sobre el analysis de superficies. También quiero agradecer a mis colegas de Oficina Romy, Robert, Anja, Phillip y todos aquellos que me ayudaron a lidiar con la frustración jugando futbolín. A pesar de que me tomo un tiempo integrarme como colombiana en medio de un ambiente un tanto aleman, gracias a ustedes también aprendí que ser diferente tiene su encanto. Gracias también a los practicantes que me ayudaron a mejorar el ingles en mis articulos y presentaciones, Mitchell Mackenzie, John Nielsen y Riley Mather, asi como a las estudiantes de maestría, Sina Smith and Berin Kackar por su trabajo en el laboratorio. Adicionalmente, agradezco a mis colegas de Siemens Erlangen Dr. Günther Schmid, Dr. Ralf Krause, Dr. Christian Reller, Dr. Bernhard Schmid y Dr. Manfred Baldauf por su apoyo científico y técnico. Igualmente, quiere expresar mi gratitud a mi mentora

en Siemens Dr. Kerstin Haese por tomarse el tiempo en este ultima año para guiar mi desarrollo profesional y los últimos pasos de mi doctorado.

Mis agradecimientos se extienden también al departamento de química de la universidad técnica de Múnich y a los miembros de TCI, quienes influenciaron mi projecto con su visión cientifica. Quiero agradecer especialmente al Prof. Eisenreich, Dr. Huber and M.Sc. Thomas Burger por su disposición para solucionar mis dudas y su colaboración con algunos análisis fisicoquímicos. También debo agradecer al Prof. Haenen y a la Dra. Shannon de la universidad de Hasselt, así como al Prof. Rosiwal y la Dra. Ghanem de la Universidad de Erlangen-Nürnberg por el material suministrado y por las valiosas discusiones técnicas.

Quiero agradecer también a mis amigos de camino, especialmente a esos que ya pueden ser llamados doctores: Carlos, Karla, Adrián, Diego, Maria Antonia, Jose, Natalia, gracias por compartir sus historias y por entender las mías, pero también por ser como mi terapia grupal, a la cual llegaba desmotivada y salía con energías renovadas para continuar. A Jairo, Carlos y Pedro gracias por leer partes de esta tesis y por sus correcciones. He decidido escribir agradecimientos en español, especialmente para mis padres de quienes estoy no solo inmensamente agradecida, sino también orgullosa por haberme dado la posibilidad de crecer pensando en grande y de seguir mis sueños, pero sobre todo por ensenarme a trabajar duro y a mirar mas allá de los limites que la sociedad impone, siempre manteniendo los pies en la tierra. Gracias porque no me dieron alas, sino que me ayudaron a construirlas y hoy puedo volar a lugares incluso más lejanos de lo que tal vez había imaginado. Gracias también a mi hermana, porque aunque estemos lejos, sé que cuento con ella y porque de alguna manera representa a esa parte que me recuerda que además de trabajar duro se debe disfrutar de lo simple de la vida. También debo especialmente agradecer a ese hombre paciente e inteligente, mi novio Pedro, que estuvo a mi lado ayudándome a escalar la montaña de la ciencia mientras lidiaba con la montaña rusa de las emociones que afloraron durante el doctorado, le agradezco por haberme brindado incansablemente su mano para continuar buscando mi propio camino. “Keep pushing” es una de las frases que me deja este doctorado. A mis padres, mi hermana y mi novio mi más profundo agradecimiento, sin ustedes esto tal vez no hubiese sido posible. Finalmente, agradezco infinitamente a todos aquellos que me dieron un empujoncito desde que llegue a Alemania, incluso aquellos que tal vez no nombro en este escrito. Todos ustedes hicieron este documento posible.

Abstract

The world is currently facing two problems that are very closely linked: climate changes associated with the high levels of CO_2 in the atmosphere and an increasing global energy demand. To address these challenges, it is crucial to integrate renewable energies and decentralize the energy system, while driving a low-carbon economy. Thus, it is required to develop technologies that utilize CO_2 as raw material and convert electrical energy into other useful forms of energy. The electrochemical reduction of CO_2 has the potential to meet these requirements and to actively contribute to cutback CO_2 from the atmosphere. However, for an industrial application there are still challenges to overcome, such as low selectivity, short durability and low current densities along with high overpotentials. In this thesis, the electrochemical reduction of CO_2 is investigated with the aim to increase selectivity towards value-added chemicals. CO_2 electrolysis was initially studied using planar electrodes such as boron doped diamond (BDD) and transition metals in H-cells. The results demonstrated the stability but low activity of BDD electrodes and indicated that growth conditions and especially grain size play an important role in their activity for CO_2 reduction towards CO and HCOOH. Considering CO as the well-accepted main intermediate to multi-carbon products, a metal screening (Fe, Co, Ni, Cu) was performed with CO and CO_2 as the reactant. It was confirmed that Cu is the only material able to electroreduce CO to multi-carbon products but it was also observed that the presence of CO can suppress the hydrogen evolution reaction. Subsequently, this thesis focuses on the electrochemical reduction of CO to ethanol, ethylene and *n*-propanol using gas diffusion electrodes and flow cells. With this set-up, it was possible to overcome the mass transfer limitations observed while using H-cells and planar electrodes. As a result, high current densities (up to $-300\,mA/cm^2$) were achieved and it was possible to directly compare CO and CO_2 as the reactant. Several advantages were demonstrated by using CO rather than CO_2. One of them is that compared to CO_2, more than two-fold higher Faradaic efficiencies can be achieved using CO. Furthermore, the study of different Cu-powders with different particle sizes indicated that compared to microparticles, nanoparticles lead to higher selectivity at higher current densities. Finally, the feasibility of a two-step electrolysis system was demonstrated at application-relevant current densities. A significant improvement in the selectivity towards multi-carbon products was achieved by introducing a gas separation technique between the two steps. Overall, this doctoral thesis aims to contribute to the research community by providing key insights into the development of the electrochemical reduction of CO_2 towards multi-carbon products as an industrial process.

Kurzzusammenfassung

Die Welt steht derzeit vor zwei Problemen, die sehr eng miteinander verbunden sind: Klimaveränderungen aufgrund des hohen CO_2-Gehalts in der Atmosphäre und eines zunehmenden globalen Energiebedarfs. Um diesen Herausforderungen zu begegnen, ist es entscheidend, erneuerbare Energien zu integrieren und das Energiesystem zu dezentralisieren, während gleichzeitig eine kohlenstoffneutrale Wirtschaft vorangetrieben wird. Daher müssen Technologien entwickelt werden, die CO_2 als Rohstoff nutzen und elektrische Energie zu anderen nützlichen Energieformen umwandeln. Die elektrochemische Reduktion von CO_2 hat das Potenzial, elektrische Energie in chemische Energie umzuwandeln und aktiv zur Reduzierung des CO_2 aus der Atmosphäre beizutragen. Für eine industrielle Anwendung sind jedoch noch Herausforderungen zu bewältigen, wie geringe Selektivität, Instabilität und geringere Stromdichten bei hohen Überspannungen. In dieser Arbeit wird die elektrochemische Reduktion von CO_2 untersucht, mit dem Ziel, die Selektivität gegenüber Wertschöpfungschemikalien zu erhöhen. Zunächst wurde die CO_2-Elektrolyse mit planaren Elektroden wie Bor-dotiertem Diamant (BDD) und Übergangsmetallen in H-Zellen untersucht. Die Ergebnisse mit BDD-Elektroden zeigten hohe Stabilität, aber geringe Aktivität für die Umwandlung von CO_2 zu CO und HCOOH. Außerdem wurde gezeigt, dass Wachstumsbedingungen und insbesondere die Korngröße eine wichtige Rolle bei ihrer Aktivität zur CO_2-Reduktion spielen. Ein Metall-Screening (Fe, Co, Ni, Cu) mit CO und CO_2 als Edukte wurde durchgeführt, unter Berücksichtigung von CO als Zwischenprodukt bei der elektrochemischen Herstellung von kohlenstoffhaltigen Produkte. Das Metall-Screening bestätigte, dass Cu das einzige Material in Lage ist, CO zu kohlenstoffhaltigen Produkten mit mehr als eine Kohlenstoffverbindung zu elektroreduzieren. Dazu wurde gezeigt, dass die Wasserstoffentwicklungsreaktion mit der Anwesenheit von CO unterdrückt wird. Des Weiteren beschäftigt sich diese Arbeit mit der elektrochemischen Reduktion des Hauptzwischenprodukts Kohlenmonoxid zu Ethylen, Ethanol und *n*-Propanol. Dafür wurden die Experimente unter Verwendung von Gasdiffusionselektroden und Durchflusszellen durchgeführt. Mit diesem Aufbau war es möglich, die bei der Verwendung von H-Zellen und planaren Elektroden beobachteten Stofftransportlimitierungen zu überwinden. Damit war es auch möglich hohe Stromdichten zu erreichen (bis $-300\,mA/cm^2$) sowie CO und CO_2 als Reaktanten direkt zu vergleichen. Durch die Verwendung von CO anstatt von CO_2 als Reaktant wurden mehrere Vorteile gezeigt. Eine davon ist, dass mit CO im Vergleich zu CO_2 mehr als doppelt so hohe Faraday-Wirkungsgrade erzielt werden können. Darüber hinaus hat die Untersuchung

verschiedener Cu-Pulver mit unterschiedlichen Partikelgrößen gezeigt, dass Nanopartikel im Vergleich zu Mikropartikeln bei höheren Strömen zu einer höheren Selektivität bei höheren Stromdichten führen. Schließlich wurde ein integriertes Zweistufige-Elektrolyse-System aufgebaut und optimiert. Die Ergebnisse zeigten die Machbarkeit einer zweistufigen Elektrolyse von CO_2 bei anwendungsrelevanten Stromdichten. Allerdings wurde bewiesen, dass eine CO_2 Abtrennung zwischen den beiden Schritten notwendig ist, um die Selektivität zu kohlenstoffhaltigen Produkten zu verbessern.

Contents

1 Introduction

1.1 Research context

The rapid increase in energy demand, together with the climatic changes associated with the increasing CO_2 concentration in the atmosphere, requires a rethinking of the energy system and the use of fossil fuels. This implies worldwide research and development of new technologies that can assure a carbon-neutral economy. The following paragraphs aim to provide an overview of the current challenges that motivate the investigation of the electrochemical reduction of CO_2 together with the basic requirements and the state of the art of this technology to finally define the scope of this thesis.

1.1.1 Traditional energy system and CO_2 emissions

The energy business, which includes generation, distribution, and consumption, has been expanding among others because of population and economy growth [1–3]. The urban population of the world has grown rapidly from 746 million in 1950 to 3.9 billion in 2014 and a 2.5 billion increase is expected by 2050 [4]. This implies a significant increase in energy demand. According to the International Energy Agency (IEA) the global energy consumption grew by 2.3 % in 2018, nearly twice the average rate of growth since 2010 [5]. Traditional energy generation systems based on fossil fuels (coal, crude oil and natural gas) and nuclear power, cause several negative effects on the climate and the ecosystems on which we depend [2, 6]. The high concentration of CO_2 in the atmosphere is one of the negative consequences that has caught more attention due to its accelerated increase since the industrial revolution [7]. A global average annual concentration of CO_2 in the atmosphere of 407.4 ppm was reported in 2018, up 2.4 ppm since 2017. This is a major increase, taking into account that CO_2 ranged between 180 and 280 ppm in pre-industrial years [5]. Alongside agricultural and industrial activities, the energy generation sector has been a major contributor to this high level of CO_2 in the atmosphere [8]. In 2018 global energy related CO_2 emissions reached a historic value of 33.1 Gt CO_2 as shown

in Fig. 1.1. This is the highest rate of growth since 2013, and 70 % higher than the average increase since 2010 [5].

Although it is still not totally understood, how the anthropogenic CO_2 emissions directly affect earth's climate; it has been widely accepted that the increase of CO_2 concentration in the atmosphere is directly linked to an increase in global temperature [6–8]. Likewise, the increase in global temperature has been correlated to catastrophic effects on the ecosystem [6, 8, 9]. The link between traditional energy systems with CO_2 emission and climate warming has caught the attention of politicians, scientists, businessmen as well as the general public. This brought 195 countries at the United Nations Climate Change Conference held in Paris in 2015 to agree on a plan for the reduction of CO_2 emissions and other greenhouse gases to hold global temperatures well below 2 °C above pre-industrial levels and to pursue efforts to limit the temperature increase to 1.5 °C [10].

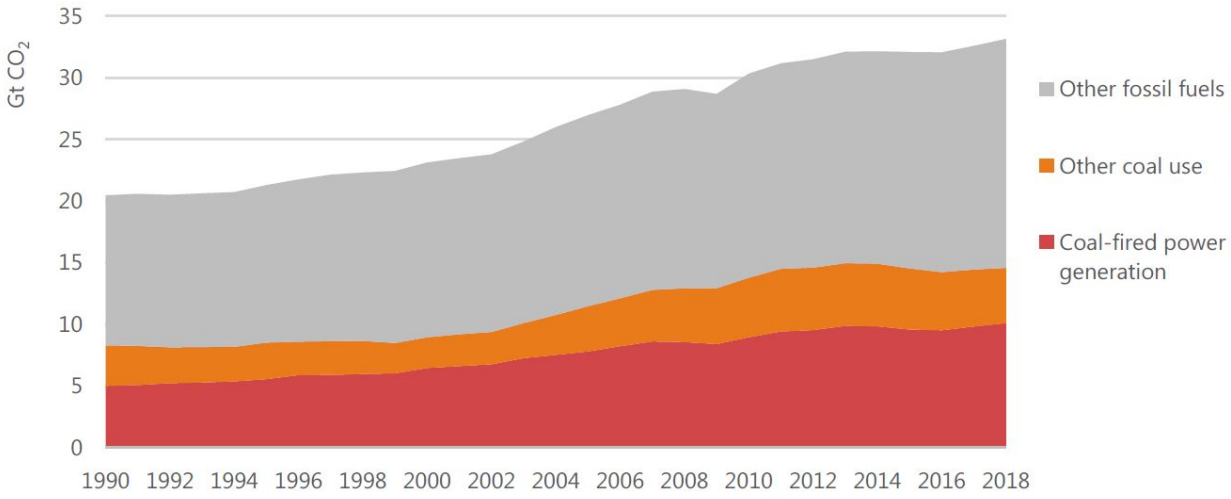

Figure 1.1: Global energy-related CO_2 emissions by source. Source: IEA(2019) Global Energy and CO_2 Status Report [5]. All rights reserved

1.1.2 Energy system transformation

In order to mitigate global climate change and to achieved the goals set in the Paris agreement, global energy demand should be covered by a secure affordable and reliable energy supply that can assure reduced emissions of greenhouse gases [11–13]. Meeting global energy demand in a sustainable way will require not only increased energy efficiency and new methods of using existing carbon based fuels but also a significant amount of new carbon-neutral energy [1, 12]. The integration of renewable energies in the traditional system contributes to a more sustainable energy supply due to the lower consumption of fossil raw materials and the consequent reduction in emissions of greenhouse gases [12]. In fact, in 2018 energy efficiency together with

the integration of renewable energy contributed to a significant restrain on global emissions growth, as shown in Fig. 1.2. Nearly 215 Mt of emissions were reduced due to the transition to renewable energy (green) in the power sector. Without the improvement in efficiency and the transition from coal to gas as well as from fossil fuels to renewable energy sources, emissions growth in 2018 would have been 50 % higher. However, the transition was not fast enough to keep the rapid pace of electricity demand and CO_2 emissions [5].

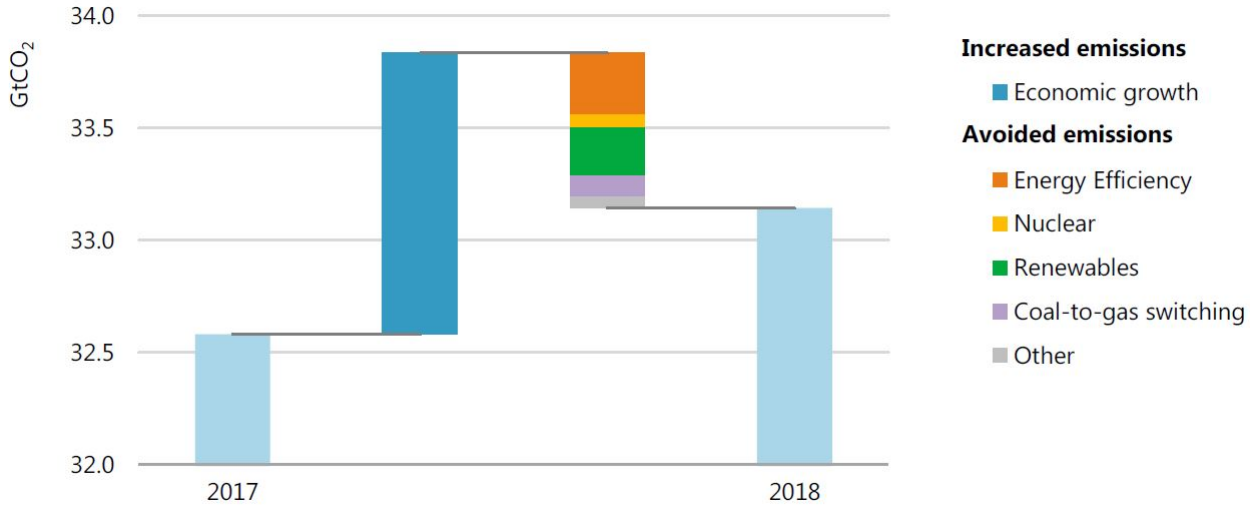

Figure 1.2: Change in global energy related CO_2 emissions and avoided emissions, 2017-18. Source: IEA(2019) Global Energy and CO_2 Status Report [5]. All rights reserved

In Europe, CO_2 emissions fell by 1.3 % (50 Mt). This decline was driven by a drop of 4.5 % in Germany, as both oil and coal combustion slumped sharply, while the power generation from renewable energy reached a record high of 37 % of the electricity mix [5]. This can be considered as a positive result of the German energy system transition known as the "Energiewende", which targets are: reduction of CO_2 emissions by 80–95 % in 2050 relative to 1990, phasing out nuclear power until 2022, as well as maintaining high competitiveness and security of supply [11].

The main sources of renewable power in Germany are wind and solar [12, 14, 15]. These sources generate (almost) no air, land, or water pollution and no CO_2 emissions. In terms of sun and wind renewable energy is abundant and minimal geopolitical stress is caused by its production [1]. Especially solar is considered the largest source of energy, which is becoming the lowest cost resource on a straight energy production basis [16]. However, with these sources the power generation is intermittent and is not always available when and where energy is needed [15]. Thus, energy storage and decentralization of the system represent a major challenge.

Despite electricity generation, other areas such as transport and industrial process are still predominantly depending on fossil fuels [14]. A direct transition from fossil fuels to renewable energies in this sectors requires a fundamental transformation of infrastructures along the entire energy chain from conversion over distribution to end use [11]. It is well recognized that the energy transition can only be successful through the inclusion of these areas, especially with regard to the reduction of CO_2 emissions [12].

In addition to the transformation of the energy system, it is also necessary to remove CO_2 from the atmosphere in order to achieve the targets set in the Paris agreement, as reported recently by the Intergovernmental Panel of Climate Change (IPCC) [17]. Carbon can be captured from large point sources or directly be removed from the air using chemical sorbents that interact strongly with CO_2 such as amine and ammonium [18, 19]. A direct air capture technology has been recently introduced in the industrial sector by the company *Climeworks*, whose vision is to capture 1 % of global emissions by 2025 [20, 21]. While carbon capture is a promising technology to reduce the high levels of CO_2 in the atmosphere, the further utilization of CO_2 as a raw material should be addressed in order to achieve a neutral carbon circular economy.

1.1.3 Sector coupling and Power to X technologies

As aforementioned, the complete transition to renewable energy sources requires also the transition from large scale energy production to local generation, storage and flexible consumption. This can also be understood as a decentralization of the energy system. To address this challenge, a new concept has been introduced in Germany, “sector coupling”, which consists in interconnecting the energy consuming sectors with the power producing sectors [14, 22]. Within this concept, “Power to X technologies” (P2X) have emerged and are gaining importance in the scientific community as well as in the industrial sector [14].

The energy system transformation requires, therefore, two phases for its implementation as shown in Fig. 1.3. In phase 1, which is currently being introduced, the electricity is fed into the traditional energy system. The distribution mechanism is combined with electricity storage using batteries and fuel cells. These electrochemical storage technologies are currently propelled by the automotive industry leading to higher efficiencies and lower prices. In Phase 2, the energy sector should merge with other sectors. This, as mentioned above, is known as sector coupling and can be implemented using P2X technologies. An important requirement for phase 2 is a low cost of renewable energy, which should become lower than the cost for conventional fossil or nuclear energy generation [23]. The current trends suggest that this requirement can be fulfilled in a short term as reported by the International Renewable Energy Agency (IRENA). They have tracked and analyzed the cost evolution of renewable power and confirmed the status of renewable power as a highly cost-effective energy source [24].

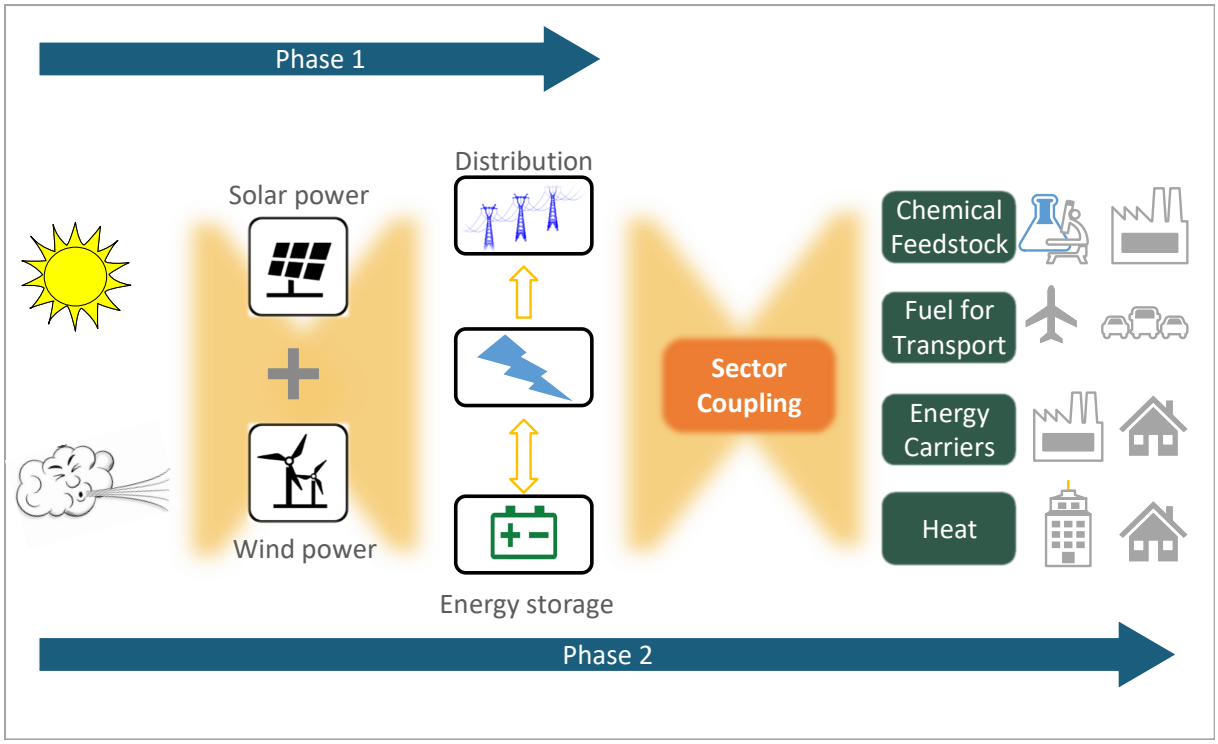

Figure 1.3: Phases of the energy system transformation. Adapted from [23]

Power to X technologies allow the conversion of electrical power from a renewable source into an X useful form of energy, where X can be among others gas, liquid or heat [14]. Converting power to gas or liquid can also refer to the conversion of electrical energy into chemical energy or synthetic energy carriers [14]. This is especially valuable in sectors that are still dependent of fossil fuels or petrochemicals and where the direct use of renewable energy remains a challenge. In these cases, using fuels synthesized from clean electricity and CO_2 might be the best approach for a carbon neutral economy.

Electrochemical processes are the gist of some P2X technologies. These are environmentally friendly, can be operated under relatively mild conditions and can also be coupled with renewable electricity sources at remote locations [13, 25]. Water electrolysis is one of the basic examples of a P2X technology, where water is electrochemically reduced to H_2 and oxidized to O_2. In this way, electrical energy can be stored in the chemical bonds of H_2 as a gas. However, H_2 as a storage option is limited due to high cost, security challenges and the need for a special infrastructure for its storage and transport [26]. An alternative to improve energy density and storage ability is the electrochemical conversion of water to H_2 followed by a thermochemical synthesis with CO_2 to obtain CH_4 (methanation) [27]. This option delivers a higher energy density product than H_2, is compatible with the current infrastructure and contributes to the utilization of CO_2. However, it should be taken into account that renewable electricity is in this case only used for the production of H_2, while the methanation itself is the result of a well established catalytic reaction at high temperatures [27].

A new promising approach is the electrochemical reduction of CO_2 in aqueous electrolytes, where even higher energy dense synthetic carriers, as well as gas and liquid chemical products can be obtained. With this technology multi-carbon products, which are usually obtained from fossil sources, can instead be electrochemically synthesized from CO_2 and water using renewable energy as driving force [28]. Thus, the electrochemical reduction of CO_2 has the potential to trigger a sustainable carbon neutral economy by integrating renewable energy in the chemical sector and hence reducing CO_2 emissions. Nevertheless, CO_2 electrolyzers still have to overcome challenges such as low selectivity, high overpotentials and fast degradation. This technology can only be industrially deployed by achieving long-term stable electrolysis with high conversion rates and suitable product selectivity at high current densities [29–31]. For this reason, the electrochemical reduction of CO_2 has gained attention in the scientific community and has become a major topic that requires further investigation.

1.2 CO_2 electrochemical reduction

In the last three decades, several researchers have demonstrated that CO_2 can be activated by an electrocatalytic process in aqueous electrolytes at ambient pressure and temperature [28, 29, 32–37]. In this electrocatalytic process the reduction of CO_2 and H_2O takes place at the cathode, while the oxidation of H_2O occurs at the anode. For the purpose of this thesis, the attention will be directed to the cathodic reaction, where CO_2 is reduced to value-added chemicals. The electrochemical reduction of CO_2 ($ERCO_2$) can follow a two-, six-, eight-, 12-, or even 18-electron reduction pathway to obtain various gaseous and liquid products. Up to 16 different CO_2 reduction products have been reported including ethylene glycol and propionaldehyde among others [35]. Equations (1.1 - 1.7) show the half-cell electrochemical reaction as well as the thermodynamic electrode potentials versus the reversible hydrogen electrode (V vs RHE) for the seven most common products that can be obtained from the $ERCO_2$ [35].

$$CO_2(g) + H_2O(l) + 2\,e^- \rightleftharpoons CO(g) + 2\,OH^- \qquad -0.10\,V \text{ vs RHE} \quad (1.1)$$

$$CO_2(g) + H_2O(l) + 2\,e^- \rightleftharpoons HCOO^-(aq) + OH^- \qquad -0.03\,V \text{ vs RHE} \quad (1.2)$$

$$CO_2(g) + 6\,H_2O(l) + 8\,e^- \rightleftharpoons CH_4(g) + 8\,OH^- \qquad 0.17\,V \text{ vs RHE} \quad (1.3)$$

$$CO_2(g) + 5\,H_2O(l) + 6\,e^- \rightleftharpoons CH_3OH(g) + 6\,OH^- \qquad 0.03\,V \text{ vs RHE} \quad (1.4)$$

$$2\,CO_2(g) + 8\,H_2O(l) + 12\,e^- \rightleftharpoons C_2H_4(g) + 12\,OH^- \qquad 0.08\,V \text{ vs RHE} \quad (1.5)$$

$$2\,CO_2(g) + 9\,H_2O(l) + 12\,e^- \rightleftharpoons C_2H_5OH(l) + 12\,OH^- \qquad 0.09\,V \text{ vs RHE} \quad (1.6)$$

$$3\,CO_2(g) + 13\,H_2O(l) + 18\,e^- \rightleftharpoons C_3H_7OH(l) + 18\,OH^- \qquad 0.21\,V \text{ vs RHE} \quad (1.7)$$

Since CO_2 electrolysis is usually performed in an aqueous environment, hydrogen evolution also takes place as shown in equation (1.8), being a competition reaction to the $ERCO_2$.

$$2\,H_2O + 2\,e^- \rightleftharpoons H_2 + 2\,OH^- \qquad 0\,V \text{ vs RHE} \quad (1.8)$$

CO_2 can be electrochemically reduced to several products at similar potentials, according to equations (1.1) to (1.7). However, the practical potentials required for CO_2 reduction reactions are much more negative than the equilibrium ones, indicating that CO_2 reduction is generally more difficult to take place in comparison with H_2 evolution [33]. An explanation for this can be the increased amount of reaction intermediates, which generally correlates with the number of electrons required to form certain products. Since the activation energy for each intermediate needs to be overcome to obtain the final product, the formation of multiple intermediates with electron transfer require highly negative potentials to proceed, resulting in much more negative potentials than the overall theoretical equilibrium potential for each product [38, 39]. Another explanation is the lack of a suitable catalyst. Based on several experimental studies an overpotential of $\sim 1\,V$ is usually required to drive the $ERCO_2$ [33, 35]. Thus, the selectivity to one or another product can not only be controlled by the potential applied. Instead, several variables such as electrocatalyst, electrolyte, electrochemical reactor as well as electrode design play a role in the product spectrum that can be obtained from the electrochemical reduction of CO_2.

1.2.1 Electrocatalysts

The electrochemical synthesis of products from CO_2 is a complex multi-step reaction with multiple adsorbed intermediates (*CO, *COH, *CHO, among others) [38, 40, 41]. The catalyst provides reactive sites that allow the reduction of CO_2. Thus, the reaction mechanisms for the various products are affected by the binding strength of reactants and intermediates on the catalyst surface during the electrocatalytic reduction of CO_2 [38]. Different materials have been tested as electrocatalyst [37, 42]. The majority of the research community has focused on the study of transition metals, while some studies have shown that non-metallic materials such as boron doped diamond electrodes are also able to electrochemically activate CO_2.

1.2.1.1 Transition metals

Transition metals have been extensively studied as electrocatalysts [32, 33, 43–45]. Hori et al. was one of the first groups that contributed to understanding the electrochemical conversion of CO_2 on transition metals. They carried out CO_2 reduction on various metal electrodes at

a constant current of −5 mA/cm² in 0.5 M $KHCO_3$ [32, 33, 43]. In all the metals tested, CO_2 is first reduced to CO or HCOOH and, depending on the ability of each metal to bind these intermediates, different products can be obtained as follow [32, 33]:

(i) Metals that require a high overvoltage to produce hydrogen (Pb, Hg, In, Sn, Cd), produce formate as the main CO_2 reduction product. They also have negligible CO adsorption properties and very low amounts of CO have been detected as product.

(ii) Metals that bind CO strongly (Ni, Fe, Pt, Ti) are poisoned by CO, and consequently, H_2 evolves from the competing water reduction as the main product.

(iii) Metals that bind CO weakly (Au, Ag, Zn, Pd, Ga) produce mostly CO, as the produced CO is released from the surface before it can be further reduced to products such as alcohols and hydrocarbons.

(iv) Metals with intermediate binding energy for CO (Cu) produce CH_4, C_2H_4 and alcohols among other multi-carbon products.

Most of Hori's results were confirmed by Azuma et al. [44] testing transition metals in a different electrolysis cell and using potentiostatic but not galvanostatic methods. In a more recent publication, Kuhl et al. [45] performed experiments with seven transition metals analyzed before by Hori et al. [33] but using their own improved product analysis methodology. This study, contrary to Hori's work, reported that all of the seven transition metals studied (Au, Ag, Zn, Cu, Ni, Pt and Fe) are capable of producing methane or methanol [45]. They demonstrated the importance of measuring over a wide range of potentials with methods capable of identifying and quantifying even minor products. However, it should be taken into account that even when methanol and methane were found as CO_2 reduction products using transition metals such as Ni, Fe and Zn, the hydrogen evolution was, in this case, the main product leading to very low efficiencies for the C_1 products found. Thus, copper seems to be the only metal able to reduce efficiently CO_2 into multi-carbon products such as ethylene, ethanol and propanol [33, 44, 45]. Kuhl et al. [35] found 16 products out of the $ERCO_2$ on copper. They analyzed the gas products during the electrolysis with a gas chromatograph and an aliquot of the liquid products was taken at the end of the experiment for analysis with 1D ^{1}H NMR. These techniques allow reproducibility and are used nowadays by numerous research groups including us.

The most intensively studied electrocatalysts are: Ag, for the production of CO; Sn, on which formate is produced; and Cu, on which multi-carbon products are formed. While major progress regarding stability and selectivity has been made for the production of formate and CO, the formation of multi-carbon products involving multiple proton and electron transfer has still several challenges to be addressed. Some of the challenges to overcome with Cu as electrocatalyst are

the high overpotentials required, the fast deactivation and the simultaneous formation of several compounds, which lead to low selectivities.

Recently, a large portion of the scientific community has focused on the investigation of Cu as the only metal that can reduce CO_2 to hydrocarbons and alcohols at appreciable levels. One main reason for this unique catalytic activity of copper is attributed to the appropriate binding strength of intermediates (such as -CO, -COH, -CHO and -CH3) on the copper surface during the electrochemical reduction of CO_2 [38, 46]. Several efforts have been made including the study of mechanisms based on density functional theory calculations [38, 47, 48]; the modification of Cu surface structure [49, 50]; the development of nanostructured catalysts to increase the number of active sites [51–55], as well as bimetallic catalysts [56]; and even exploring catalysts beyond just simple metallics, such as Cu/N- dopped carbon-based materials that have shown interesting catalytic abilities [57]. While significant progress has been made, there is still a long path to go in the development of suitable catalysts.

1.2.1.2 Boron-doped diamond electrodes

Carbon electrodes, including glassy carbon, graphite, carbon nanotubes and boron-doped diamond (BDD), offer several properties over solid metal electrodes in many different electrochemical applications. Boron-doped diamond (BDD) is a synthetic diamond in which boron atoms replace a part of carbon atoms. With this substitution, diamond can become electrically conductive [58]. Some of the advantages of BDD electrodes for the electrochemical reduction of CO_2 are: chemical inertness in acid and alkaline media, mechanical durability, low background currents (low capacitance), and a wide potential window for water electrolysis [59, 60]. Electrodes with these characteristics applied in the CO_2 electrochemical reduction have the potential to provide long-term stability and suppression of the hydrogen formation, known as the competing reaction for CO_2 reduction.

For commercial and laboratory electrode production chemical vapor deposition (CVD) is the most popular growth technique. During CVD a plasma is created using either hot filaments (HF-CVD) or microwaves (MWP-CVD). A carbon source such as methane and dopant, boron, in gaseous form is fed into the CVD reactor in the presence of H_2. The employed growth parameters are highly important as they will control properties such as doping level, surface termination, the ratio of non-diamond carbon (sp^2) to diamond (sp^3), the thickness of the film, texture and grain size [60]. This can lead to the following categories of BDD: ultra-crystalline (UCN), the grain size <10 nm; nanocrystalline (NC), grain size in the range of 10 nm-1 µm; microcrystalline (MC), grain size >1 µm [60]. BDD characteristics such as sp^2 hybridization or non-diamond-carbon (NDC) incorporation, boron content and surface termination define

the CO_2 adsorption/desorption ability of the electrode, the conductivity and in general the electrochemical properties that influence the reduction of CO_2 [60, 61].

Einaga et al. have reported several studies using BDD as cathode for the electrochemical reduction of CO_2 including the investigation of applied potentials and electrolytes such as sea water [62], ammonia [63], and alkali-metal cations [64]. Products such as CO, HCOOH, and HCHO together with H_2 have been reported. Furthermore, Birdja et al. [65] have provided some mechanistic insights for the CO_2 reaction on BDD using $HClO_4$ and $NaClO_4$ as electrolytes. However, further investigation is required to demonstrate long-term stability, CO_2 reaction path on BDD, the effect of the anionic species in electrolyte, and the influence of growth parameters in the performance of BDD as cathode for the CO_2 electrochemical reduction.

1.2.1.3 Effects of catalyst size and morphology

The performance of an electrocatalyst not only depends on the material but also on the morphology. Some studies have shown that nanostructured catalysts are capable of providing more active sites (under-coordinated sites such as edge sites and corner sites) compared to bulk metal catalysts where all the atoms sit on a flat surface [39, 66, 67]. The increased active surface sites on nanocatalysts may cause an enhanced catalytic performance since the catalytic activity is proportional to the number of active surface sites [66]. Additionally, nanostructured catalysts, have shown an increased tolerance to heavy metal impurities in an electrolyte, improving the catalytic stability of the electrochemical reduction of CO_2. Hori et al. [33] have demonstrated that a flat catalyst can be poisoned by an unavoidable ppm concentration of heavy metal impurities (such as Fe or Pb) in the electrolytes, resulting in the degradation of the electrocatalytic activity for CO_2 reduction. Nanostructured electrocatalysts can adapt to contamination or impurities much better because of their large surface area and thus improving catalytic stability [66].

The study of Cu nanoparticles was initially performed covering Cu foils with polycrystalline Cu nanoparticles (50-100 nm). Tang et al. [46] reported that Cu nanoparticle covered electrodes exhibited a better selectivity towards C_2H_4 and CO formation in comparison with an electropolished Cu electrode and an argon gas sputtered Cu electrode. The increased catalytic selectivity for C_2H_4 formation in CO_2 reduction performance was explained by the roughened Cu surface which was able to provide a greater abundance of undercoordinated sites. Reske et al. [68] examined the catalytic behavior of Cu nanoparticles (CuNPs) with different particle size in the range of 2-15 nm. Interestingly, a significant increase of H_2 and CO selectivity was observed on CuNPs while the reduction to hydrocarbons was lower compared to the bulk Cu foil. On the other hand, Manthiram et al. [69] have demonstrated that CuNPs supported on glassy carbon (CuNPs/C) exhibited a 4-fold higher methanation current densities compared to the high-purity Cu foil counterpart and a Faradaic Efficiency (FE) of 80 % for CH_4

was achieved. Furthermore, Baturina et al. [70] have shown that Carbon black supported Cu nanoparticles are more selective towards C_2H_4 generation versus electrodeposited Cu. In this case, the particle size range was 10-30 nm. Song et al. [57] performed $ERCO_2$ using a carbon nanospike (CNS) film with electronucleated Cu nanoparticles (10-30 nm). With this electrode a low overpotential and high Faradaic efficiency towards ethanol was reported. Additionally, Kim et al. [52] reported selective conversion of CO_2 to multi-carbon products, while suppressing C_1 formation by performing $ERCO_2$ on cube-like CuNPs deposited onto carbon paper support. This indicates that catalyst support plays also an important role in the selectivity. This has directed the investigation focus on the nanostructured Cu catalyst supported on carbon based electrodes including gas diffusion electrodes [71, 72]. While significant progress has been made in the last five years regarding selectivity, overpotential and current densities towards multi-carbon products using Cu nanoparticles, further investigation is required to understand the influence of material dimensions on the selectivity of the electrochemical reduction of CO_2.

1.2.2 Electrolytes

Electrolytes provide a medium to transfer coupled electrons and protons (e^-/H^+). The type and concentration of electrolytes affect the conductivity and pH, and thus, the performance of the electrolyzer. Experiments in different electrolyte species and concentrations revealed that the product distribution of the reduction reaction depends strongly on the pH at the reaction boundary, which is different from the pH bulk and it is affected among others by the electrolyte species and concentration [33, 43]. Most studies in electrochemical CO_2 reduction have been performed in weakly acidic or alkaline CO_2-saturated aqueous electrolytes containing inorganic salts with HCO_3^-, SO_4^{2-}, or Cl^- anions and alkali metal cations e.g., Na^+ and K^+.

Ions adsorbed on an electrode surface can block surface sites and can thereby decrease the current density, stabilize intermediates, and modify the potential of the outer Helmholtz layer in the electrical double layer and the electrode surface [43, 73, 74]. In general, smaller cations have larger hydration powers, and consequently, have less adsorption on electrode surfaces. Smaller cationic species can deliver more water molecules from their solvation shell to the electrode than bigger cations. Thus, H_2 production increases with smaller cation size, i.e. Li^+ with a hydration number of 22 shows a larger H_2 formation than Cs^+ with a hydration number of 6 ($Li^+ > Na^+ > K^+ > Rb^+ > Cs^+$). Meanwhile, cations can affect relative concentrations of charged species (such as anion radical intermediates) close to the electrode, thus affecting product selectivity and current density. Cations adsorbed on a cathode repel H^+ ions from the cathode. This explains the experimentally observed trend of decreased H_2 evolution when larger cations are present in the electrolyte [74]. Additionally, cation adsorption may stabilize "CO_2^-*" on the cathode surface and hence favor the reduction of CO_2. Large cations were found to benefit the formation of

HCOOH on a Hg electrode, C_2H_4 on a Cu electrode [43, 73], and CO on a Ag electrode [74]. In general, CO_2 reduction has been shown to be favorable in Na^+, K^+, and Cs^+ solutions.

Anionic species with different buffer capacities affect the local pH at the electrode and hence the nature and selectivity of products formed [43]. A high local pH inhibits H_2 evolution and CH_4 formation because of low proton concentration, while the reduction of CO_2 to C_2H_4 is favored. The buffer capacity of anions impacts the availability of protons, which in turn affects reaction kinetics. For the weakly-buffered electrolytes such as $KHCO_3$ a sudden increase in local pH is observed during electrolysis as the hydroxide generated as a by-product of water-splitting cannot diffuse away fast enough or be immediately buffered by the solution. The majority of the studies that have reported a high selectivity towards C2 products on nanostructured and oxide derived Cu [52, 75, 76] have used $KHCO_3$ at low concentrations in H-cells. Here, the poor buffering capacity of the electrolyte causes the pH close to the electrode to quickly increase, helping to promote C2 products and suppress the competing CH_4 and H_2 reactions.

The majority of studies have been performed using neutral-pH catholytes such as bicarbonate-based salts. Only recently, experiments on gas-diffusion layers and flow cells have used KOH directly as a bulk catholyte [71, 72, 77, 78]. By using an alkaline catholyte directly, CO_2 reduction products have been observed at lower overall onset potentials than in neutral conditions on Au, Cu, and Ag catalysts [72, 77, 78]. This can be associated with higher conductivity of OH^- than HCO_3^-. However, the interaction between unreacted CO_2 and hydroxide is problematic for overall stability. While an alkaline catholyte may provide optimal cathode performance, it comes at the cost of system stability due to the interaction between CO_2 and hydroxide. A portion of the CO_2 on the boundary interface will be converted to bicarbonate by interacting with hydroxide, and then subsequently into carbonate. This carbonate could lead to salt deposits on the GDE, which is particularly an issue for scale-up [79]. This will not only decrease CO_2 utilization for the electrochemical conversion, but it might over a long enough operating time also decrease the pH at the reaction boundary and reduce the concentration of expensive KOH catholyte, itself energy-intensively produced through electrochemical reactions [80].

1.2.3 Electrode and cell design

Electrodes play an important role in the performance of heterogeneous electrochemical conversion of CO_2. In general, electrodes comprise a catalyst and substrate that should activate CO_2 and conduct electrons with low resistance. The processes occurring at the electrode–electrolyte interface and within the electrode determine performance and durability of the electrolysis. Thus, the main goal while designing electrodes and cells is the optimization of all the transport processes involved in the electrolysis, i.e. charge, heat and mass transport of reactants and products to and out of the electrocatalyst [29]. For the study of CO_2 electrochemical reduction

it should also be taken into account that the electrochemical cell or electrolyzer design has a profound effect on mass transport and thus on the performance of the reaction.

Up to date, there is no standard experimental setup or methodology established for the $ERCO_2$ and thus a variety of electrolyzer architectures have been developed [29, 81]. However, electrolyzers can be classified generally in two main groups H-Cells and flow cells. As depicted in Fig. 1.4 and 1.6, in each of these configurations CO_2 is supplied to a catalyst layer that is fully or partially immersed in a conductive electrolyte. The CO_2 fed can diffuse through the hydrodynamic boundary layer of a saturated bulk electrolyte as in a standard H-cell configuration or from a nearby gas-phase with a much shorter diffusion pathway when using gas diffusion electrodes in a flow cell [80]. A significant amount of fundamental studies and catalytic materials are still developed, tested and characterized in classical H-cell configurations and planar electrodes, in which the developed catalyst is deposited. Recently, it became obvious that high current density catalyst testing is a necessary step to properly evaluate materials for the up-scaling of the electrochemical CO_2 reduction, since catalytic behavior can be strongly affected by mass transport conditions [71, 72, 80]. This led to the introduction of gas diffusion electrodes and flow cells for the study of $ERCO_2$. Gas diffusion electrodes have been in general tested using flow cells. However, some authors have also investigated the performance of gas diffusion electrodes in H-Cells.

1.2.3.1 H-cells

H-type cells (H-cells) are typical and commonly used as lab-scale electrochemical reactors. The H-cell is usually made of glass and encompasses two compartments and three electrodes, i.e., working electrode, reference electrode, and counter electrode as depicted in Fig. 1.4. The cathodic and anodic chambers are separated by a proton-conducting or an anion-exchange polymer membrane. This setup allows ionic conductivity, preventing the transport of cathodic products to the anode where they can be oxidized [82]. A schematic of the electrochemical reduction of CO_2 on a planar electrode is given in Fig. 1.5. In this kind of setups the dissolution of CO_2 in the aqueous electrolyte and the long diffusion pathway lead to low CO_2 concentration at the electrode surface. This, together with a low surface area limits the performance of the $ERCO_2$. Furthermore, in an H-cell the electrolysis is operated as a semi-batch process, where the mass transport of liquid products can be arduous since the electrolytes are not continuously recirculated. However, a significant part of the scientific community and the majority of studies about electrocatalyst development for $ERCO_2$ published in the last 15 years have been performed in this type of cells.

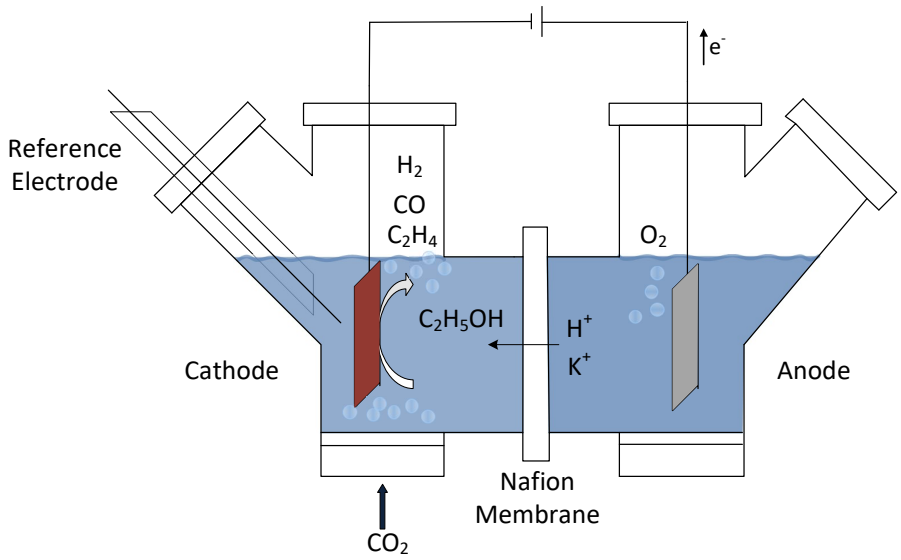

Figure 1.4: Schematic representation of an H-type electrochemical cell

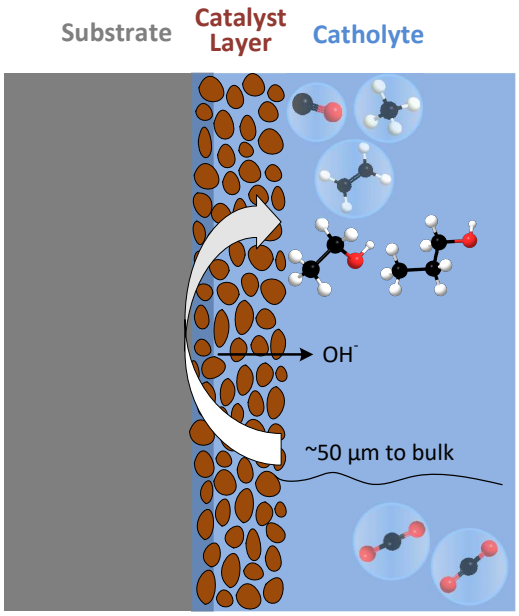

Figure 1.5: Representation of the electrochemical reaction on a planar electrode. Adapted from [80]

1.2.3.2 Flow cells

This type of setup consists of a collection of gaskets that are pressed together forming three flow channels, one for the gas, one for the catholyte and another for the anolyte. An ion-exchange membrane separates the cathode and the anode. Layers of a sealing material in between the gaskets, assure a leak-free system. The electrodes are usually placed on a metallic frame that allows an electrical connection with the current source. Cathode and anode performance can be monitored by using external reference electrodes. In this configuration, CO_2 is provided from one side of a gas diffusion electrode, while the other side of these porous electrode is in contact with the flowing catholyte [81, 82]. This makes CO_2 mass transfer to the catalyst much more effective than for the planar electrode because the distance over which mass transfer through the electrolyte occurs is smaller [83]. In addition, the liquid products are also transported out of the reaction zone by circulating the electrolyte. Consequently, a pump is required for the circulation of each electrolyte and an electrolyte reservoir is also introduced for the operation of a flow cell. In general, the operation of a flow cell demands a more complex periphery than a batch cell. As mentioned above, the configuration of the cell can vary from one research group to another. However, the schematic shown in Fig 1.6 should give a general idea of the architecture, from which all other setups can be derived.

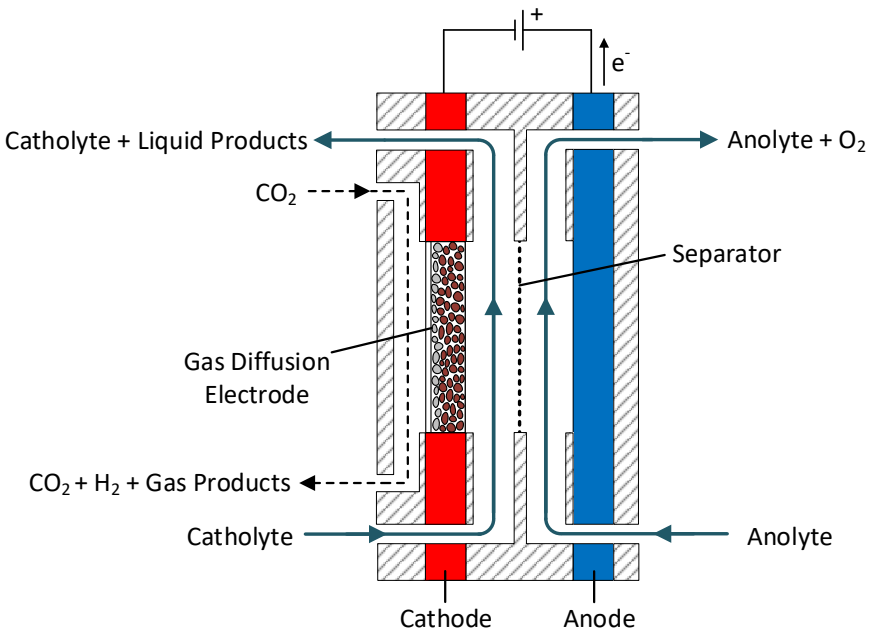

Figure 1.6: Schematic representation of an electrochemical flow cell. Adapted from [84]

1.2.3.3 Gas diffusion electrodes

In general, a gas diffusion electrode (GDE) consists of a porous material that allows a three phase boundary, where catalyst, electrolyte and gaseous reactant meet. Some GDEs use an electrically conductive reinforcement web, on which different mixtures of catalyst particles and binder materials are casted. The composition of the applied mixtures varies making the electrode more or less porous and hydrophobic [79]. Other types of GDEs are comprised of a catalyst layer and a substrate, which serves multiple functions: firstly it provides a porous medium through which reactant gas, CO_2, can diffuse from flow-field channels to the catalyst layer; secondly it allows the transport of product from the catalyst layer into flow channels or the electrolyte; and lastly it is conductive with low resistance [29, 83]. Porous carbon layers known as Gas Diffusion Layers (GDL) are commonly used as substrate. GDLs are formed from carbon fibers or pressed carbon particles and consist of a macroporous diffusion medium (DM) typically treated with PTFE to be hydrophobic and a microporous layer (ML). Catalyst particles mixed with a (ionic) binder are deposited onto the ML to form the catalyst layer [83]. Different ionomers are employed to work as binders for the fixation of the catalyst on the surface to provide ionic conductivity within the catalyst layer [81, 83]. A schematic of this type of GDE is given in Fig. 1.7.

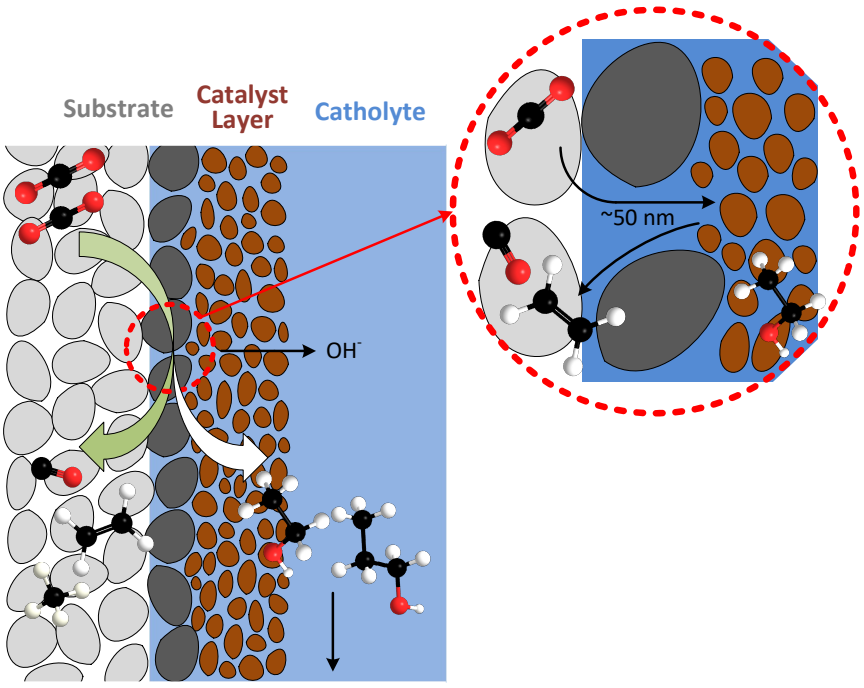

Figure 1.7: Representation of the CO_2 electrochemical reduction on a GDE made of a catalyst layer deposited onto a hydrophobic substrate with CO_2 diffusion from a nearby gas–liquid interface. Adapted from [80]

GDEs have been firstly introduced and extensively studied in fuel cells and water electrolyzers. In the case of fuel cells, an important role of the hydrophobic GDL is the removal of excess water. However, for GDEs applied in CO_2 electrolyzers, the electrolyte must be kept in contact with the catalyst surface a sufficient time for the reaction to take place. On one hand, proper wetting is prerequisite, but too much hydrophilicity that leads to a flooded electrode should also be avoided, otherwise H_2 evolution would take place instead of CO_2 reduction [81, 83]. Recent studies have shown that for $ERCO_2$ to become economically feasible it is necessary to improve the current density (>200 mA/cm^2) [23, 77]. It has been demonstrated that GDEs and flow cell systems are promising approaches for achieving this target [71, 72, 85]. The first studies regarding $ERCO_2$ on GDEs attributed the high current densities achieved to the high concentration of gaseous CO_2 at the gas/solid interface, thereby overcoming the low solubility of CO_2 in water [86]. However, recent experimental and theoretical work have demonstrated the importance of water and hydrated cations on the elementary processes involved in $ERCO_2$ [83]. Therefore, it is necessary to cover the catalyst with electrolyte to provide electrocatalytic activity. This means that although CO_2 is supplied to the GDE from the gas phase the reactant at the catalyst site should still be dissolved CO_2. However, the solubility of CO_2 in water would represent in a GDE a much lower mass-transfer resistance than in a planar electrode, since the dissolved CO_2 does not have to be transported through a bulk electrolyte [83]. In a general point of view, it can be considered that the reaction is no longer limited by the solubility of CO_2 with the introduction of a GDE. The primary difference between a planar electrode in an H-cell and a GDE in a flow cell is the CO_2 diffusion pathway to the surface of the catalyst that should be roughly 50 µm for a planar electrode in an H-cell vs 50 nm using a gas-diffusion layer in a flow cell [80]. This means that even though dissolved CO_2 is the reactant in both cases the 1000-fold lower diffusion pathway in a flow cell allows an increased current density.

1.2.4 Figures of merit

The characterization of each feature in an electrolyzer can be complex. However, there is a commonly used figure of merit to evaluate the performance of an electrochemical system known as the Faradaic efficiency (FE) or current efficiency [87]. In general, the Faradaic efficiency for a given product is defined by the following equation:

$$FE_i = \frac{z_i \cdot F \cdot n_i}{Q} \tag{1.9}$$

where z_i is the number of electrons required for each reaction, F the Faraday constant, n_i the number moles obtained for each product and Q the applied charge. The Faraday constant ($F = N_A \cdot e$) is the product of the Avogadro number ($N_A = 6.022\,141 \cdot 10^{23}$/mol) and the elementary charge ($e = 1.602\,177 \cdot 10^{-19}$ C). The applied charge ($Q = I \cdot t$) is given by the total applied current (I) and the electrolysis time (t). By definition, the FE for a continuous flow system can

also be understood as the ratio between the molar flow obtained for a specific product ($\dot{n}_i$) and the theoretical molar flow that could have been produced $\dot{n}_{i,theo.}$ with the charge applied:

$$FE_i = \frac{\dot{n}_i}{\dot{n}_{i,theo.}} \tag{1.10}$$

where $\dot{n}_{i,theo.}$ is defined by the Faraday's Law:

$$\dot{n}_{i,theo.} = \frac{n_{i,theo.}}{t} = \frac{I}{z_i \cdot F} \tag{1.11}$$

Replacing equation 1.11 in equation 1.10 and assuming ideal gas, $p \cdot V_i = n_i \cdot R \cdot T$, the Faradaic efficiency for gaseous products can be calculated as follows:

$$FE_i = \frac{z_i \cdot F \cdot y_i \cdot \dot{V}_{out} \cdot p}{I \cdot R \cdot T} \tag{1.12}$$

where $\dot{V}_{out}$ is the total gas flow at the gas outlet of the cathode and y_i is the molar fraction of a specific product measured usually by gas chromatography.

For the liquid phase the products are usually accumulated in an electrolyte reservoir and the analysis is carried out either at the end of a potentiostatic step or at the end of the experiment obtaining an average FE. The analytical method commonly used is Nuclear Magnetic Resonance (NMR). Using this method the FE for the liquid products is calculated by the ratio between the amount of substance obtained for a specific product (n_i) and the theoretical amount of substance that could have been produced $n_{i,theo.}$ with the charge applied during the time the liquid was accumulated:

$$FE_i = \frac{n_i}{n_{i,theo.}} \tag{1.13}$$

with $n_{i,theo.}$ defined by equation 1.11 and calculating n_i as follows:

$$n_i = c_{Standard} \cdot \frac{A_i}{A_{Standard}} \cdot \frac{P_{Standard}}{P_i} \cdot X_{Dilution} \cdot V_{Katolyt} \tag{1.14}$$

In this case, the molar concentration of each product is determined by comparing the intensity of a product peak and the intensity of a standard peak, being $c_{Standard}$ a known concentration, A_i the integral area of a product peak and $A_{Standard}$ the integral area of the standard peak. The signals corresponding to the standard compound and to a specific product must be normalized according to the number of protons. These are defined as $P_{Standard}$ and P_i, respectively [88, 89]. It should also be taken into account, firstly, that during the preparation of the sample to be measured by NMR, the aliquot with the obtained products is diluted in D_2O and, secondly, that the original concentration of the standard is also diluted by mixing it with D_2O and the aliquot

to be analyzed in the NMR tube. Finally, the molar concentration is multiplied by the volume of electrolyte in the reservoir to obtain the amount of moles of each product.

While the FE is calculated with the total current applied, in the literature FE charts are usually given as a function of the geometrical current density. With this, a better performance comparison for electrolyzers with variable sizes is accomplished. Another figure of merit is the stability, which describes the gradual degradation/deactivation of the electrode catalyst and the overall electrochemical cell. Unfortunately, the durability of the electrochemical cell is probably the least studied aspect of electrochemical reduction [87].

1.2.5 Target products and state-of-the-art

As aforementioned, several products can be obtained from the electrochemical reduction of CO_2. The formation of C1 products, such as CO and HCOOH, is nowadays possible at high current densities due to the adoption of gas diffusion electrodes [23, 85]. However, more sophisticated catalysts and electrochemical systems are required for the formation of C2 and C3 products with Cu [90]. Jiao et al. [87] have recently published a general techno-economic analysis of CO_2 electrolysis systems suggesting that alcohols such as ethanol and *n*-propanol could be highly promising, if current densities nearby $-300\,\mathrm{mA/cm^2}$ and high Faradaic efficiencies $\sim$60 % at moderate overpotentials are achieved. As given in Fig. 1.8, Jiao et al. summarized the general trends of Faradaic efficiencies towards the most common CO_2 reduction products reported until the end of 2016. The majority of the reported results have achieved high Faradaic efficiencies at low current densities. One of the reasons is that a large portion of the community has focused on the development of catalysts using the traditional batch cell reactors. Furthermore, long term stability was unknown for the majority of collected results, since many experiments were conducted over short periods of time lower than 5 h. In general, Faradaic efficiencies for CO and formic acid are consistently high (>80 %) at low and high current densities (cf. Fig. 1.8a). In contrast, in the case of C2 products, Faradaic efficiencies towards ethylene and ethanol tend to be low (cf. Fig. 1.8b). In the past two years, significant progress has been made on improving the Faradaic efficiency for C2 products [53, 71, 72]. For the case of C3 products, the Faradaic efficiency for *n*-propanol has been significantly low (<5 %) reflecting the energy intensive (18 electrons) reaction pathway [87].

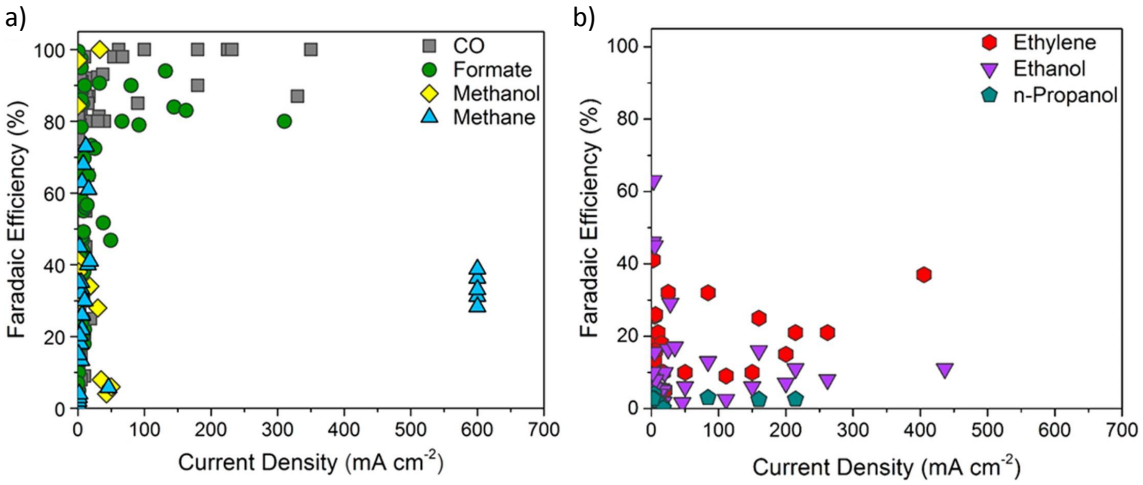

Figure 1.8: State-of-the-art Faradaic Efficiency versus total current density for: a) C1 and b) C2-C3 products. Reprinted with permission from [87]. Copyright 2019

From an economic point of view, ethylene and ethanol are highly desirable products due to the high market price (1.3 \$/kg ethylene and 1.0 \$/kg ethanol) and annual global production (140 $Mtonne_{ethylene}$/year and 77 $Mtonne_{ethanol}$/year). Furthermore, these two products have major industrial uses as chemical precursors, fuel additives, and E-fuels. While *n*-propanol currently presents low annual production (0.2 Mtonne/year) due to the difficulty of its production process [87], this chemical is an industrially important precursor with the potential of providing a high fuel efficiency due to its large energy-mass density (30.94 kJ/g) [51]. Hence, if *n*-propanol could be efficiently produced through CO_2 reduction, it could replace ethanol as a transportation fuel additive, increasing its market potential [87].

Alcohols are traditionally produced by fermentation of sugars or by conversion of petrochemicals [90–92]. Although bio-catalysis have been proven to be highly selective towards C2 alcohols, the production rates with this type of catalysts tend to be slow, water intensive, and highly sensitive due to the use of microorganisms [90]. For alcohols produced by $ERCO_2$ to become profitable, cheaper electricity costs and improved catalytic performance are needed. Nevertheless, with the current energy system transformation and with continual efforts, the introduction of C2-C3 alcohols produced from $ERCO_2$ would allow for renewable energy sources to penetrate the transportation and chemical sectors while potentially reducing CO_2 emissions [87]. Overall, further research efforts are needed to develop electrochemical systems, especially for the conversion of CO_2 into C2 and C3 products with the appropriated performance for industrial implementation.

While stable and highly efficient conversion of CO_2 to CO has been achieved at high current densities using GDEs, lower and unstable conversion have been obtained for direct $ERCO_2$ to C2 and C3 products. Despite the low conversion for multi-carbon products, several experimental and theoretical mechanistic investigations have demonstrated that CO is the main intermediate towards multi-carbon products [37, 41, 93]. Although these experimental results have provided interesting mechanistic insights, most of them have been performed using CO-saturated aqueous electrolytes and planar electrodes, where the maximum geometric current density that can be achieved is on the order of $-1\,mA/cm^2$. This low current density is attributed to the very low solubility of CO in water ($\sim$1 mM), which is lower than the solubility of CO_2 ($\sim$33 mM). Additionally, it has been shown that the selectivity towards C2 products increases in an alkaline pH environment [94]. Recently, a part of the scientific community has focused on optimizing selectivity, current density and cathode potential by studying CO_2 electrolysis using alkaline electrolytes, flow cells and Cu-GDEs, prepared with nanoparticles [71, 72]. Ma et al. [71] performed $ERCO_2$ on a GDE using Cu nanoparticles, proposing a possible reaction path, as shown in Fig. 1.9. Nevertheless, in alkaline conditions, CO_2 reacts with OH^- forming bicarbonate. This unwanted side reaction can consume more CO_2 than what is utilized for electrochemical product formation [95]. While multi-carbon products should be the target, several aforementioned issues need to be overcome for a efficient direct $ERCO_2$. As shown in Fig. 1.9, CO is a key intermediate to multi-carbon products and a better understanding of its reduction path can lead to more efficient electrolysis systems. With the aim to increase selectivity towards value added chemicals, it is worthwhile not only to investigate CO as a reactant for electrochemical reduction using GDEs and flow cells, but also to evaluate the feasibility of a two-step electrochemical reduction of CO_2.

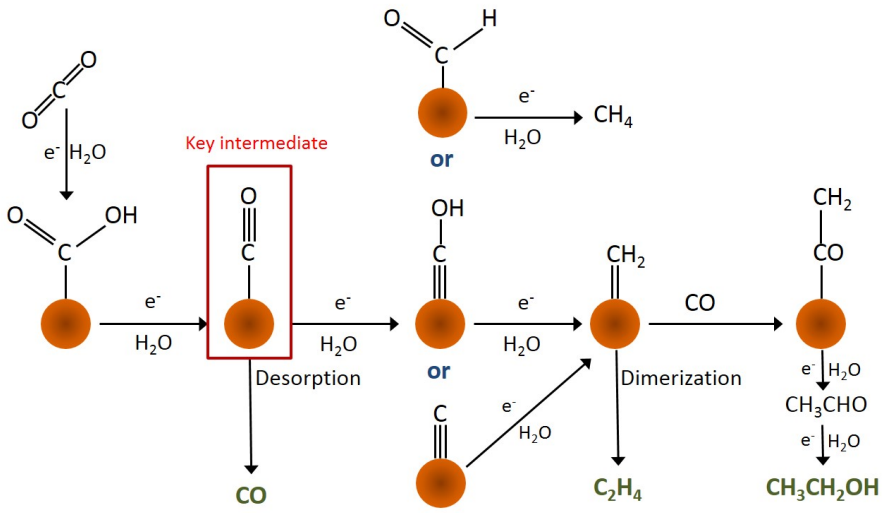

Figure 1.9: Proposed reaction pathway for the CO_2 reduction to various products (mainly C2H4 and C2H5OH) on Cu nanoparticles. Adapted from [71]

1.3 Scope of this thesis

Aiming for a carbon neutral economy and the integration of renewable electricity in the energy system, new technologies that convert electrical renewable energy into chemical energy are currently being developed. In the course of these activities, Siemens Corporate Technology has started the research project "CO_2ToValue" to investigate the fundamental feasibility of the CO_2 and renewable electricity transformation into economically and energetically valuable products. Within this frame, the present doctoral thesis focused on the experimental investigation of the electrochemical reduction of CO_2 and CO towards value-added chemicals. It is important to mention that the emphasis of this thesis was placed on the cathodic reaction, which means the reduction reaction. The oxidation reaction is out of the scope of this thesis. The main goal was to increase selectivity towards value added chemicals for an industrial application. This involves the development of a system that can be operated at high current densities.

The first objective was the study of metallic and non-metallic materials as electrocatalyst in conventional electrolysis cells known as H-Cells to gain a better understanding of the electrochemical reduction of CO_2 in a simple system. After confirming that Cu is the only material able to electrochemically reduce CO_2 and CO towards multi-carbon products, the investigation was performed in Cu gas diffusion electrodes with flow cells. Subsequently, the doctoral project focused on the electrochemical reduction of the main intermediate to hydrocarbons, specifically carbon monoxide. Here, the objective was to explore the advantages of carbon monoxide as the reactant in electrochemical reduction. Furthermore, taking into account that big steps have been made by Siemens in the electrochemical reduction of CO_2 to CO, the final objective of the thesis was to study the feasibility of a two-step electrochemical reduction of CO_2 at current densities up to $-300\,mA/cm^2$ regarding selectivity towards ethylene, ethanol and *n*-propanol. In order to achieve the above mentioned objectives the document is sectioned as follows:

Chapter 2 explores the use of non-metallic and metallic planar electrodes as electrocatalyst for the electrochemical reduction of CO_2 in H-cells. In the first, part boron doped diamond electrodes are investigated as electrocatalyst. The second part focuses on the electrochemical reduction on transition metals using either CO_2 or CO as the reactant.

Chapter 3 demonstrates the advantages of CO as reactant over CO_2 towards multi-carbon products using gas diffusion electrodes with flow cells being able with this to operate at industrially relevant current densities. Additionally, the influence of Cu particle size on the selectivity towards ethylene, ethanol and *n*-propanol is investigated.

Chapter 4 focuses on the investigation of a cascade two-step electrolysis of CO_2. Here each step is initially studied separately. Subsequently, a fully experimental demonstration of a two-step electrolysis of CO_2 is presented. With this, it was possible to provide interesting insights into the development of a cascade electrolysis as an alternative to improve the selectivity for multi-carbon products.

Chapter 5 summarizes the key findings on the strategies applied to improve the electrochemical reduction of CO_2 and draws the conclusions of this work. Additionally, some suggestions for further investigation based on chapters 2, 3 and 4 are given as an outlook.

2 CO_2 electrochemical reduction on planar electrodes

This chapter focuses on the study of conventional and novel materials as electrocatalysts for the electrochemical reduction of CO_2. The here performed material screening allowed a better understanding of the phenomena that take place during electrolysis and provided the basis for the development of a more suitable electrochemical system. Non-metallic, as well as metallic planar electrodes were investigated using H-Cells. This chapter is divided in three main sections. In section 2.1 and 2.2 boron doped diamond electrodes are investigated as catalysts for the $ERCO_2$, while in section 2.3 transition metals are studied for the electrochemical reduction of carbon monoxide and carbon dioxide. The first section is based on:

N. S. Romero Cuellar, K. Wiesner-Fleischer, O. Hinrichsen, M. Fleischer, Electrochemical Reduction of CO_2 in Water-Based Electrolytes $KHCO_3$ and K_2SO_4 Using Boron Doped Diamond Electrodes, ChemistrySelect, Volume 3 Number 13, 2018. DOI: 10.1002/slct.201702414.

Author contributions:

N. S. Romero Cuellar conducted the experiments, evaluated the results, performed the product analysis and wrote the manuscript with input from all authors. K. Wiesner-Fleischer, M. Fleischer and O. Hinrichsen supervised and guided the experiments as well as the findings of this work.

2.1 Electrochemical reduction of CO_2 in Water-Based Electrolytes $KHCO_3$ and K_2SO_4 Using Boron Doped Diamond Electrodes

2.1.1 Abstract

The performance of Boron Doped Diamond (BDD) electrodes for the electrochemical reduction of CO_2 at room temperature and in water-based electrolytes was investigated. Techniques such as linear sweep voltammetry, chronoamperometry, and chronopotentiometry were used to confirm the activity of BDD for the CO_2 reduction. Besides H_2, CO and HCOOH were found as major products with CH_3OH as minor product. The effect of anionic species with and without buffer capacity was investigated using $KHCO_3$ and K_2SO_4 as electrolytes. BDD did not show any degradation after using it in several experiments. The The Faradaic efficiency (FE) for CO in the gas phase and the concentration of HCOOH in the liquid phase were higher in K_2SO_4 than in $KHCO_3$. However, the total FE for $C1$ products was lower than 20 %. Then BDD electrodes were modified with silver, which improved the FE for CO to 68 % in K_2SO_4 at −1.8 V vs Ag/AgCl. Galvanostatic experiments were also performed for 10 hours at $-10\,mA/cm^2$ producing 30 % FE for CO in the gas phase and 43.9 mM HCOOH in the liquid phase.

2.1.2 Introduction

The electrochemical reduction of CO_2 using aqueous electrolytes and renewable energy as a current source for the production of industrial chemicals at room temperature and atmospheric pressure is a promising technique to achieve carbon neutrality and a sustainable energy economy in the chemical industry [36, 40]. Nevertheless, the industrial application of this technology requires further development of suitable catalysts [37, 96, 97]. Transition metals have been extensively studied as electrocatalysts; [32, 33, 35, 44, 45, 98]; unfortunately, low efficiency due to hydrogen evolution, poor product selectivity, high over potential and fast deactivation remain a challenge for industrial applications. Recently, it has been discovered that non-metallic carbon based electrocatalysts such as BDD and N-doped carbon, which show chemical and mechanical stability, were also active for electrochemical reduction of CO_2 [59, 62, 63, 65].

BDD electrodes were first studied as cathodes for the electrochemical reduction of CO_2 in seawater and aqueous ammonia solutions by Nakata et al [62]. They found BDD to be active for the production of HCHO, HCOOH and H_2 and attributed the high and stable Faradaic efficiency

(FE) to the sp^3-bonded carbon of BDD after using diamond electrodes with different sp^2/sp^3 ratios. An efficiency of 36 % was reported in seawater for the selective formation of HCHO. In a more recent publication, BDD was also found to be active towards CH 3 OH generation in aqueous ammonia solution. However, the high selectivity for CH_3OH production was not caused by the direct electrochemical reduction of CO_2.Instead, it was shown that the bicarbonate ions, which are formed by the reaction between ammonia and CO_2, were the reducible species [63]. On the other hand, Birdja and Koper [65] performed CO_2 electrochemical reduction on BDD electrodes using $HClO_4$ and $NaClO_4$ as electrolytes. CO, HCHO, and HCOOH were found as products depending on the applied cathodic potentia. Additionally, CH_4 was reported by the reduction of CO and HCOOH by the electrolysis of HCHO.They suggested that HCOOH and CH_3OH may not be produced directly by the CO_2 electrochemical reduction. These products should instead be the result of Cannizzaro-type disproportionation reactions, which take place at local alkaline pH values. Regarding the production of formic acid on BDD electrodes, Ikemiya et al. [64] studied the effect of alkali-metal cations (AM) such as Cs^+, Rb^+, K^+, and Na^+, using alkaline solutions (AMOH) and neutralizing them to pH 6.2 with HCl. The highest FE for HCOOH was found with Rb^+. The same effect has also been discussed on transition metals such as Ag and Cu where Cs^+ performed the best [99]. Regarding transition metals, it has also been proven that in addition to the cationic species, the anionic species can also influence the performance of electrolysis. However, the influence of the anions has never before been investigated on BDD electrodes

In this work, electrochemical reduction of CO_2 is performed on BDD electrodes in $KHCO_3$ and K_2SO_4, aiming to better understand the effect of anionic species on the formation of CO and HCOOH on this specific type of semiconductor electrodes. The best results were found in K_2SO_4, showing stable performance. Furthermore, it will be shown that electrochemical deposition of Ag on BDD improves the efficiency to carbon monoxide without compromising the stability of the BDD electrode.

2.1.3 Results and discussion

2.1.3.1 Electrode Characterization

We characterized BDD Electrodes first using Raman spectroscopy to verify the presence of sp^3-bond carbon as shown in the supporting information (2.7). The electrochemical behavior of the BDD electrodes was first evaluated by means of linear sweep voltammetry (LSV) in both the presence and absence of CO_2, which can indicate BDD activity. In LSV, the working electrode potential (E_{WE}) is varied linearly with the time between two values. Faradaic current will flow when the potential reaches values at which the species in solution can undergo electrochemical

conversions [100]. In a N_2 environment at the cathode, the only reaction expected is hydrogen evolution reaction (HER). On the other hand, in a CO_2 environment, the reduction of H^+ protons and the CO_2 reduction reaction (CO_2RR) should occur simultaneously [101]. Fig. 2.1 depicts voltammograms for BDD electrodes in the presence of an inert gas such as N_2 and in CO_2. It can be noticed that Faradaic current started flowing at a lower potential (−1.1 V vs Ag/AgCl) in a CO_2 atmosphere than in N_2 (−1.3 V vs Ag/AgCl). However, low current is only achieved until around −1.8 V vs Ag/AgCl, where a rise of the curve is observed. The Faradaic current flowing in the presence of CO_2 between −1.1 V and −1.8 V suggests that the BDD electrode is active for the CO_2RR. In addition, the delay on the exponential behavior of the current in CO_2 relative to that in N_2 suggests that the presence of CO_2 or its reaction products could make the H_2 evolution reaction happen at more negative potentials.

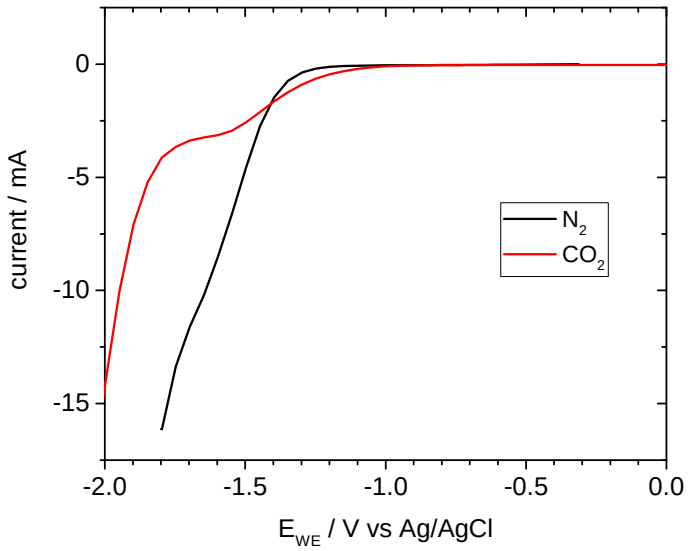

Figure 2.1: Linear sweep voltammogram for BDD electrodes at 50 mV/s in 0.1 M $KHCO_3$ in presence of N_2 (black) and CO_2 (red).

2.1.3.2 CO_2 Reduction Products

In order to confirm the activity of BDD for the CO_2RR and its products, potentiostatic experiments were performed, in which the working electrode potential (E_{WE}) was increased 0.1 V every 20 min from −1.4 V to −2.1 V vs Ag/AgCl. The gas products were analyzed at each potential using gas chromatography. The reaction products in both electrolytes for the gas phase were CO and H_2 with traces of CH_4 at the most negative potential. Fig. 2.2 depicts the results of the Faradaic efficiency for CO in $KHCO_3$ and K_2SO_4. Products accumulated in the liquid phase were analyzed using NMR after the end of the experiments, in which HCOOH and CH_3OH were detected as liquid products as shown in Table 2.1.

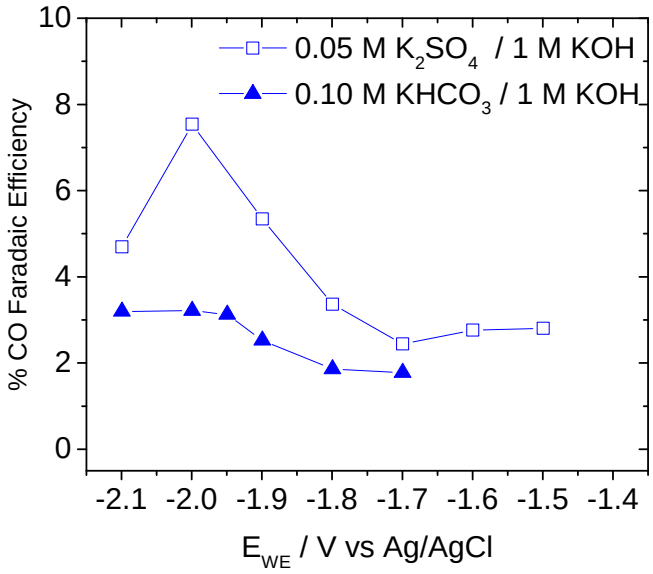

Figure 2.2: Faradaic efficiencies of CO for the electrochemical reduction of CO_2 on BDD electrodes in 0.1 M $KHCO_3$ (▲) and in 0.05 M K_2SO_4 (□).

Table 2.1: Concentration in mM of the liquid products for the electrochemical reduction of CO_2 on BDD and Ag-BDD electrodes in 0.1 M $KHCO_3$ and 0.05 M K_2SO_4

			average current	Concentration / mM	
Method	Electrolyte	Electrode	mA	HCOOH	CH_3OH
potentiostatic	0.05 M K_2SO_4	BDD	9.31	11.38	0.05
	0.10 M $KHCO_3$	BDD	9.34	5.74	0.01
	0.05 M K_2SO_4	Ag-BDD	16.22	11.29	0.01
galvanostatic	0.05 M K_2SO_4	Ag-BDD	9.99	43.94	0.02
	0.10 M $KHCO_3$	Ag-BDD	9.97	14.54	0.01

The formation of CO using BDD has been reported by Birdja & Koper [65] and Jiwanti et al. [63] with Faradaic efficiencies lower than 1 %. Nevertheless, Jiwanti et al. experiments were performed in aqueous ammonia at lower working electrode potentials than in this work. They found methanol as the main product of the reaction, in which CO_2 was only fed into the electrolyte before the electrolysis. Thus, the high selectivity to methanol was presumably caused by the reduction of bicarbonate HCO_3^- and not of CO_2. In our experiments, $KHCO_3$ was used as electrolyte, which dissociates to potassium ions K^+ and bicarbonate ions HCO_3^-. In addition, CO_2 was constantly supplied to the solution. Small quantities of methanol were found not only in $KHCO_3$ but also in K_2SO_4, where the presence of bicarbonate should be lower, since the only source is the CO_2 in solution. Our results suggest that methanol was likely not a product of HCO_3^-, since a higher methanol concentration was obtained in K_2SO_4 than in $KHCO_3$.

Formaldehyde, which was found by Nakata et al. [62] and Birdja & Koper [65] as a product of CO_2RR on BDD, is not present in our product spectrum. This can be attributed to different

factors: first, our experiments were run at higher cathodic potentials, reaching current densities around $-10\,mA/cm^2$; secondly, the electrolytes used in our experiments are different than the ones used in the two studies mentioned above; lastly, formaldehyde could be an intermediate for the liquid products we found, namely HCOOH and CH_3OH.

Birdja and Koper used 0.001 M $HClO_4$ + 0.099 M $NaClO_4$ as electrolyte, in which CO, HCHO and HCOOH were found as products [65]. They proposed a mechanism based on the Cannizzaro-type reactions, [102] suggesting that the formation of HCOOH under reducing conditions might be the result of a disproportionation reaction of HCHO, which is promoted by the OH^- ions produced during the direct reduction of water. As explained by Kortlever [37], H_2 can evolve from two different reactions: it could be the result of proton reduction at less negative potentials and a very acidic media with pH of 1, or it could be produced by direct water reduction with pH 3 and more negative potentials producing OH^- [37].

Our experiments were run at bulk pH values between 5 and 9 and at potentials at which HER takes place, so that a high presence of OH^- in the vicinity of the electrode was expected. Based on Birdja's and Koper's results our experiment conditions should promote the disproportionation reaction converting HCHO into HCOOH and CH_3OH. In fact, HCOOH and CH_3OH were found as products in the liquid phase as shown in Table 2.1. Therefore, it can be assumed that formaldehyde is not observed in our product spectrum because it is fully converted into carboxylic acid and alcohol.

In order to examine a possible non-electrochemical reaction of formaldehyde due to a high concentration of OH^- in the vicinity of the electrode, a solution of 0.01 M HCHO + 1 M KOH was prepared without applying current density and without the presence of CO_2 . Additionally, 0.01 M HCHO was mixed with 1 M $KHCO_3$ to rule out a loss of product before the product analysis. Both samples were analyzed after 24 hours using NMR. The NMR results depicted in Fig. 2.14 in the supporting information show that HCHO is converted into HCOOH in a high concentration of OH^- but not in the presence of HCO_3^-. This indicates that HCOOH can be a product of the disproportionation reaction of HCHO in alkaline media. A quantification of CH_3OH in the presence of HCHO using 1D ^1H NMR is complicated due to overlapping peaks; however, the presence of CH_3OH was confirmed with 13C NMR. Taking into account the above mentioned facts, Faradaic efficiencies were only calculated for CO and not for HCOOH and CH_3OH, since these two products are not the results of an entirely electrochemical reduction of CO_2, but of a disproportionation reaction of HCHO.

2.1.3.3 Electrolyte Effect: Anionic species

Fig. 2.2 and Table 2.1 show a higher FE for CO and higher concentration of HCOOH in potassium sulphate than in bicarbonate, which can be attributed to the difference of pH values close to the electrode. It is known that there are differences between the pH values in bulk and close to the electrode. Tracking the change of the local pH value is not an easily accomplished task. Therefore, we measured the bulk pH before and after the electrolysis. There was no significant change using $KHCO_3$, while an increase from 5.5 to 8.5 was observed in K_2SO_4. A similar effect was investigated by Hori on Cu electrodes [33]. He explained that the buffering effect of HCO_3^- can neutralize the OH^- produced while HER takes place, mitigating the pH enhancement at the electrode and promoting the H_2 evolution rather than the CO_2 reduction. In contrast, electrolytes such as K_2SO_4 are not able to neutralize OH^-. This results in a pH increase in the vicinity of the electrode, slightly suppressing the HER and favoring the CO_2RR. Thus, a more alkaline media not only suppresses the HER and promotes the CO_2 reduction, but it also enhances the formation of HCOOH and CH_3OH due to the Cannizzaro reaction on BDD electrodes. Our results are then in agreement with Hori's observations [33] and with Birdja's and Koper's results [65], who demonstrated that the formation of carboxilic acids and alcohols is the result of Cannizzaro-type reactions and that the lower the electrolyte buffer capacity, the higher the possibility of disproportionation reactions occurring. However, from this type of reaction a conversion of HCOOH and CH_3OH in a 1 : 1 ratio is expected [103], which is not the case. The lower concentration of CH_3OH suggests that part of the HCOOH could also be a product of the direct reduction of CO_2 on BDD. The activity of BDD for the conversion of CO_2 into HCOOH has been reported by Ikemiya et al. [64].

Fig. 2.3 shows a possible reaction path based on our experimental results and the above mentioned comparison with the literature. Thus, products such as CO, HCOOH and HCHO can be expected from the electrochemical reduction of CO_2. Nevertheless, it should be taken into consideration that a disproportionation reaction of HCHO into HCOOH and CH_3OH may occur, which can change the product concentration associated with the electrochemical reaction.

To ensure the stability of the electrode after using it with different electrolytes and pH values, SEM images of the BDD electrodes before and after electrolysis were taken. No significant differences were observed in the BDD surface morphology, as shown in Fig. 2.12 and 2.13 in the supporting information.

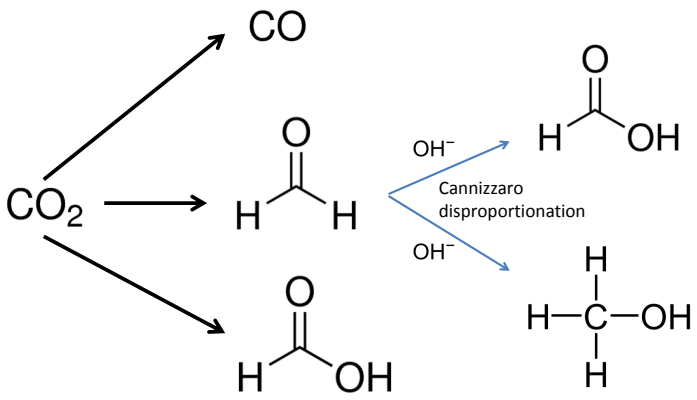

Figure 2.3: Possible reaction path for the reduction of CO_2 on BDD electrodes

2.1.3.4 Ag Electro-Deposition

Although it has been observed that the Faradaic efficiency for C_1 products can be improved by using an electrolyte such as K_2SO_4, hydrogen is still the main product of the electrolysis. One could expect that performing electrolysis at lower potentials than the HER onset potential could be a way to fully use the advantage of BDD due to its large water decomposition window. However, we could not obtain measurable products at potentials at which HER does not take place.

Our results show that BDD is not as active for CO_2 reduction as transition metals [32]. Products such as CO and HCOOH have also been reported for the electrochemical reduction of CO_2 on Ag electrodes [104] achieving FE for CO over 90 % [29]. The reaction path for the conversion of CO_2 to CO and HCOOH with both Ag [32] and BDD [64] is related to a $\cdot CO_2$ radical adsorbed on the electrode surface. However, some of the HCOOH and methanol seem to be the product of a Cannizzaro-type disproportionation as reported by Birdja and Koper [65]. Another important observation when comparing BDDs with transition metals is the working electrode potential to achieve a maximum Faradaic efficiency for CO. In Fig. 2.2 the maximal FE for CO is achieved at −2 V vs. Ag/AgCl, which is higher than a working electrode potential of −1.6 V vs. Ag/AgCl reported for Ag [29, 105]. Nevertheless, the stable performance of BDD over time, as observed in Fig. 2.16 of the supporting information, makes this kind of electrode interesting for long term experiments.

With the aim of using the advantage of BDD regarding stability while suppressing the hydrogen evolution, Ag nanoparticles were electrodeposited on BDD as described in the experimental section. Chronoamperometry was performed again in K_2SO_4 and Fig. 2.4 shows the enhancement

of the BDD activity to carbon monoxide on Ag-BDDs. As expected, the presence of Ag does not only increase the activity for the conversion of CO_2 to CO, but it also reduces the over-potential at which the highest FE for CO is obtained from −2 V to −1.8 V vs. Ag/AgCl. On the other hand, when looking at the accumulated liquid products of the potentiostatic experiments, no increase of HCOOH and CH_3OH is observed on Ag-BDD compared to BDD. Thus, our results suggest that the modification of BDD with Ag leads to the decrease of working electrode potential as well as the increase in the activity towards CO. For a better understanding and comparison of the Ag modification effect, the behavior of the current density with the applied potential is shown in Fig. 2.15 in supporting information.

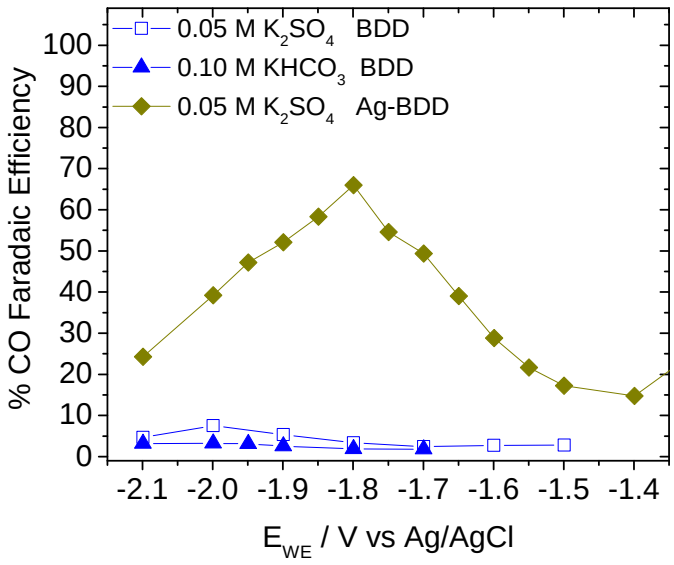

Figure 2.4: Electrochemical reduction of CO_2 on BDD electrodes in 0.1 M $KHCO_3$ (▲) / 0.05 M K_2SO_4 (□) and Ag-BDD electrodes in 0.05 M K_2SO_4 (◆).

2.1.3.5 Galvanostatic Measurements

Taking into account the fact that industrial electrochemical processes are preferably performed using galvanostatic methods [106], and that long-term stability of the catalyst is one of the characteristics necessary to scale up the CO_2RR [97], Ag-BDD electrodes were tested at a constant current density of $-10\,mA/cm^2$ for 10 hours in both K_2SO_4 and $KHCO_3$ obtaining stable FE for CO in both cases as depicted in Fig. 2.5 and Fig. 2.6 respectively. Besides that, the effect of the anionic species is observed again, obtaining higher concentrations in K_2SO_4 than in $KHCO_3$, which confirms the influence of the electrolyte buffer capacity on the liquid products, regardless of electrode modifications. For comparison, a galvanostatic experiment using a non-modified BDD electrode is also shown in Fig. 2.16 in the supporting information.

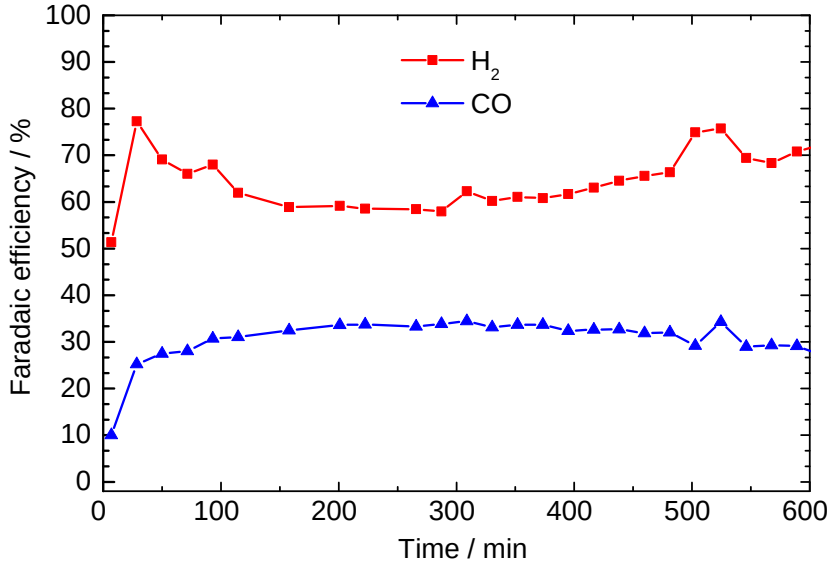

Figure 2.5: Electrochemical reduction of CO_2 on an Ag-BDD electrode in 0.05 M K_2SO_4 at $-10\,mA/cm^2$

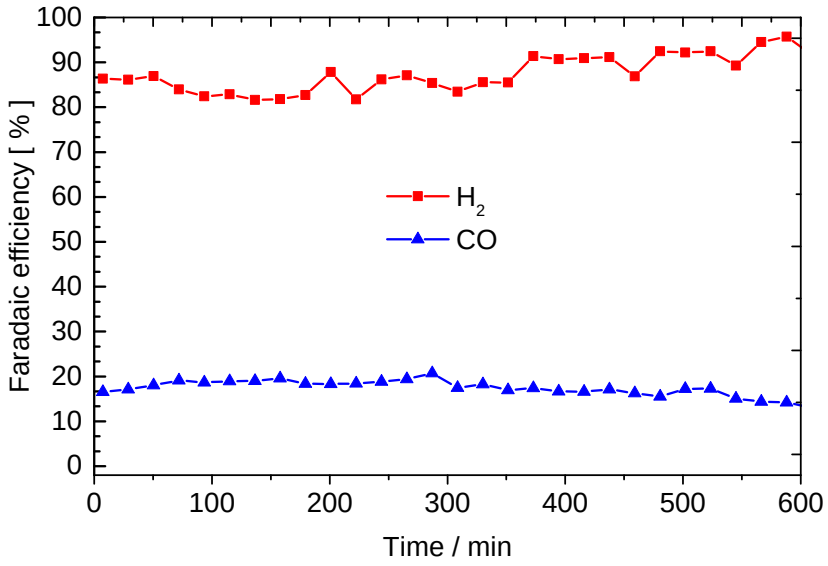

Figure 2.6: Electrochemical reduction of CO_2 on an Ag-BDD electrode in 0.1 M $KHCO_3$ at $-10\,mA/cm^2$

Long term galvanostatic measurements allow us to elucidate another difference on the mechanism for the liquid products between BDD and Ag-BDD. As mentioned above CO and HCOOH have been reported as the two products expected with Ag catalyst, where CO is the main product [104]. CO, HCOOH, HCHO and CH_3OH were found using BDD electrodes [65]. Our results suggest the existence of two possible reaction paths for HCOOH formation as depicted in Fig. 2.3. One is the direct conversion of CO_2 to HCOOH; the other is the disproportionation reaction of HCHO that generates CH_3OH and HCOOH. The increase on the HCOOH concentration in the experiments with Ag-BDD indicates that the direct path to HCOOH is

favored. However, the presence of CH_3OH with a similar concentration using BDD and Ag-BDD suggests that a Cannizzaro-type reaction takes place in both cases.

2.1.4 Conclusions

After performing electrochemical reduction of CO_2 on BDD electrodes in electrolytes with different buffer capacities such as $KHCO_3$ and K_2SO_4, it was confirmed that the BDD activity to obtain CO and HCOOH is enhanced by the electrolyte without buffer ability, in which the CO_2 reduction should occur at a local alkaline pH, suppressing the HER and promoting the formation of carbon monoxide and formic acid. However, the Faradaic efficiency of CO_2 reduction products is low due to the poor activity of BDD and an alkaline media is not enough to completely suppress the HER. It was also shown that the modification of BDD by Ag electrodeposition leads to the increase of CO without either compromising the stability of the electrode or decreasing the production of HCOOH in the liquid phase. This was confirmed by performing galvanostatic measurements at $-10\,mA/cm^2$. Thus, transition metal deposition on BDD could, for instance, be a viable alternative to deal with some of the catalyst challenges in the CO_2 electrochemical reduction, which could even be used as an electrode in photo-electrochemical processes.

Acknowledgments

The authors thank Prof. Nakata from the Tokio University of Science and Prof. Einaga from the Keio University for providing us the BDD electrodes and for the valuable discussions. Special thanks to Prof. Eisenreich from the Technical University of Munich for his support with the NMR measurements, as well as, Dr. Rucki and Dr. Scheithauer from Siemens AG for the FEG-SEM and XPS analysis. N.S. Romero would like to express her particular gratitude to the TUM Graduate School for financial support.

2.1.5 Supporting Information

2.1.5.1 Experimental

Materials and Methods For all the experiments, a two compartment H-type cell made of glass was employed, using (5 ml) electrolyte volume in each compartment. Cathode and anode were separated by a Nafion® 117 membrane (DuPont). The electrolysis was carried out either in 0.1 M $KHCO_3$ or 0.05 M K_2SO_4 as catholyte and 1 M KOH as anolyte, prepared from high purity reagents (Sigma Aldrich) and deionized water. Boron Doped Diamond (BDD) with p-type surface and a boron content of 10 000 ppm was used as a working electrode. BDD was deposited on Si(100) wafers using Microwave Plasma Assisted Chemical Vapor Deposition (MWP-CVD) [64]. The wafer was cut with a laser technique to obtain rectangular pieces (18 mm $\times$ 7 mm). A Pt wire (Goodfellow) and an Ag/AgCl electrode (C3 Prozess- und Analysentechnik GmbH) were used as a counter electrode and reference electrode, respectively.

A Bio-logic VSP 150 potentiostat (Seyssinet-Pariset, France), was controlled by the EC-Lab® software, so that different techniques were recorded without returning to an open circuit for each electrolysis experiment. Electrochemical reduction of CO_2 was performed either using chronoamperometry, in which the electrolysis potential is applied for a certain amount of time, or chronopotentiometry, where the current density is constant.

At the beginning of each experiment 10 sccm N_2 (Linde 5.0) was supplied to the cathode for 1 hour and a linear sweep voltammetry was carried out. High Purity CO_2 (Linde 5.0) was then fed for 1 hour and a second linear sweep voltammetry was performed, followed by either chronoamperometry or chronopotentiometry. CO_2 was supplied at a constant flow of 10 sccm into the electrolyte during the electrochemical reduction, so that, CO_2 bubbles were constantly flowing through the electrolyte from the bottom of the cell to the gas outlet. The pressure of CO_2 inside the cell was maintained at atmospheric pressure with 0.1 bar overpressure to ensure the transport of the gas to the gas chromatograph.

Product Quantification For the quantification of the gas products, a Gas Chromatograph 7890B Agilent (Santa Clara, USA) was used with Helium as carrier gas in a configuration optimized for this application. An aliquot of the gas product (1 ml) was automatically injected every 20 minutes from the cell to the gas chromatograph during the electrolysis. An example of a gas chromatogram is shown in Fig. 2.10. For the liquid phase an aliquot of the catholyte was taken right after the experiment for subsequent analysis. The liquid products were analyzed and quantified using ^1H Nuclear Magnetic Resonance NMR spectroscopy using a 500 MHz Bruker (Bruker BioSpin, Karlsruhe, Germany) following the method described by Kuhl et al. [35] The

water peak was suppressed by a pre-saturation sequence. Electrolyte containing CO_2 reduction products (300 ml) was mixed with sodium fumarate (50 ml), which was used as internal standard in D_2O (250 ml) for the quantification. In order to make sure that the detected products were the result of the electrolysis and not impurities from another source, the electrolyte was analyzed before and after the electrolysis. An example of an NMR spectrum is shown in Fig. 2.11.

Ag nanoparticles were electrodeposited on BDD in a two-electrode system at −10 V with respect to a Pt counter electrode in aqueous 0.1 M $AgNO_3$ for 40 seconds. The distance between the electrodes was approximately 10 cm in an H-cell. To confirm the presence of Ag on the electrodes, X-ray Photoelectron Spectroscopy (XPS) was performed with a Quantum 2000 X-ray microprobe. The results are depicted in Fig. 2.12 and 2.13.

2.1.5.2 Boron Doped Diamond Electrode - Characterization

Raman spectroscopy was performed using WITec Raman microscope (Ulm, Germany) with a green laser (532 nm). The analysis of the spectra is based on Ivandini's and Einaga's study [107]. The presence of Boron is confirmed by the bands at approx. 500 and 1200 cm^{-1}. Sp^3 hybridization is confirmed by the peak at 1331 cm^{-1}. The absence of peaks between 1300 and 1500 cm^{-1} suggests that there is no sp^2 hybridization at the BDD surface.

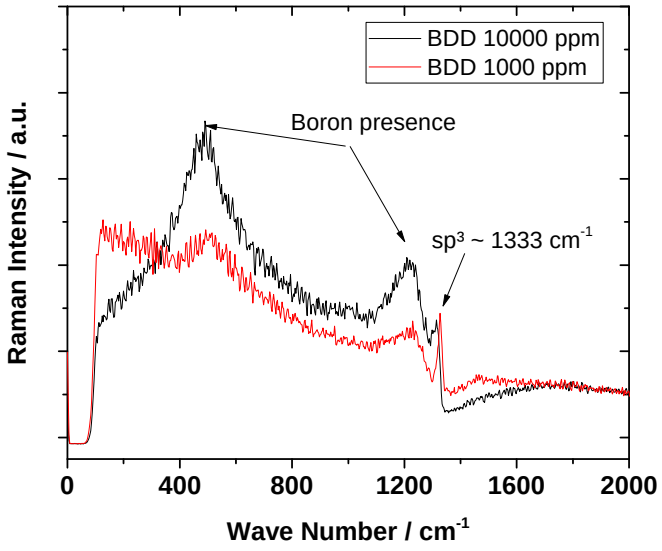

Figure 2.7: Raman spectra of a 1000 ppm BDD electrode and a 10 000 ppm BDD electrode

2.1.5.3 Field-Emission Gun - Scanning Electron Microscope (FEG-SEM) images of BDD electrodes

Images of the BDD electrodes before and after electrolysis were taken using a FEI STRATA 400 Dual Beam ^{TM} system.

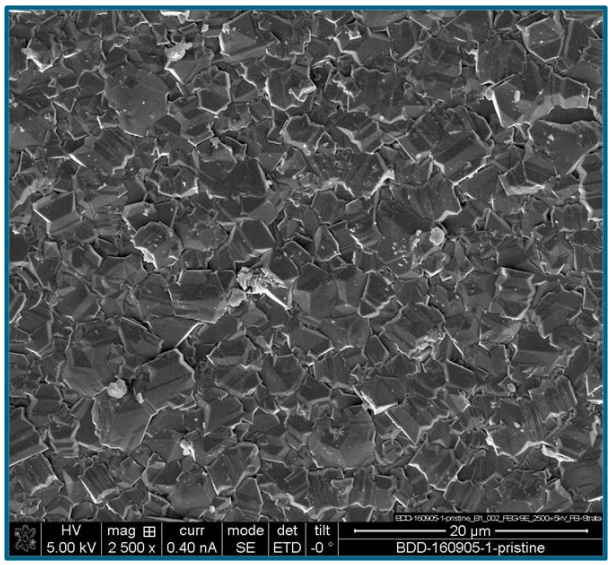

Figure 2.8: FEG-SEM results for BDD electrode before electrolysis

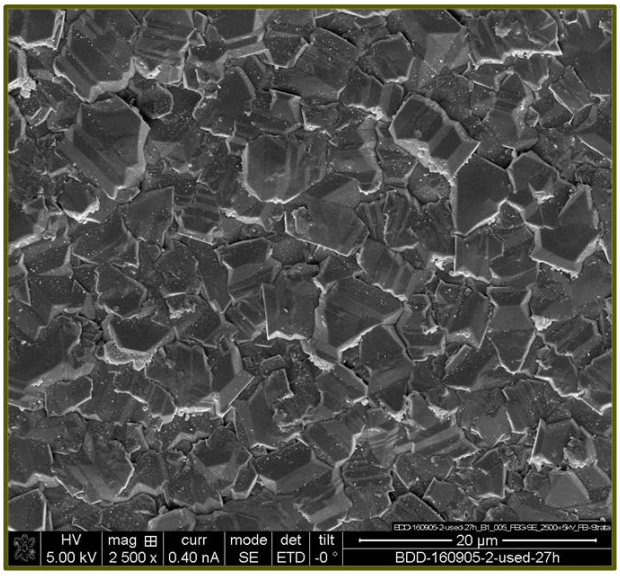

Figure 2.9: FEG-SEM results for BDD electrode after electrolysis

2.1.5.4 Gas Products Analysis: Gas Chromatography

A Gas Chromatograph 7980B Agilent with three columns (Porapak QS 80-100 mesh, 60/80 Molsieve 4 and 80/100 Hayesep Q) and Helium as carrier gas was used for the quantification of the gas products.

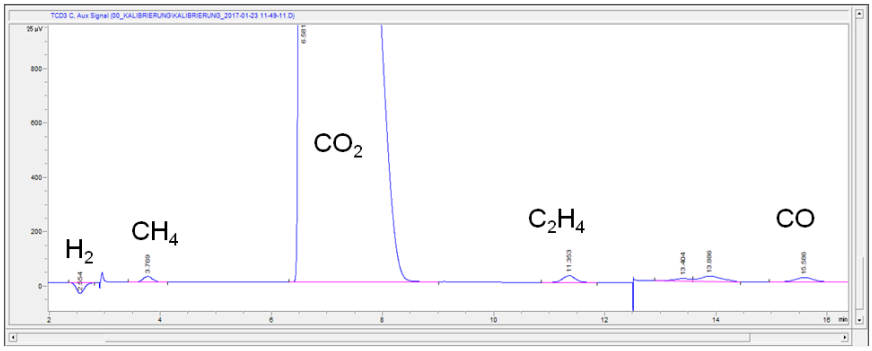

Figure 2.10: Gas chromatogram of a calibration gas for the possible gas products of the CO_2 electrochemical reduction

2.1.5.5 Liquid Products Analysis: Nuclear Magnetic Resonance (NMR)

Two products were detected in the liquid phase namely $HCOO^-$ (8.4 ppm) and CH_3OH (3.35 ppm). Potassium fumarate (6.49 ppm) was used as internal standard with water suppression (4.7 ppm).

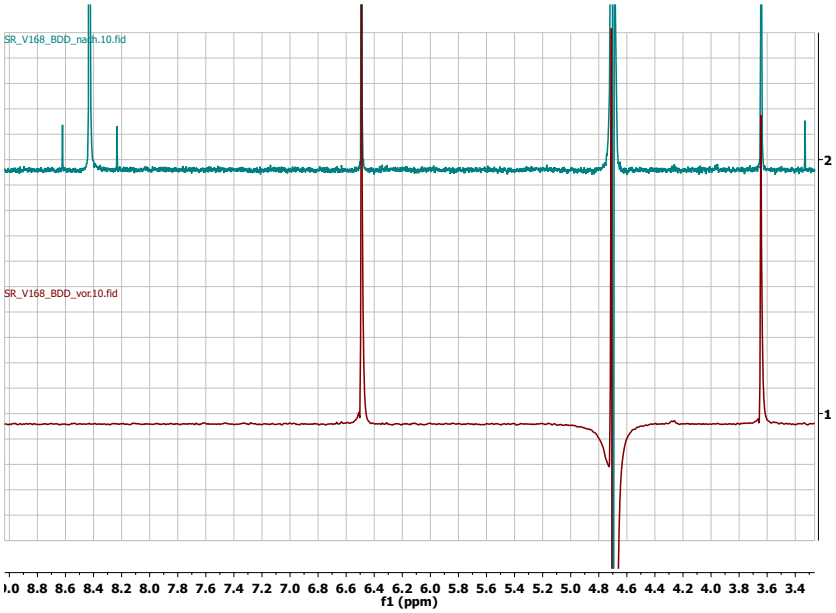

Figure 2.11: ^1H NMR spectra before (bottom) and after (top) CO_2 electrochemical reduction on BDD electrodes

2.1.5.6 Characterization of BDD before and after Ag-deposition

The XPS analysis of BDD electrodes was performed with a Quantum 2000 X-ray microprobe.

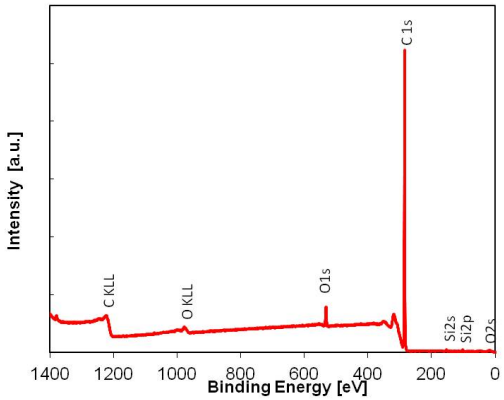

Figure 2.12: X-ray Photoelectron Spectroscopy (XPS) elemental analysis results for BDD electrode before electrolysis

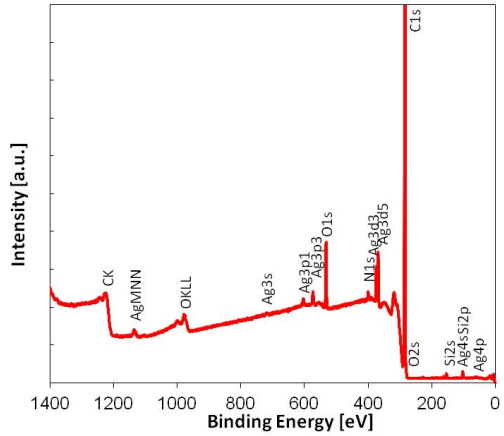

Figure 2.13: X-ray Photoelectron Spectroscopy (XPS) elemental analysis results for Ag-doped-BDD before electrolysis

2.1.5.7 ^{1}H NMR results for the disproportionation reaction of HCHO

Fig. 2.14 shows $HCOO^-$ (8.4 ppm) as result of the disproportionation reaction of HCHO (3.3 ppm/4.9 ppm) in KOH and CH_3OH (3.35 ppm). Potassium fumarate (6.49 ppm) was used as internal standard.

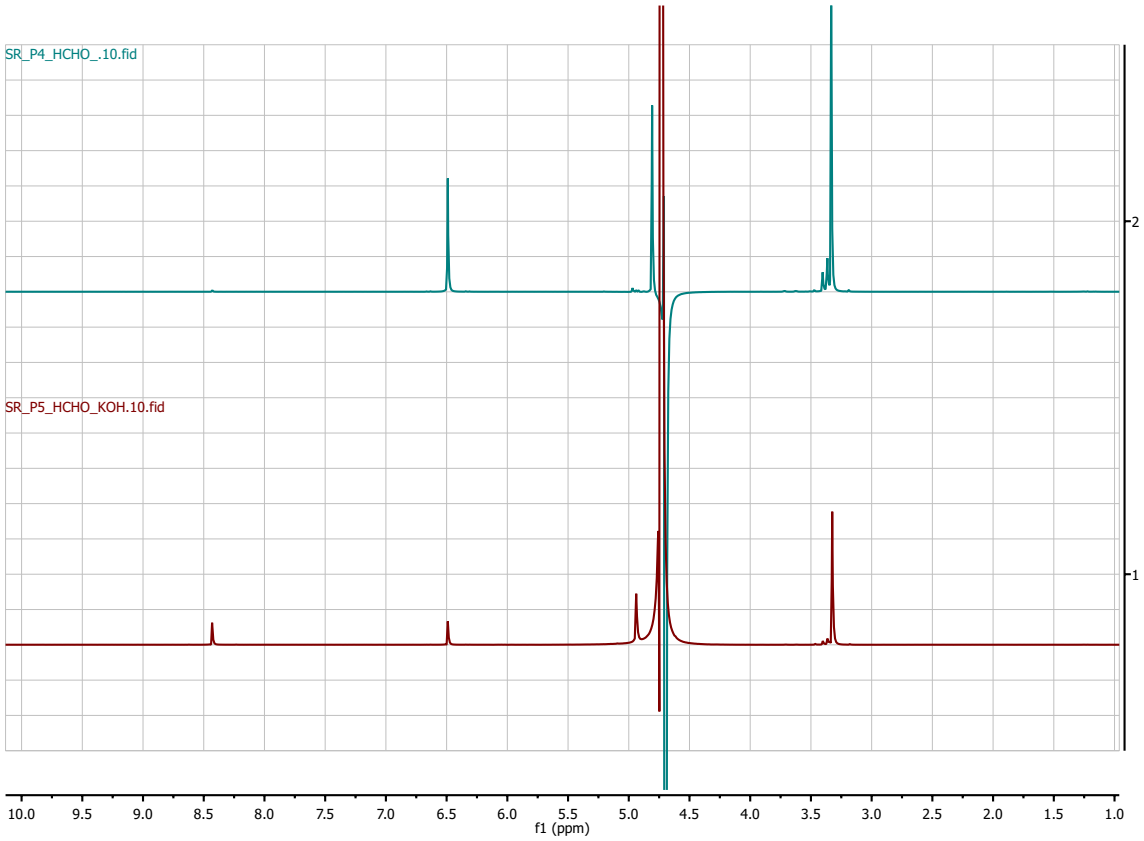

Figure 2.14: NMR spectra for HCHO in $KHCO_3$ (top) and in KOH (bottom)

2.1.5.8 Current density vs. working electrode potential

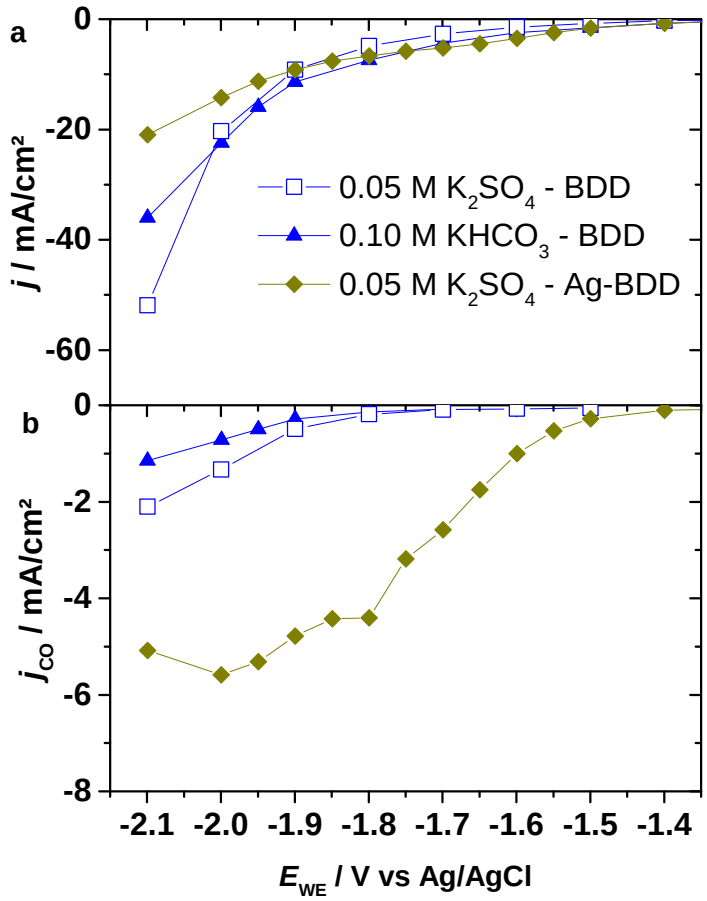

Figure 2.15: (a) Total current density vs. applied working electrode potential (b) current density for the conversion of CO on BDD electrodes in 0.1 M $KHCO_3$ (▲) / 0.05 M K_2SO_4 (□) and Ag-BDD electrodes in 0.05 M K_2SO_4 (◆).

2.1.5.9 Galvanostatic experiment on BDD electrode without Ag deposition

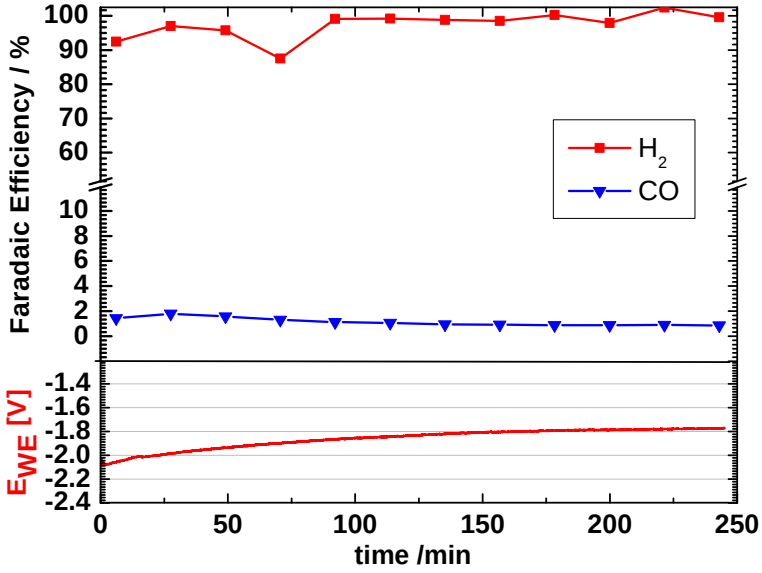

Figure 2.16: Electrochemical reduction of CO_2 on a BDD electrode in 0.05 M K_2SO_4 at $-10\,mA/cm^2$

2.2 Electrochemical reduction of CO_2 on nanocrystalline BDD electrodes

Boron-Doped Diamond (BDD) electrodes have been proven to be active for the electrochemical reduction of CO_2. Although, it is know that the feed gas and operation parameters set for chemical vapor deposition (CVD) play a decisive role in the properties of BDD electrodes for general electrochemical applications; scarcely information has been reported in the literature regarding the properties of the BDD electrodes used specifically for the electrochemical reduction of CO_2 and how these properties affect their performance as cathodes. Thus, further investigation about the effect of variable parameters by the growth of the electrode is required. Accordingly, nanocrystalline (NC) BDD electrodes with different growth conditions, were characterized by a master student as a part of her thesis [108], within the frame of the here presented doctoral thesis. The aim of this study was to address the influence of BDD preparation parameters such as boron- and CH_4-content on electrochemical reduction of CO_2. The electrodes were characterized before electrolysis by scanning electron microscopy (SEM) and Raman spectroscopy in order to determine the qualitative differences on the surface regarding grain size as well as boron, diamond (sp^3), and non-diamond (sp^2) incorporation. Linear-voltammetry, chronoamperometry, and chronopotentiometry were the techniques used for the electrochemical characterization. The main products gained from the electrochemical reduction of CO_2 with NC BDD electrodes were CO and HCOOH. Regarding the boron-content (in the range studied 1-2 %), no significant effect was observed besides the expected increase in conductivity with higher boron concentration. In contrast, it was found that a low concentration of methane during the preparation of the electrode leads to a higher HCOOH Faradaic efficiency.

2.2.1 Growth conditions for nanocrystalline BDD electrodes

The electrodes were provided by the Institute for Material Research at the Hasselt University in Belgium. The nanocrystalline BDD layer was deposited on 20 mm-20 mm p-type (100) Si-substrates. All the samples were grown by microwave plasma enhanced chemical vapor deposition (MWP-CVD) in a A 2.45 GHz ASTex 6500 series reactor. The reactor was fed with a plasma feedgas consisting of H_2, Trimethylborane (TMB) as boron source and CH_4 as carbon source with a total flow rate of 500 sccm. The microwave power corresponds to 3600 W, the pressure was kept constant at 45 torr (equivalent to approximately 0.06 bar). The thickness was determined *in-situ* from the interference fringes of the reflection spectrum of a 473 nm laser, and the deposition run was stopped once the desired thickness of 150 nm was reached. The coated wafers were cut with the laser cutter to obtain 20 mm x 7 mm electrodes. The methane concentration in the feed gas was varied in the range of 0.5-1.5 % and TMB/CH_4 ratios of 10.000 ppm

(1 %) to 20.000 ppm (2 %) with 1.0 % CH_4 concentration. The sample morphologies of the films were investigated by electron microscopy using a FEI Quanta 200F field emission gun scanning electron microscope (FEG-SEM). The resulting grown morphologies for each sample are summarized in Table 2.2.

Table 2.2: SEM-micrographs of nanocrystalline BDD on Si-wafers. CH_4 concentration varying between 0.5-1.5 % with a constant boron content of 10.000 ppm. B/C ratios varying from 10.000 ppm to 20.000 ppm

Sample	10000x SEM	100000x SEM
0.50% 10,000 ppm	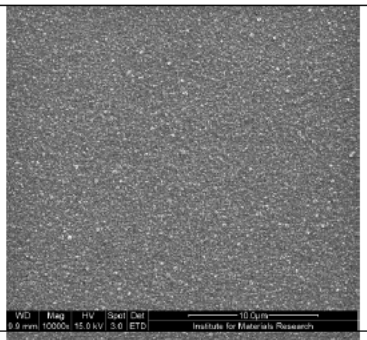	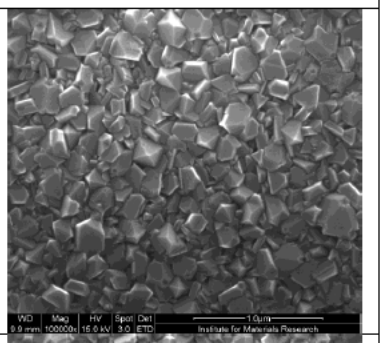
1.0% 10,000 ppm		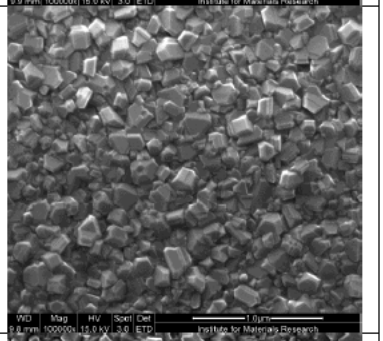
1.5% 10,000 ppm	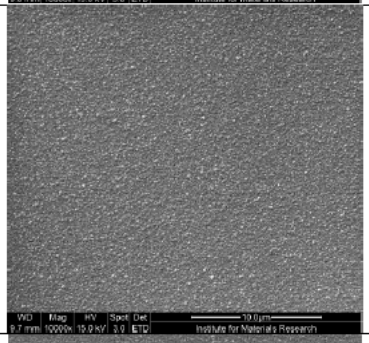	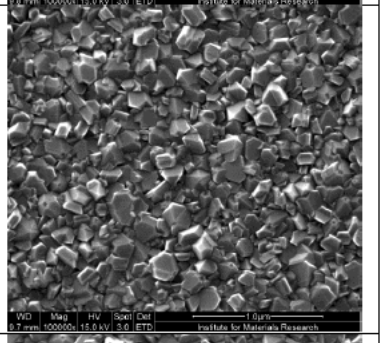
1.0% 20,000 ppm		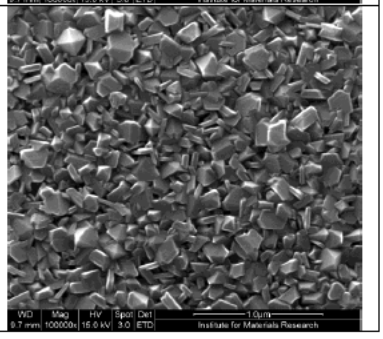

2.2.2 Effect of methane concentration on boron-doped diamond electrodes

As mentioned above the concentration of the carbon source, in this case methane (CH_4), influences material-specific parameters such as grain size and non-diamond carbon (NDC) incorporation, which can be determined by the presence of sp^2 hybridized atomic orbitals. The methane concentration was varied in the range 0.5-1.5 % at a constant B/C ratio of 10.000 ppm. The resulting electrodes named 1.0 % B/C_0.5 % CH_4, 1.0 % B/C_1.0 % CH_4, 1.0 % B/C_-1.5 % CH_4 were characterized in terms of their structure as well as their electrochemical properties. Fig. 2.2 depicts homogeneous BDD layers with angular shaped grains and flat edges. It can be observed that higher CH_4 concentration leads to a smaller grain size and more grain boundaries, hence a larger resistivity is expected, as has been reported in the literature for nanocrystalline and microcrystalline BDD [109]. Additionally, the CH_4 concentration of the feed gas can also affect the sp^2/sp^3 hybridization and the boron incorporation, which can be determined using Raman spectroscopy.

Fig. 2.17 presents Raman spectra for the three samples examined. A sharp peak at 520 cm^{-1} and a signal at 950 cm^{-1} are observed for all the samples. These two signals correspond to Si of the first and second order, which were not observed in section 2.1.5.2 for microcrystalline (MC) electrodes with a thicker BDD film. In this case, the thin coating layer of the nanocrystalline (NC) BDD makes silicon visible in the spectrum. The presence of boron is confirmed by the bands at $\sim$500 cm^{-1} and $\sim$1200 cm^{-1}, which are attribute to to the B-B and B-C vibration, respectively. Pure diamond contains only sp^3 carbon bonds, which in Raman spectra results in a single peak occurring at 1332 cm^{-1}. As the boron incorporation increases the diamond (sp^3) peak shifts to slightly low wavelengths, moves from being symmetrical to deforming asymmetrically, and its intensity decreases [60]. From the spectra obtained and based on the band at $\sim$1200 cm^{-1}, it can be interpreted that even having a constant boron source a decreasing methane concentration leads to an increasing boron incorporation, which makes the electrode more conductive. The interpretation of the Raman spectra for nanocrystalline BDD films is more complicated than for microcrytalline BDD films as selection rules break down [60]. Non-diamond carbon incorporation (sp^2) is thought to occur predominantly at grain boundaries. Thus, sp^2 can be electrochemically significant in nanocrystalline BDD films given that the grain boundary density is notably higher than in MC. In the three NC BDD samples studied, sp^2 hybridization is confirmed by the signal at 1575 cm^{-1}. However, in Fig. 2.17 the intensity of the sp^2 peak is larger for the sample prepared with the lowest methane concentration than for the other two samples. Considering the grain boundary density and that NDC incorporation should occur predominantly at grain boundaries, it would be expected to have a larger sp^2 presence in the sample 1.0 % B/C_1.5 % CH_4. Here it should be taken into account that NDC bonds are more polarisable than diamond carbon bonds and that the sp^3 peak intensity decreases with

increasing boron doping levels [60]. Thus, the intensity of the spectra in this case does not totally represent the actual sp^2/sp^3 ratio in the BDD electrode.

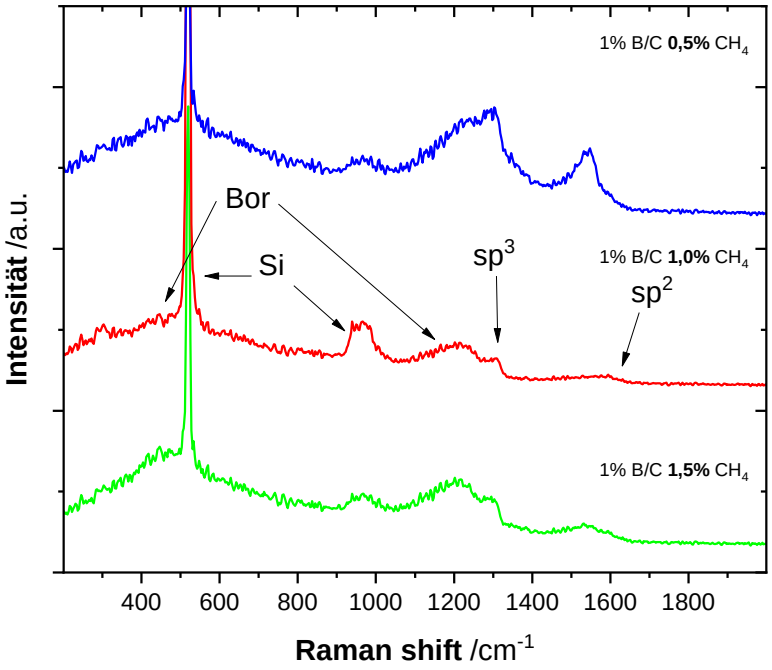

Figure 2.17: Raman spectra for the samples

The electrochemical behavior of the BDD electrodes was characterized following the experimental procedure described in section 2.1.5.1. Experiments were performed in a two compartment H-type cell with 0.1 M $KHCO_3$ as catholyte and 1 M KOH as anolyte. Potential variation series were conducted and repeated twice with the same electrode from −1.4 V to −2.1 V vs. Ag/AgCl. CO and H_2 were the two components found in the gas outlet, while in the liquid phase HCOOH was detected. The Faradaic efficiency for CO as main gas product, the total current density and the partial current density as function of the applied potential are shown in Fig. 2.18. The highest Faradaic efficiencies for CO were obtained with the sample prepared with the highest CH_4 concentration (1.0 % B/C_1.5 % CH_4). The Faradaic efficiency decreased with more negative potentials. Furthermore, with the same sample very low current densities were achieved. In contrast, the sample prepared with the lowest CH_4 concentration (1.0 % B/C_-0.5 % CH_4) reaches the highest current densities with increasing Faradaic efficiency for CO at more negative potentials. Considering that the samples will the lowest CH_4 content is the more conductive, as mentioned above, the better performance of this sample can be attribute to the conductivity. Interestingly, this is also the sample with the larger grain size, which will explain the lower Faradaic efficiency compared to 1.0 % B/C_1.5 % CH_4 that presented the lowest grain size. This indicates, that a lower grain size, which means a larger grain boundary density might

make the electrode more active for the reduction of CO_2 to CO since more CO_2 molecules can be adsorbed, assuming that CO_2 is adsorbed at the grain boundaries. Nevertheless, taking into account that electrons are also needed for the reaction, a lower conductivity decreases the ability of the electrode to reduce CO_2. This might explain the CO Faradaic efficiency decrease observed at more negative potentials for the sample 1.0 % B/C_1.5 % CH_4, which was the less conductive. This suggests that a compromise between conductivity and grain size needs to be reached for the preparation of BDD as cathodes in the electrochemical reduction of CO_2.

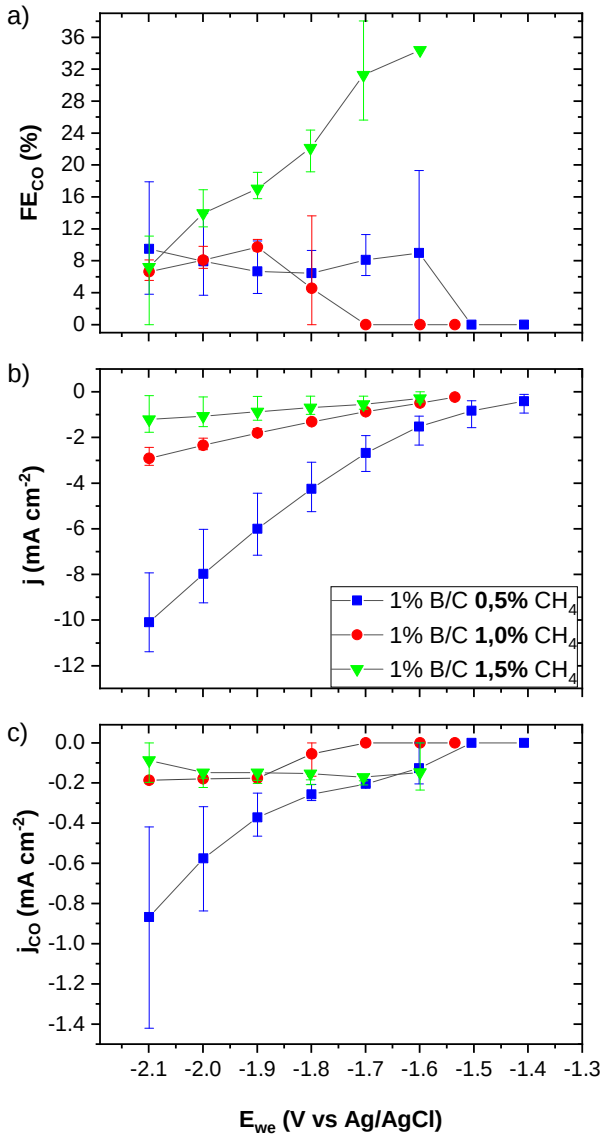

Figure 2.18: Potentiostatic electrochemical reduction of CO_2 with nanocrystalline BDD grown with different CH_4 concentrations. a) Faradaic efficiency for CO, b) total current density achieved, c) CO partial current density as function of the applied potential.

Galvanostatic experiments were performed at a current density of –2 mA/cm^2 over 3.5 h. While the gas products were monitored during electrolysis, the liquid products were collected at the

end of the experiment and analyzed by NMR as described in section 2.1.5.1. A stable performance of the electrodes regarding the production of CO is demonstrated in Fig. 2.19. As expected, when setting the same current density for all the samples, a more negative working electrode potential is observed for the less conductive sample (1.0 % B/C_1.5 % CH_4). Nevertheless, similar Faradaic efficiencies for CO (∼10 %) are obtained with all the samples. In contrast, a clear difference is observed in the liquid phase, in which a higher Faradaic efficiency for HCOOH was achieved with the sample that was prepared with lower CH_4 concentration (1.0 % B/C_0.5 % CH_4). In general, it was observed for nanocrystalline electrodes that the carbon source content in the gas supplied to the CVD reactor for the growth of BDD films plays a role in the performance of the electrode. The results demonstrate that higher Faradaic efficiencies for CO and HCOOH can be achieved with electrodes prepared with a low CH_4 concentration (0.5 %).

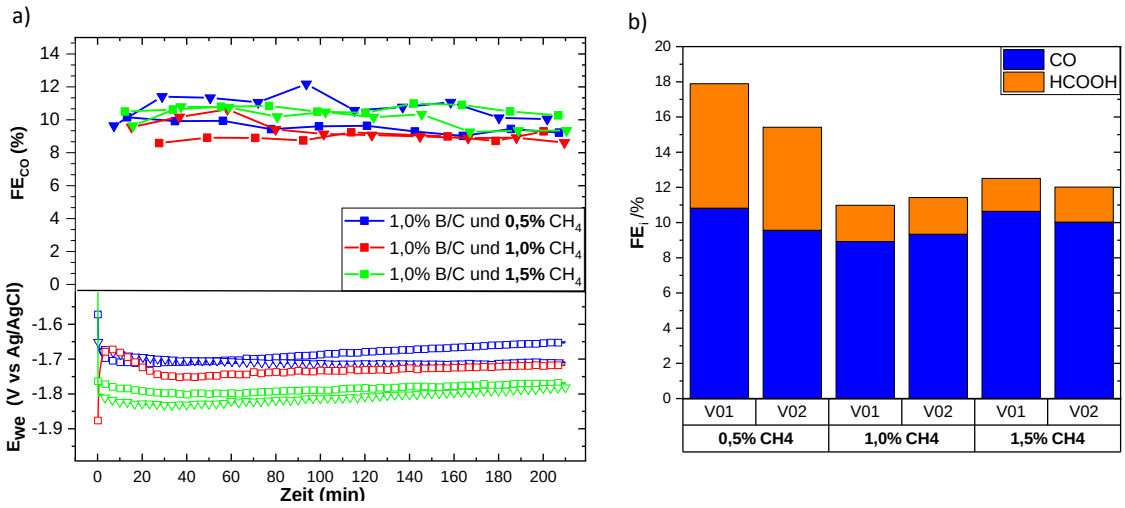

Figure 2.19: Galvanostatic electrochemical reduction of CO_2 with nanocrystalline BDD grown with different CH_4 concentrations. a) Faradaic efficiency for CO and corresponding working electrode potential for CO_2 at -2 mA/cm^2. b) Cumulative Faradaic efficiency for the liquid (HCOOH) and the gas phase (CO) after 210 min electrolysis.

2.2.3 Effect of B/C content on boron-doped diamond electrodes

Aiming to evaluate the influence of the B/C content use for the growth of BDD films, the performance of two electrodes was investigated. One electrode was prepared with a TMB/CH_4 ratio of 10.000 ppm (1 %), the other one with a B/C ratio of 20.000 ppm (2 %), both with 1.0 % CH_4 concentration. As depicted in the SEM images given in Table 2.2 the sample prepared with a larger B/C ratio (2.0 % B/C_1.0 % CH_4) shows more edges and some grains with smaller size

than the sample with lower B/C ratio (1.0 % B/C_1.0 % CH_4). In Fig. 2.20 can be observed that, as mentioned above the, silicon peak overlap the boron band at $-500\,cm^{-1}$. However, the boron band at $-1220\,cm^{-1}$ is visible in both cases. The sp^3 ($-1332\,cm^{-1}$) and sp^2 ($-1575\,cm^{-1}$) peaks for the sample 2.0 % B/C_1.0 % CH_4 were shifted to lower wavelengths and deformed asymmetrically. As expected the sp^3 peak lost intensity with a larger B/C content while the signal for sp^2 became much more intense. This behavior was expected for samples with and increased boron incorporation and is in accordance with the literature [60]. With a raise of boron incorporation the the disordered structure of amorphous carbon increases, shifting the signals of the spectrum and making them asymmetric.

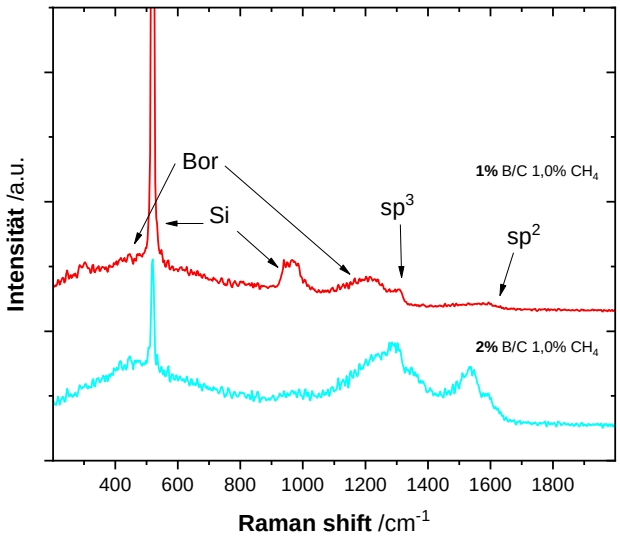

Figure 2.20: Raman spectra for the samples

The electrochemical performance of the two samples with different B/C content was also tested conducting potentiostatic and galvanostatic electrochemical reduction of CO_2 in the same potential range (from $-1.4\,V$ to $-2.1\,V$ vs. Ag/AgCl) and at the same current density ($-2\,mA/cm^2$) as described in section 2.2.2. The results of the potential variation are depicted in Fig. 2.21. A higher Faradaic efficiency for CO was achieved with the sample with lower B/C concentration ratio (1.0 % B/C_1.0 % CH_4). A maximum efficiency is observed at a working electrode potential of $-1.9\,V$ vs. Ag/AgCl. While a high boron incorporation leads to higher conductivity and thus higher total current densities are achieved; a less conductive electrode leads to higher Faradaic efficiency.

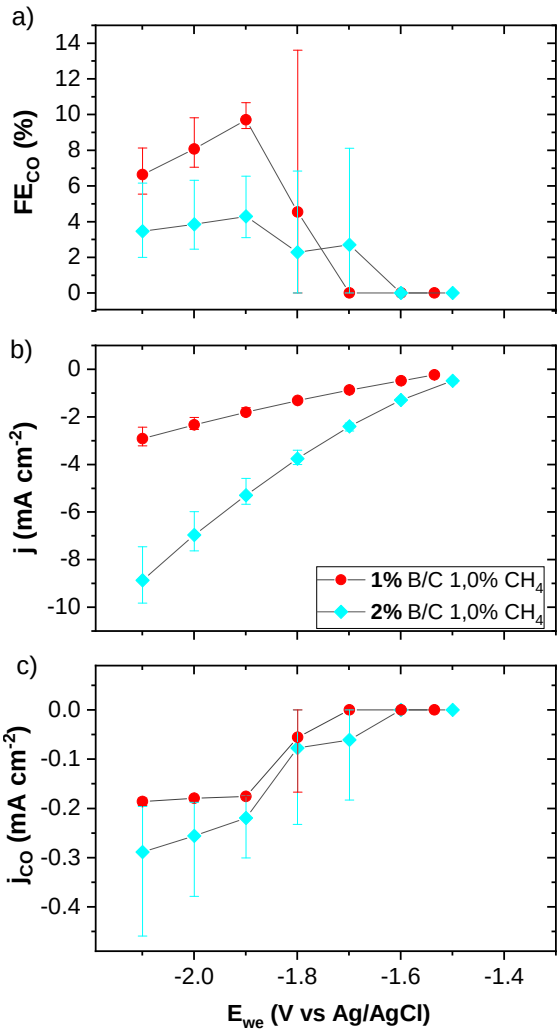

Figure 2.21: Potentiostatic electrochemical reduction of CO_2 with nanocrystalline BDD grown with different B/C concentration ratios. a) Faradaic efficiency for CO, b) total current density achieved, c) CO partial current density as function of the applied potential.

In the results of the galvanostatic experiments summarized in Fig. 2.22 no significant difference regarding the performance of the electrodes was evident. In general, ∼9 % CO and ∼3 % HCOOH Faradaic efficiencies were achieved with a stable performance in all the cases. Since nanocrystalline boron doped diamond electrodes have scarcely been explored, there is no reference in the literature for a direct comparison. However, Xu et al. [61] have recently studied the effect of doping level on MC BDD electrodes (grain sizes are in the range of 1 µm to 10 µm) for the electrochemical reduction of CO_2. They tested samples with varying boron content from 0.01 to 2.0 %. The highest Faradaic efficiency for HCOOH was found using the samples with a boron content of 0.1 %, while the samples with 2 % boron content showed the highest Faradaic efficiency for CO and a lower Faradaic efficiency for HCOOH compared to the samples with

boron content 0.1 to 1.0 %. In that case, high boron content BDD is prejudicial for production of formic acid. On the contrast, it is preferred for producing CO [61]. While the Raman analysis, of the two NC BDD samples tested in this work, confirms a larger incorporation of boron for the electrode with a higher B/C ratio; no significant influence on the activity of the electrode was evident after galvanostatic electrochemical characterization. Nevertheless, both samples are more selective for CO than HCOOH, contrary to the MC BDD electrodes tested by Xu et al. On one side the selectivity differences could be attribute to the grain size. On the other side it should be considered that the carbon concentration used for the MC BDD might differ from the carbon concentration of the NC BDD samples and that the electrolysis was performed in different electrolytes and cells. Since no samples with a B/C content under 1 % were available for the investigation, the trends observed are not conclusive. Thus, it would be worthwhile to further investigate the effect of boron content in NC BDD electrodes in a wider range and compare it with MC BDD prepared with the same carbon source concentration.

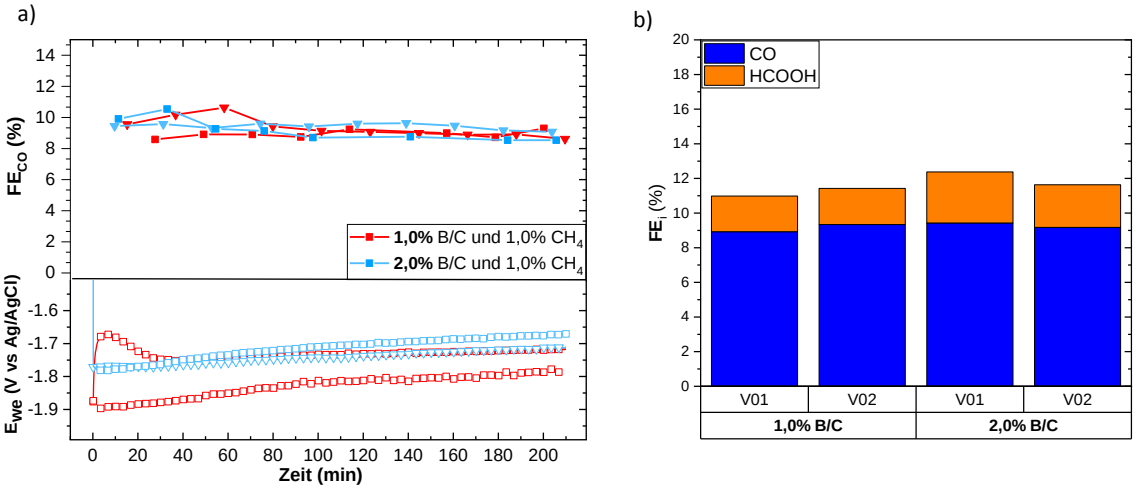

Figure 2.22: galvanostatic electrochemical reduction of CO_2 with nanocrystalline BDD grown with different B/C concentration ratios. a) Faradaic efficiency for CO and corresponding working electrode potential for CO_2 at -2 mA/cm^2. b) Cumulative Faradaic efficiency for the liquid (HCOOH) and the gas phase (CO) after 210 min electrolysis.

In the first scientific reports regarding electrochemical reduction of CO_2 on BDD no much information was given with respect to the properties of the BDD used. The first efforts focused mainly on the products that could be obtained and the electrolysis conditions that affect the selectivity. After performing electrochemical reduction of CO_2 with and NC BDD as well as with MC BDD electrodes (cf. section 2.1) and after comparison with the literature, it became evident that the performance of the electrode depends not only on the content of the feed gas used for BDD growth but also on the conditions such as time, temperature and pressure that

determine the type of crystal NC or MC. This study made evident that the specific feed gas content that leads to a more active MC BDD electrode might have a different effect on a NC BDD film. While the NC BDD films tested here were more active to CO, the MC BDD electrodes reported in the literature were more selective for HCOOH [61]. This can be attribute to the incorporation of non diamond carbon (sp^2), that is thought to occur predominantly at grain boundaries. Even when using the same B/C ratio, the sp^2 incorporation in a MC BDD film was not observable since the grain boundary density is significantly lower than in a NC BDD film, were sp^2 hybridization was confirmed (cf. Fig. 2.20). Additionally, comparing the results from section 2.1 with the present results for the sample with a boron content of 1.0 %, it is also evident that a higher efficiency for CO at the same potentials is achieved with NC BDD (cf. Fig. 2.21) than with MC BDD (cf. Fig. 2.2) using the same electrolyte in the same cell.

2.2.4 Conclusion

The aim of this investigation was to obtain some insights regarding the effect of BDD growth parameters on the electrochemical reduction of CO_2. On one hand, the carbon source, i.e. the methane concentration, was varied from 0.5 % to 1.5 % CH_4 maintaining the B/C content constant at 1.0 % B/C; on the other hand, the boron content was modified from 1.0 % to 2.0 % B/C with a constant methane concentration of 1.0 % CH_4. The results demonstrate that carbon source concentration (methane), as a variable parameter in the growth of NC BDD films, plays an important role in the ability of the electrode to electrochemically reduce CO_2. Higher Faradaic efficiencies for CO and HCOOH were achieved with the sample prepared with the lowest methane concentration. Besides the methane concentration, the B/C concentration ratio was also investigated by characterizing two samples with 1.0 % and 2.0 % B/C content. Although no significant difference was observed in the performance of these two samples, further investigation is necessary to understand the role of the boron concentration on NC BDD films at B/C concentration ratios lower than 1.0 %. In addition, it was found that NC BDD electrodes are more selective towards CO than MC BDD electrodes with the same boron content. In general, BDD electrodes showed stability but low activity for $ERCO_2$. However, it would be worthwhile to investigate NC and MC BDD samples prepared in the same reactor with similar conditions in order to provide more conclusive trends.

2.3 Transition metal electrocatalysts for CO and CO_2 electroreduction

The activity of transition metals for the reduction of CO_2 have been extensively studied [33, 35, 44]. The majority of the studies indicate that product yield and composition depend on the binding energy of CO as mentioned in section 1.2.1.1. However, only few experimental studies have specifically investigated the electrochemical reduction of CO on transition metals. In this work Ni, Co, Fe, and Cu were investigated as electrocatalyst using either CO_2 or CO as reactant. The electrochemical reduction was carried out using a glass H-Type cell as described in section 1.2.3.1. A volume of 4.5 ml electrolyte was used for each compartment with 0.1 M $KHCO_3$ (Sigma Aldrich, purity 99.98 %) as catholyte and 1 M KOH (Sigma Aldrich, purity 99.98 %) as anolyte. Metal foils, Fe, Co, Ni, Cu (GoodFellow, purity 99.99 %, thickness 0.5 mm) were mechanically polished with sand paper (3M, P1200), ultrasonicated and rinsed with deionized water prior to electrolysis. Each foil was attached to a Pt or Cu wire enabling electrical contact with the potentiostat. This connection was isolated using a teflon tube and teflon tape. A Pt wire (Goodfellow) and an Ag/AgCl electrode (C3 Prozess- und Analysentechnik GmbH) were used as a counter electrode and reference electrode, respectively. 10 sccm CO_2 or CO were supplied to the cathode compartment one hour before the experiment to assure saturation of the reactant in the electrolyte. During electrolysis the same volumetric flow was constantly supplied. Potentiostatic and galvanostatic experiments were performed over 60 or 90 min. Gas products were analyzed during electrolysis by GC, while liquid products were collected at the end of the experiment and analyzed by NMR as described in section 2.1.5.1.

2.3.1 Electrochemical reduction of CO_2 on Fe, Co, Ni, Cu

Table 2.3 summarizes the results of the $ERCO_2$ performed with Cu, Ni, Fe, and Co in comparison with the results reported by Hori et al. [33] and Kuhl et al. [45]. Average current densities (j), working electrode potentials (E_{WE}), and Faradaic efficiencies (FE) are given. It is important to mention that neither Hori et al. nor Kuhl et al. included Co in their investigations. In general, the products found and the FE achieved are comparable with the results reported in the literature for Ni, Fe and Cu. It can be observed that HCOOH is found as a product using any metal but with a higher FE when using Cu. Furthermore, CH_4 and MeOH were formed using Ni and Cu, while ethylene, ethanol, acetate, and n-propanol were only produced, when using Cu, as also reported by Kuhl et al. [45]. In contrast, with Fe and Co mainly H_2 was obtained. The literature attribute the low activity of Fe and Ni to the binding strength of CO. Calculations using density functional theory (DFT) predict a CO adsorption energy for Cu of −0.75 eV, while for Ni −1.95 eV have been reported [110]. Considering that the CO adsorption energy calculated

Table 2.3: Electrochemical reduction of CO_2 on transition metals compared to data from Hori et al. [33] and Kuhl et al. [45].

		E_{WE} V Ag/AgCl	j mA/cm^2	Faradaic Efficiency (%) CO	CH_4	C_2H_4	MeOH	EtOH	Acetate	PrOH	HCOOH	H_2	Total
Cu	This work	-1.60	6.04	2.26	19.96	12.54	0.056	5.55	4.32	5.14	7.11	20.85	77.79 [a]
	Hori	-1.64	5.00	1.30	33.30	25.50		5.70			9.40	20.50	95.70
	Kuhl	-1.65	5.90	1.10	24.40	26.00	0.020	9.70			2.00	22.60	85.82 [b]
Ni	This work	-1.55	3.57		2.26		0.252				0.36	93.00	95.86
	Hori	-1.68	5		1.80	0.10					1.40	88.90	92.20
	Kuhl	-1.60	5		0.50	0.05	2.300				0.06	106.00	108.91
Fe	This work	-1.08	3.57								0.07	87.76	87.83
	Hori	-1.11	5									94.8	94.80
	Kuhl	-1.14	5.3		0.01							99	99.01
Co	This work	-1.34	3								2.32	99.65	101.97

[a] Value does not include additional products found such as ethyleneglycol, allyl alcohol and propionaldehyde.
[b] Value does not include additional products found such as hydroxyacetone, ethyleneglycol, acetone, allyl alcohol, *n*-propanol and propionaldehyde.

for Co, −1.65 eV [110], is in between Cu and Ni, it would be expected to obtain better results with Co than with Ni but it is not the case. Hence, this suggests that the CO binding ability of each metal is not the only determining factor in the activity for the reduction of CO_2. It seems that the ability of each transition metal to bind H* also plays a role.

2.3.2 Electrochemical reduction of CO on Fe, Co, Ni, Cu

The same four transition metals where studied as electrocatalyst for the reduction of carbon monoxide by performing potentiostatic and galvanostatic experiments. In order to assure saturation of the reactant, 10 sccm CO were supplied to the cell over one hour prior to electrolysis. The potentials set were selected based on linear voltammetry performed prior to electrolysis with each metal. Galvanostatic experiments were performed at a current density of $-10\,mA/cm^2$. Table 2.4 summarizes the results showing average values for either the obtained current or potential and for the Faradaic efficiencies achieved. Traces of HCOOH were found using all the metals even though no CO_2 was supplied to the cell. In the literature, it is well accepted that CO is not an intermediate for HCOOH. Thus, the HCOOH found might be the result of the low amount of CO_2 that is formed in the electrolyte due to the carbonate equilibrium reaction since $KHCO_3$ was used as the catholyte. Furthermore, the high H_2 production even using Cu can be attributed to the lower solubility of carbon monoxide in water ($\sim$1 mM), which is lower than the solubility of CO_2 ($\sim$33 mM). This leads to a lower supply of CO than of CO_2 to the reaction boundary. Thus, in this kind of set-up a direct comparison of CO_2 and CO as the reactant can not be assured. Regarding the results for Ni, Fe, and Co, methanol was observed in all the cases but only when performing galvanostatic experiments, in which higher potentials were achieved. Considering that Ni, Fe and Co can bind CO stronger than Cu it is expected to need more energy for their further reaction of CO in this kind of metals. Here, the ability of this metals to bind hydrogen should also be taken into account. The results suggest that in Ni, Fe, and Co the H_2

Table 2.4: Electrochemical reduction of CO on transition metals

Metal	Type of experiment	E_{WE} V Ag/AgCl	I mA	Time s	Faradaic Efficiency (%) CH_4	C_2H_4	MeOH	EtOH	C_2	C_3	HCOOH	H2	Total
Cu	Potentiostatic	-1.5	3.32	3650	0.89	10.52		2.14	5.73	12.72		50.08	82.07
		-1.6	12.58	4200	3.22	8.49	0.016	1.45	1.41	2.81	0.03	64.30	81.72
		-1.7	40.97	3600	0.91	4.52	0.048	1.45	0.56	0.77	0.14	78.05	86.44
	Galvanostatic	-1.58	10	4227	1.36	4.73	0.037	0.48	10.50	1.12	0.12	80.67	99.01
Ni	Potentiostatic	-1.5	1.38	4500			2.110					92.19	94.30
		-1.6	27.50	4500			0.021				0.057	97.03	97.11
	Galvanostatic	-1.65	10	4200			0.293				0.120	92.70	93.12
Fe	Potentiostatic	-1.3	1.13	4774								110	110.00
		-1.40	5.47	4226								115	115.00
		-1.5	40.84	5620							0.125	92.98	93.11
	Galvanostatic	-1.52	10	8258			0.017				0.160	95.98	96.16
Co	Potentiostatic	-1.30	2.09	4249							0.353	73.35	73.71
		-1.40	3.13	3600								94.14	94.14
		-1.50	14.65	4200							0.111	100.15	100.27
	Galvanostatic	-1.46	5	5534			0.093				0.065	97.67	97.83
		-1.53	10	7085			0.048				0.074	96.36	96.48

evolution reaction requires less energy. Furthermore, with the high formation of H_2 it would be expected to obtain methane, since H* should be around CO*. Here is important to keep in mind that the liquid products were accumulate during the electrolysis, while the gas products are analyzed online. Hence, the formation of methane traces can not be totally ruled out, since the amount of CH_4 might have been under the detection limit of the used GC. On the other hand, when comparing the formation of MeOH using the four metals investigated, Ni shows the higher FE in both the galvanostatic and the potentiostatic experiments. This suggest that the formation of MeOH might be favored by a catalyst that binds CO stronger, which could also be the explanation for the usually low Faradaic efficiencies reported in the literature for methanol using Cu.

While the results from Tables 2.3 and 2.4 indicate that this kind of set-up is not suitable for a direct comparison of CO_2 and CO as reactants, the high formation of hydrogen opens the opportunity to study the hydrogen evolution reaction (HER) in the presence of CO and CO_2. With this purpose linear voltammetry experiments were performed at 50 mV/s after bubbling either N_2 as inert gas or CO and CO_2. The experiments were started at a low reduction potential, which increased at a ratio of 50 mV/s. Once the potential reaches values at which the species in solution can undergo electrochemical conversions, Faradaic current will flow. In the case of the reduction reaction a negative current is obtained as response. Hence, once an increase in the reduction current (more negative values) is observed for the case of Ni, Fe and Co it can be assumed that mainly HER is taking place based on the very low efficiencies observed for CO_2 reduction products. In the case of Cu, HER and $ERCO_2$ should take place simultaneously.

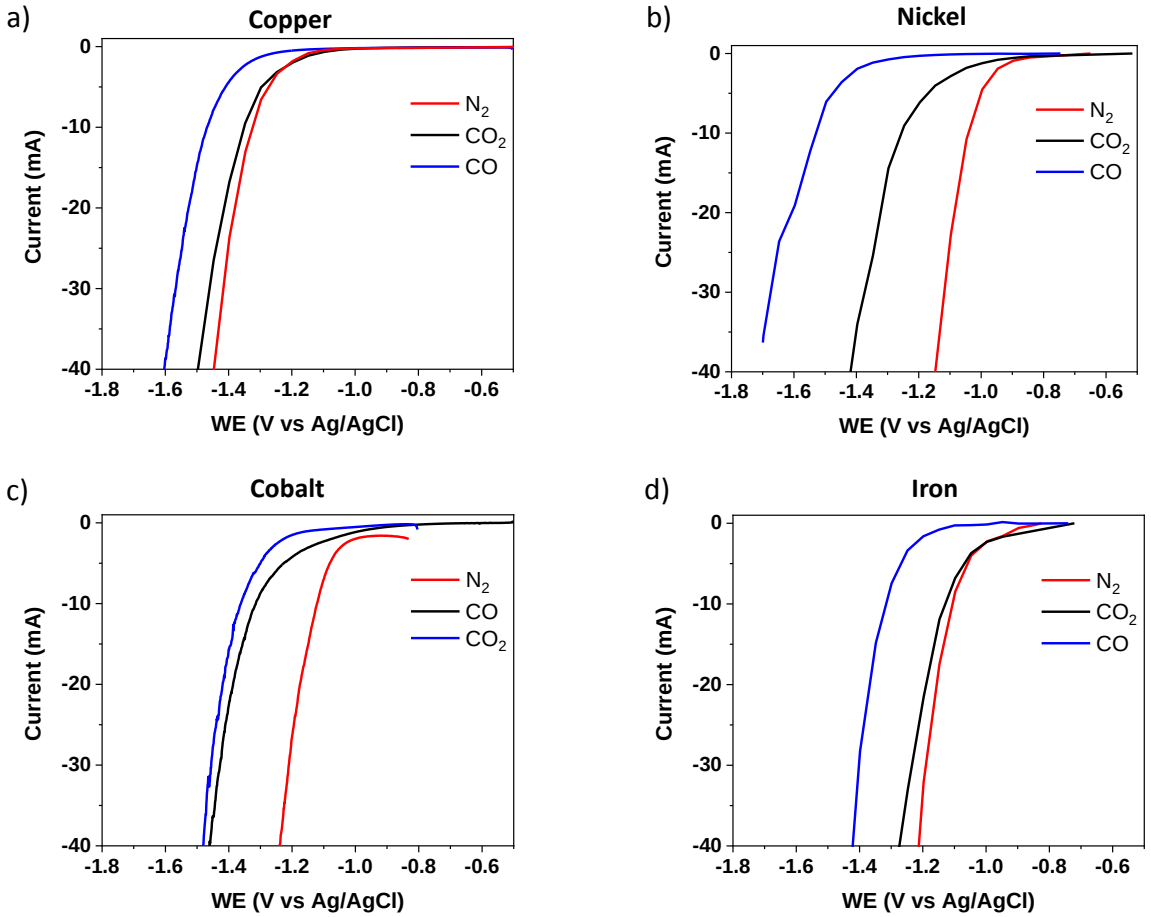

Figure 2.23: Linear Voltametry in the presence of N_2, CO_2, and CO for: a) Copper, b) Nickel, c) Cobalt, d) Iron.

As given in Fig. 2.23 in all the cases the HER is shifted to more negative potentials in the presence of CO than in the presence of CO_2. DFT calculations suggest that the observed potential shift using CO arises from adsorbate-adsorbate interactions between *CO and *H on intermediate and strong binding metals, which weakens the *H binding energy [111]. It can be observed that in the presence of N_2 the onset potential for HER is about 0.2 V lower with Ni, Fe, and Co than with Cu. This indicates that Ni, Fe, and Co are more active for HER than Cu. Using Ni the HER activity is suppressed in the presence of both CO and CO_2 so that the onset potential becomes more negative. It should also be noticed that HER suppression is stronger with CO than with CO_2. In the case of Fe, the presence of CO_2 does not inhibit significantly the HER activity, while with CO the onset potential is shifted to the left. Using Co no significant difference in the polarization curves for CO and CO_2 was detected. However, HER activity suppression is observed using both reactants in comparison to the inert gas. When using Cu and N_2 or CO_2 no significant difference in the curves is observed, which is expected since both reactions seem to happen simultaneously. In the presence of CO, the polarization curve was shifted to more negative potentials, indicating also a suppression of the HER. However, in the potentiostatic experiments performed at −1.6 V vs Ag/AgCl a higher efficiency for carbonaceous products

was obtained with CO_2 than with CO, which can be explained by the lower amount of CO available on the reaction boundary due to the lower solubility. This indicates that while the CO presence might suppress the HER on Cu, a lower amount of reactant supplied to the reaction zone favors the HER over CO reduction.

2.3.3 Conclusion

While all metals tested showed activity for MeOH and HCOO-, Cu was confirmed to be the only electrocatalyst active for the formation of multi-carbon products. Nevertheless, the formation of methanol seems to be more favorable in Ni than in Cu, suggesting that for the formation of methanol a stronger CO binding is required as what Cu can offer. Furthermore, Ni, Fe, and Co are highly active for hydrogen formation at lower potentials than Cu, which makes the competition between HER and $ERCO_2$ challenging in this kind of transition metals, leading to higher efficiencies for HER than to CO_2 or CO reduction products. In general, the lower solubility of CO than CO_2 in water makes the comparison of the two reactants difficult. Nevertheless, it was found that the presence of CO in general has a suppressing effect on the hydrogen evolution reaction, which leads to higher onset potentials for HER. this was more evident for metals with a stronger CO* binding energy. Based on the aforementioned results Cu was selected as the active material for further investigation of $ERCO_2$ in flow cells as will be described in the following chapters.

3 Advantages of CO over CO_2 as reactant for electrochemical reduction to ethylene, ethanol and *n*-propanol on gas diffusion electrodes at high current densities

This chapter is based on:

N. S. Romero Cuellar, K. Wiesner-Fleischer, M. Fleischer, A. Rucki, O. Hinrichsen, Advantages of CO over CO_2 as reactant for electrochemical reduction to ethylene, ethanol and *n*-propanol on gas diffusion electrodes at high current densities. Electrochimica Acta 2019, 307, 164-175. DOI: 10.1016/j.electacta.2019.03.142.

Author contributions:

N. S. Romero Cuellar prepared the Cu electrodes, performed the electrochemical experiments, analyzed the products, evaluated all the results and wrote the manuscript with input from all authors. A. Rucki conducted SEM and TEM characterization of Cu particles as powder and at GDL surface before and after electrolysis. K. Wiesner-Fleischer, M. Fleischer and O. Hinrichsen supervised and guided the findings of this work. All authors discussed the results, contributed and revised this manuscript.

3.1 Abstract

The electrochemical conversion of CO_2 to value-added chemicals is a technology gaining broader interest as society moves towards a carbon-neutral circular economy. Nonetheless, there are still several challenges to overcome before this technology can be applied as an industrial process. In the reaction path of the electrochemical reduction of CO_2 with Cu as an electrocatalyst, it is known that carbon monoxide is the key intermediate to chemicals such as ethylene, ethanol, and *n*-propanol. However, a better understanding of the electrochemical reduction of CO is still necessary to improve selectivity and efficiency at high current densities. In this work, the electrochemical reduction of CO_2 and CO towards C2 and C3 products is investigated using gas diffusion electrodes in a flow cell. Thereby the electrochemical reaction is not limited by the solubility of the feed gas in the electrolyte, and current densities of industrial relevance can be achieved. The electrodes are prepared using commercial Cu-powders consisting either of nano- or microparticles that are deposited on gas diffusion layers. Potentiostatic experiments show that with CO as the reactant, higher current densities for C2 and C3 products can be achieved at lower working electrode potentials compared to CO_2 as the reactant. Galvanostatic CO electrochemical reduction at $-300\,mA/cm^2$ with Cu-nanoparticles (40-60 nm) results in a cumulative Faradaic efficiency of 89 % for C2 and C3 products. This represents a two-fold increase in selectivity to ethylene and a three-fold increase towards ethanol and*n*-propanol compared to the selectivity obtained with CO_2 as the reactant. This enhancement of selectivity for C2 and C3 products at current densities of industrial relevance with CO as reactant provides a new perspective regarding a two-step electrochemical reduction of CO_2.

3.2 Introduction

The electrochemical reduction of CO_2 is an opportunity to support a low carbon economy by producing value-added chemicals out of CO_2 while utilizing low-cost renewable energy [28, 96]. For decades the combustion of fossil fuels has been the least expensive means of electricity production, resulting in emission of carbon dioxide [28], a compound which has been shown to be responsible for climate change [1]. Over the last few years the cost of renewable electricity has decreased drastically and currently tends to be competitive with traditional electricity production technologies, and soon will become the least expensive source of energy [112]. However, the challenges of intermittency of energy production and grid balancing remain [28]. Within this context, electrochemical conversion of CO_2 to fuels and feedstock using aqueous electrolytes and renewable energy is a very attractive option to close the carbon cycle [28, 29, 33, 96, 113]. In order to make that possible, high conversion at high current densities and low

overpotentials, together with a selective and long term stable operation have to be achieved [30, 96, 113, 114].

Different products can be obtained from the electrochemical reduction of CO_2 by using specific transition metals as electrocatalysts. Depending on the ability of each metal to adsorb CO, known as the main intermediate in the CO_2 reduction reaction, different products can be generated [33, 93]. These electrocatalysts have been extensively studied in the last decade focusing mainly on three approaches: the first being the electroreduction of CO_2 to syngas, i.e. a mixture of CO and H_2, using Ag and Au electrodes, which is getting closer to practical applications [85, 115, 116]; the second is the conversion of CO_2 to formate on Sn electrodes with Faradaic efficiencies (FE) over 70 % at current densities between $-100\,mA/cm^2$ and $-300\,mA/cm^2$ [117, 118]; and the third and most challenging approach is the reduction of CO_2 to C2 and C3 hydrocarbons such as ethylene, ethanol and *n*-propanol, which occurs when using Cu as electrocatalyst [35, 40, 53, 119].

Taking into account that it is possible to electroreduce CO_2 into more than ten products with Cu as an electrocatalyst [35, 94, 120], there are still a number of opportunities to explore, especially regarding the ability of copper to convert carbon monoxide into C2 and C3 products [121]. Although poor selectivity and stability, together with high overpotentials [35], seem to be the main challenges, significant improvements have been made reaching lower activation overpotentials and high Faradaic efficiencies to ethylene and ethanol [52, 53, 57, 71, 119, 122, 123]. Several studies regarding Cu catalyst structure [53, 55, 124] and Cu oxidation states [53, 76] have been performed. Recently the introduction of gas diffusion electrodes with nanostructured surfaces on carbon gas diffusion layers have enabled process operation at current densities around $-150\,mA/cm^2$ in flow cells, improving selectivity and activity towards ethylene [53, 71, 119, 125]. To our knowledge, the best results up to now have been achieved under alkaline conditions using flow cells [71, 119]. However, the formation of carbonates out of CO_2 in an alkaline medium (equations (3.1) and (3.2)) [33, 126] can lead to complications for up-scaling, since the non desired reaction rate between CO_2 and the electrolyte would be higher than the reaction rate of the desired electrochemical reactions [54]. The use of CO instead of CO_2 as the reactant in alkaline conditions should not represent drawbacks since CO does not react with aqueous electrolytes.

$$CO_2 + OH^- \rightleftharpoons HCO_3^- \tag{3.1}$$

$$HCO_3^- + OH^- \rightleftharpoons CO_3^{2-} + H_2O \tag{3.2}$$

Within this context, a two-step electrochemical reduction of CO_2 has been proposed as an alternative to increase the selectivity towards ethanol and acetate, in which CO_2 is reduced to CO as the first step, followed by CO reduction to hydrocarbons [54, 121, 127, 128]. However, the CO

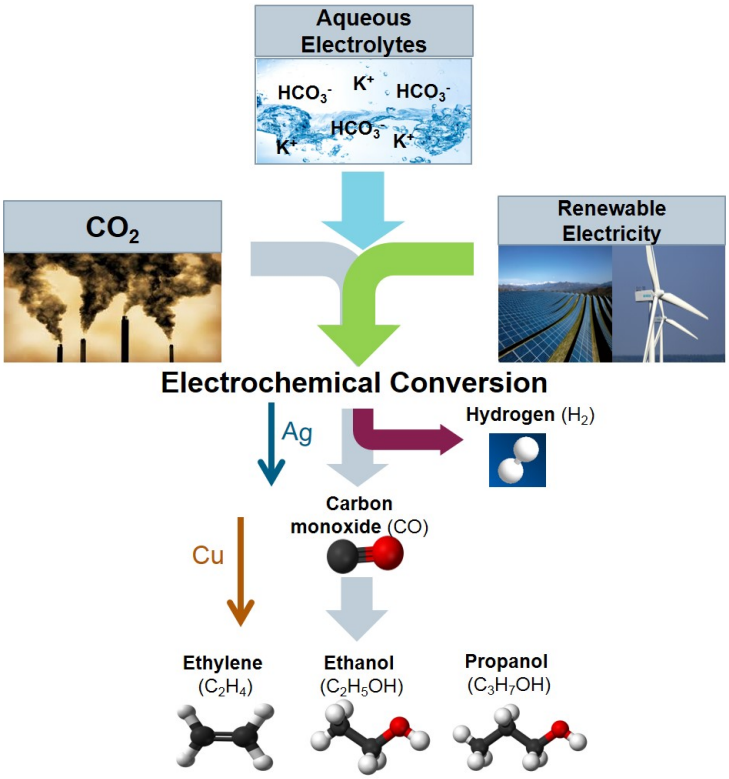

Figure 3.1: Concept scheme of a two-step CO_2 electrochemical reduction

electroreduction has been mainly investigated in setups where the electrochemical reaction is limited by the solubility of CO in aqueous electrolytes, reaching geometrical partial current densities for hydrocarbons lower than $-1\,mA/cm^2$ [93, 94, 121, 129, 130]. There is scarce research on CO electrolysis performed in flow cells with gas diffusion electrodes [54, 120]. Recently, Han et al. [54] reported CO electrochemical reduction using Cu-nanoparticles on gas diffusion electrodes with a maximal FE for ethylene of 17.8 % and a partial current density for ethylene of $-50.8\,mA/cm^2$. The formation of liquid products in their case has not been addressed. Furthermore, Schmid et al. [120], as part of their investigation of the CO_2 electrochemical reduction mechanisms at high current densities, performed galvanostatic CO bulk electrolysis at a current density of $-170\,mA/cm^2$ using an in situ-grown copper nano-dendritic catalyst on a gas diffusion layer. They reported an increment in the selectivity towards acetate and ethanol, but no significant increase in the ethylene Faradaic efficiency compared to the one achieved with CO_2 as reactant, which was around 40 % FE. Nevertheless, the nanodendritic Cu electrode decreases its activity dramatically after the first hour of experiment. With the progress made regarding Cu nanostructured-GDEs [71], flow cells [114] and the high Faradic efficiencies achieved in the conversion of CO_2 to CO at high current densities [85], a two-step electrochemical reduction as depicted in Fig. 3.1 becomes certainly worthy of further exploration.

In order to get some insights about the feasibility of a two-step electrochemical reduction of CO_2 , we compare CO_2 and CO as reactants regarding selectivity towards C2 and C3 products using gas diffusion electrodes, a flow cell, and a mild electrolyte ($KHCO_3$). This

allows a straight comparison of the electrochemical reduction of CO and CO_2 . The overall cathodic half reactions using either CO_2 or CO as the reactant are shown in Table 3.1. For each reactant we studied four commercial Cu-powders with different particle sizes in the nano- and micro-scale, aiming to obtain further knowledge about the effect of morphology on the electrochemical activity. These Cu-powders were deposited onto carbon based gas diffusion layers, obtaining gas diffusion electrodes. We also investigated the stability of the system by performing 20 hours electrolysis. Additionally, the catalyst layers were characterized by TEM and XRD before and after electrolysis. The obtained results show a remarkable increase in the selectivity towards ethylene (C_2H_4), ethanol (C_2H_5OH), and *n*-propanol (C_3H_7OH) using CO as the reactant instead of CO_2 .

Table 3.1: CO_2 and CO electroreduction reactions in aqueous solutions for the most frequent products [35, 113, 121]

CO_2 as reactant	**CO as reactant**
$CO_2 + H_2O + 2\,e^- \rightleftharpoons CO + 2\,OH^-$	
$CO_2 + H_2O + 2\,e^- \rightleftharpoons HCOO^- + OH^-$	
$CO_2 + 6\,H_2O + 8\,e^- \rightleftharpoons CH_4 + 8\,OH^-$	$CO + 5\,H_2O + 6\,e^- \rightleftharpoons CH_4 + 6\,OH^-$
$CO_2 + 5\,H_2O + 6\,e^- \rightleftharpoons CH_3OH + 6\,OH^-$	$CO + 4\,H_2O + 4\,e^- \rightleftharpoons CH_3OH + 4\,OH^-$
$2\,CO_2 + 8\,H_2O + 12\,e^- \rightleftharpoons C_2H_4 + 12\,OH^-$	$2\,CO + 6\,H_2O + 8\,e^- \rightleftharpoons C_2H_4 + 8\,OH^-$
$2\,CO_2 + 9\,H_2O + 12\,e^- \rightleftharpoons C_2H_5OH + 12\,OH^-$	$2\,CO + 7\,H_2O + 8\,e^- \rightleftharpoons C_2H_5OH + 8\,OH^-$
$3\,CO_2 + 13\,H_2O + 18\,e^- \rightleftharpoons C_3H_7OH + 18\,OH^-$	$3\,CO + 10\,H_2O + 12\,e^- \rightleftharpoons C_3H_7OH + 12\,OH^-$

3.3 Experimental

3.3.1 Cathode preparation

Cu-powders delivered by Sigma Aldrich were used for the preparation of the electrodes. Three Cu-powder samples consist of nanoparticles with different particle size ranges, namely 40-60 nm, 60-80 nm, and <100 nm. The last one is passivated with <3 % oxygen. These particle size ranges were selected based on previous studies that reported high efficiencies for C2 and C3 products [54, 71, 119]. Additionally, for comparison between micro- and nanoparticles a Cu powder with a particle size of 5 µm was also included in the study. Hereafter, when making comparisons and mentioning microparticles we will be referring specifically to a particle size of 5 µm. In total, four different electrode ensembles were investigated. These four electrode types were all prepared with a method similar to the one reported by Ma et al. [71], in which 60 mg of Cu-powder with 40 mg of 20 % Nafion® dispersion and 2 ml iso-propanol were ultrasonicated and directly deposited onto a carbon-based gas diffusion layer (GDL) H23C2 from Freudenberg. In order to restrict the deposition to the desired area and improve the reproducibility of the deposition, a frame with a free surface of 40 mm × 100 mm was placed on top of the GDL. These dimensions enable the preparation of two electrodes per batch. The deposition process

was repeated three times and the electrode was then dried under an Ar atmosphere with a flow of 0.5 L/min for at least 12 h at room temperature. Catalyst loading was calculated from the weight difference of the GDL before and after deposition, the material loss within the entire preparation process was calculated to be in the order of 40 %, resulting in a final catalyst loading of $\sim$3 mg/cm^2. SEM and TEM micrographs of Cu-Powders and Cu- electrodes as well as a FIB cut of a GDL after deposition of copper nanoparticles are shown in Fig. 3.8 and 3.9 of the supporting information.

3.3.2 Electrolysis

A MicroFlow® cell (Electrocell) with a geometric electrode area of 10 cm^2 was used for all of the experiments. The cell consisted mainly of three compartments: gas, catholyte and anolyte. The standard PTFE flow frames were modified from the original MicroFlow® cell to improve the fluid transport in the gas and electrolyte compartments and avoid leaks between gas and catholyte compartments. Additionally, support structures were added to the PTFE frames for better mechanical stability of the GDE and the membrane.

1 M $KHCO_3$ was used as catholyte and 2.5 M KOH as anolyte. Catholyte and anolyte were separated by a cation exchange membrane, Nafion® 117 (DuPont). The electrolytes were supplied to the cathode and anode using micro diaphragm liquid pumps (NFB 25 KPDCB-4A, KNF) operated at constant flow of 100 mL/min. The gas inlet was controlled with a mass flow controller SFC5400 (Sensirion) at a constant flow of 50 50 mL/min. Gas product and catholyte were collected in a catholyte reservoir, where gas and liquid phases were separated. The liquid outlet of the reservoir was sent back to the cell, while the gas outlet of the reservoir was measured with a flow meter before entering the gas chromatograph. Anolyte circulated constantly in a separate closed system between reservoir and anode, while the gas products of the anode left the system without being measured. A schematic of the setup is shown in Fig. 3.11 of the supporting information.

Electrochemical reduction of CO_2 and CO was performed using potentiostatic and galvanostatic techniques. For the potentiostatic experiments, the working electrode potential (V_{WE}) was increased 0.1 V every 22 min in the range at which the desired C2 and C3 products were observed with both reactants CO_2 and CO (between −1.2 V and −1.5 V *vs.* Ag/AgCl). In the galvanostatic experiments the current was varied from −1000 mA to −3000 mA. Current densities were calculated by dividing the applied current by the geometrical electrode area (10 cm^2). Long term experiments were also performed in the galvanostatic mode, measuring the gas products every 22 min and the liquid products after the first hour and at the end of the experiment.

The electrolysis was performed in a flow-by operation mode, in which the feed gas, CO or CO_2, enters the gas compartment at the top of the cell, passes by the GDE and leaves the cell together with the gas product at the bottom. A flow-by operation mode enables a CO/CO_2 diffusive mass transport into the pores of the GDE [85].

3.3.3 Product analysis

Gas chromatography and ^1H Nuclear Magnetic Resonance (NMR) were used for quantification of gas and liquid products, respectively. A gas chromatograph, 7890B Agilent (Santa Clara, USA), was used with Helium as the carrier gas, which enables the detection of H_2 as a negative peak. A thermal conductivity detector (TCD) and three serially connected columns were used: a HayeSeP Q-column which plays a safety role, a Porapak Q-column for the separation of CH_4, CO_2 and C_2H_4, and a molecular sieve 5 Å-column to separate N_2, O_2, and CO. 1 mL of the gas product was automatically injected every 20 minutes from the cell to the gas chromatograph during the electrolysis. The liquid products were measured taking aliquots of 1 mL from the catholyte reservoir at the end of each current density or potentiostatic step, right after the GC injection. These aliquots were analyzed by ^1H NMR spectroscopy. The NMR measurements were performed in a 500 MHz Bruker (Bruker BioSpin, Karlsruhe, Germany) following the method described by Kuhl et al. [35] and Schmid et al. [120]. The water peak was suppressed by a pre-saturation sequence. Electrolyte, containing CO_2 reduction products (300 mL), was mixed with sodium fumarate (50 mL), which was used as internal standard in D_2O (250 mL) for the quantification.

3.3.4 Electrode surface analysis before and after electrolysis

The different Cu-powders used, as well as the electrodes before and after long term experiments were examined with scanning electron microscopy with a field emission gun (FEG-SEM, FEI Strata 400 Dual BeamTM system) operated at 5.00 kV. Moreover, particle size distribution of the nano-powders and morphology were determined by transmission electron microscopy (TEM) bright field imaging with a JEOL 2200FS operated at 200 kV. Crystal structure and composition were characterized with a desktop X-ray powder diffraction system for polycrystalline material analysis (XRD, D2 Phaser Bruker).

3.4 Results and Discussion

3.4.1 CO_2 electrochemical reduction: potential variation

The electrocatalytic activity for CO_2 reduction of four commercial Cu-powders deposited onto a gas diffusion layer was investigated by performing potentiostatic experiments at room temperature using 1 M $KHCO_3$ as the catholyte. Fig. 3.2 shows the partial current densities for C1 (1a), C2 (1b) and C3 (1c) products plotted as a function of the working electrode potential. A table listing the Faradaic efficiencies for each product can be found in Table 3.4 of the supporting information. The partial current densities for CO, HCOOH, CH_4, and CH_3OH were summed and plotted as C1 products, where CO and HCOOH were the major C1 products. Regarding the ability of the four ensembles to reduce CO_2 into C1 products, a higher activity was observed in general when using Cu-nanoparticles than using Cu 5 µm. Between the three Cu-nanopowders no significant difference was observed from −1.2 to −1.4 V *vs.* Ag/AgCl. However, at a potential of −1.5 V *vs.* Ag/AgCl a higher partial current density for C1 was achieved using Cu<100 nm.

Fig. 3.2b depicts the partial current densities for C2 species with C_2H_4 and C_2H_5OH as major products and CH_3COO^-, C_2H_4O, $C_2H_6O_2$ as minor products. In general, at a working electrode potential of −1.2 V *vs.* Ag/AgCl mainly acetate was observed. The formation of ethanol was first detected at −1.3 V in all the electrodes besides the one with CuNPs 40 nm-60 nm, which produced ethanol at −1.2 V. Ethylene production started at −1.4 V when using nanoparticles and at −1.3 V when using Cu 5 µm. At the highest potential investigated, the smallest Cu-nanopowder ensemble was observed to be the most active for the reduction of CO_2 into C2 products.

Regarding C3 products *n*-propanol was the major product found and only traces of allyl-alcohol and acetone were detected. *n*-Propanol was first detected at a working electrode potential of −1.3 V *vs.* Ag/AgCl using Cu-microparticles, while using nano-particles the onset potential was −1.4 V *vs.* Ag/AgCl as shown in Fig. 3.2c.

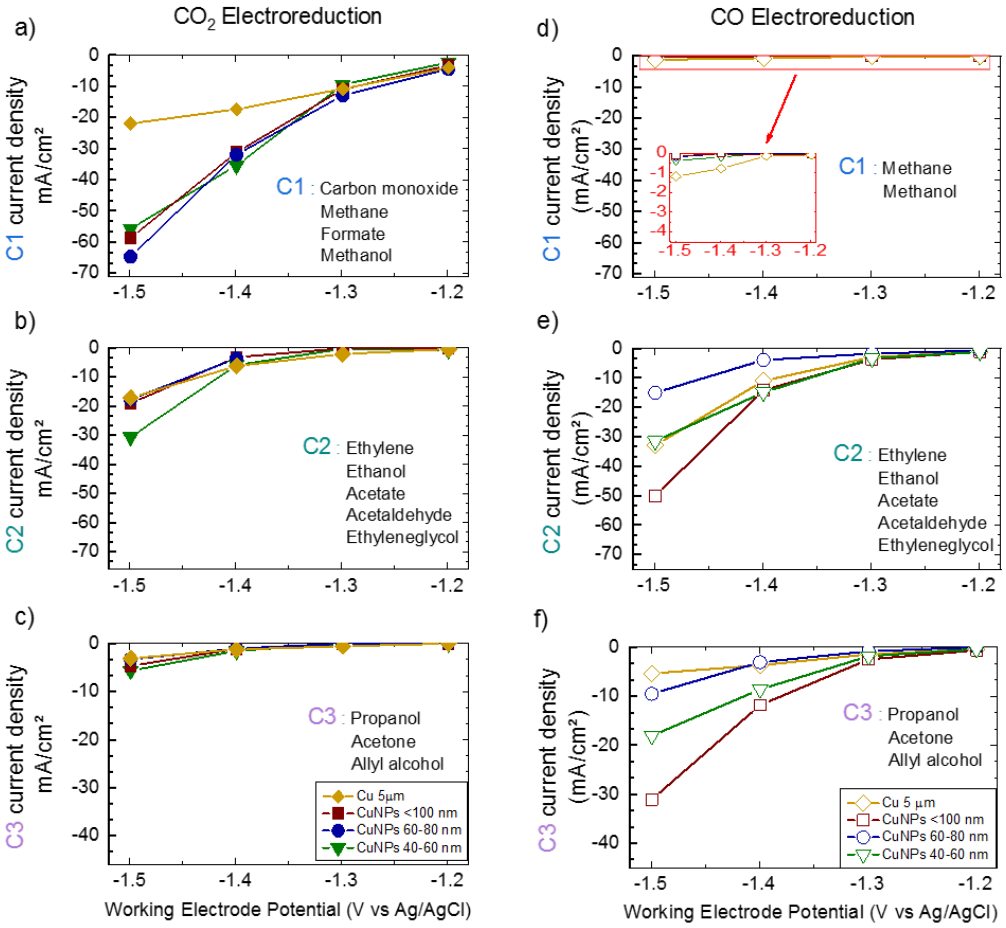

Figure 3.2: Partial current densities for C1, C2 and C3 products after CO_2 electroreduction (a, b, c) and CO electrochemical reduction (d, e, f)

In general, it can be observed that when using CO_2 as the reactant, most of the achieved current density was utilized for the formation of C1 products, mainly CO and HCOOH. Additionally, it should be noticed that the partial current density for C1 products using microparticles was much lower than it was when using nanoparticles. No significant differences in the partial current densities of C2 and C3 products were observed among the four particle sizes used. This suggests that at low potentials the further reduction of CO_2 to C2 and C3 products might have been more effective using microparticles than using nanoparticles.

Furthermore, taking a look into the Faradaic efficiencies of the major C2 and C3 products found, namely ethylene, ethanol and *n*-propanol, it can be noticed in Fig. 3.3a that up to a potential of −1.4 V *vs.* Ag/AgCl, the electrode with Cu 5 µm delivered higher Faradaic efficiencies for ethylene than those prepared with nanoparticles. Once a potential of −1.5 V *vs.* Ag/AgCl was achieved, the electrode with CuNPs 40-60 nm became more active for ethylene than the electrode with Cu5 µm. A similar behavior was observed for ethanol between potentials −1.3 V and 1.4 V *vs.* Ag/AgCl. Besides that, a large portion of the current was used for the conversion

of CO_2 to CO, resulting in Faradaic efficiencies for CO between 20 % and 40 % as shown in Table 3.31 of the supporting information.

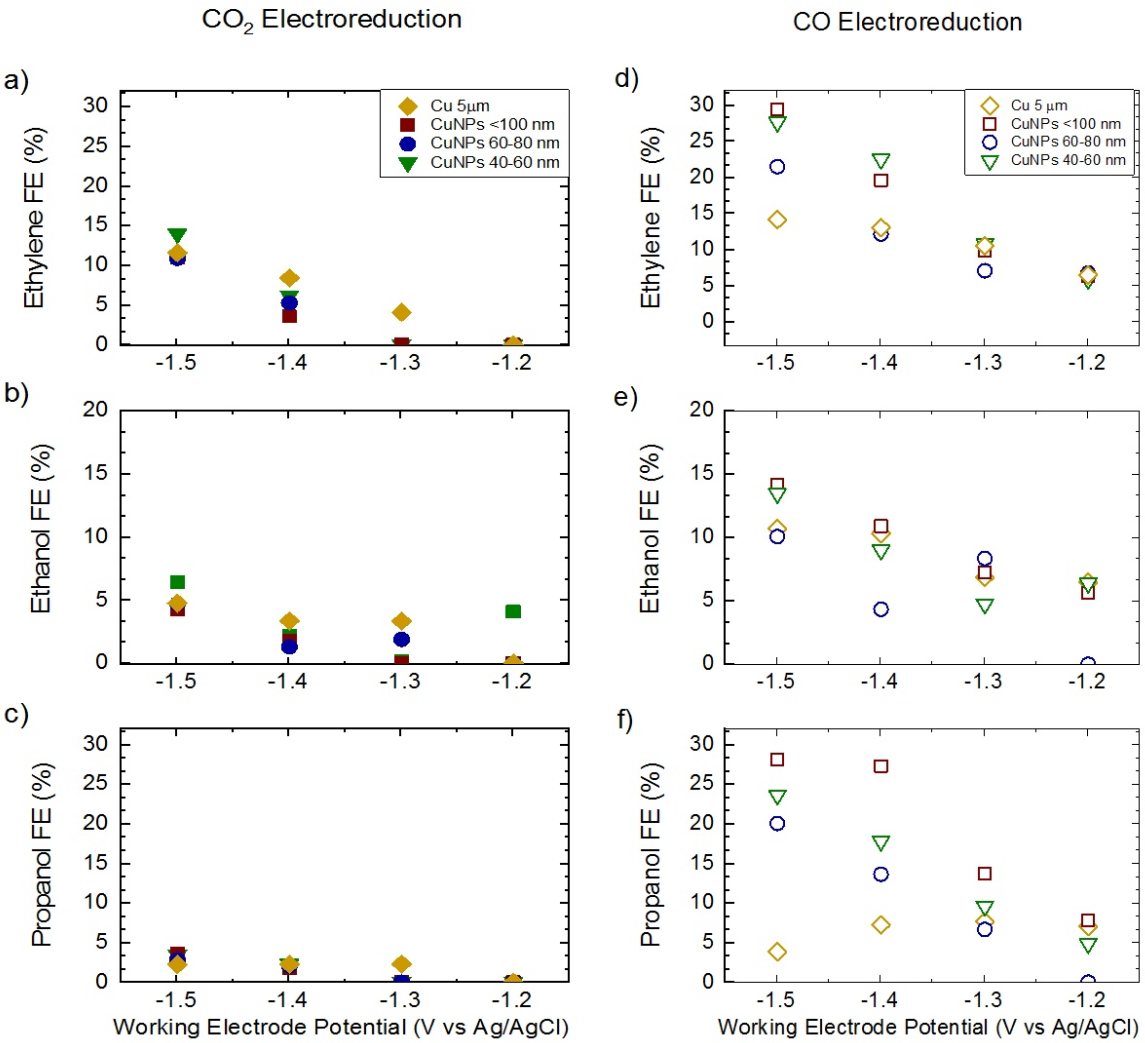

Figure 3.3: Faradaic efficiency for ethylene, ethanol and *n*-propanol using CO_2 (a, b, c) and CO as reactant (d, e, f)

3.4.2 CO electrochemical reduction: potential variation

The same four commercial Cu-powders mentioned above were investigated using CO as reactant at room temperature in 1 M $KHCO_3$ as catholyte. As depicted in Fig. 3.2d some traces of CH_4 and CH_3OH were found as C1 products at working electrode potentials higher than −1.4 V *vs.* Ag/AgCl when using Cu-nanoparticles, while with Cu-microparticles CH_4 was observed at

−1.3 V. However, the sum of partial current densities for C1 products did not exceed −2 mA/cm^2 for any of the electrodes investigated.

Regarding C2 products, acetate, ethylene and ethanol were detected at −1.2 V *vs.* Ag/AgCl in all the electrodes, which is 200 mV less than with CO_2 as reactant. This lower working electrode potential for ethylene and ethanol using CO as reactant is consistent with recent studies [119, 130] and suggests an improvement in energy efficiency under CO conditions. Furthermore, acetate decreased at more negative potentials, while ethylene and ethanol increased using nanoparticles, specifically with the sample CuNPs <100 nm, reaching C2 partial current densities of −50 mA/cm^2 at −1.5 V *vs.* Ag/AgCl.

The production of C3 products was remarkably higher using CO compared to CO_2 as the reactant. *n*-Propanol, the main C3 product, was observed in all cases at the lowest potential investigated, −1.2 V *vs.* Ag/AgCl, as shown in Fig. 3.2f. All electrodes behaved quite similarly at low potentials until −1.3 V. At more negative potentials when CO was the reactant, partial current densities for C3 products using nanoparticles were approximately four times higher than when CO_2 was used.

Focusing on the Faradaic efficiencies for the main C2 and C3 products depicted in Fig. 3.3, namely ethylene, ethanol and *n*-propanol, the same trend as before was observed. For these three products, the electrodes prepared with nanoparticles became more active than the electrode with microparticles (Cu 5 µm) when using CO as the reactant. With the three nanoparticle ensembles studied, the selectivity for ethylene, ethanol, and *n*-propanol was increased with more negative working electrode potentials. Microparticles appeared to be slightly more active towards ethylene at lower potentials than nanoparticles. However, when working at more cathodic potentials nanoparticles sharply increased their activity in respect to C2 products, while microparticles showed a steady increase in ethylene and ethanol FE and a decrease in the selectivity towards *n*-propanol. This behavior can be explained by the higher GDE roughness and higher active-center density for the CO reaction with the use of nanoparticles compared to microparticles with the same catalyst loading.

With CO as reactant a partial current density of −50 mA/cm^2 was achieved for C2 products at −1.5 V *vs.* Ag/AgCl, with an ethylene FE of 29.4 % and an ethanol FE of 14 %. Additionally, the formation of *n*-propanol rose to a partial current density of −40 mA/cm^2 with 28 % FE at the same potential. Thus, our results show that even using a mild electrolyte, a high selectivity towards C2 and C3 products can be achieved at moderate potentials by using CO as reactant.

3.4.3 Current density variation

Galvanostatic experiments were performed on all the electrodes with CO and CO_2 as reactants at geometrical current densities in the range −100 to −300 mA/cm^2. This range was selected with the aim of operating at industrially relevant current densities, while following the trend observed during the potentiostatic experiments. Fig. 3.4 depicts the Faradaic efficiencies for the main C2 and C3 products found, namely ethylene, ethanol and *n*-propanol. With CO_2 as the reactant, it can be observed in Fig. 3.4a-c that microparticles were more active towards ethylene and ethanol at current densities under −150 mA/cm^2 . However, at current densities over −150 mA/cm^2 their activity decreased. This might indicate that a limiting current density is achieved with the use of microparticles. On the contrary, an enhancement in the FE for ethylene was observed with the increase of current density in all the nanoparticle ensembles investigated. A maximum FE for ethylene formation of 32 % was achieved at −300 mA/cm^2 using CuNPs 60-80 nm. From the samples investigated using CO_2 as the reactant, this showed the highest FE towards ethylene and ethanol.

While microparticles (5 µm) decrease their activity at current densities over −150 mA/cm^2, nanoparticles became more selective with higher current densities. This can be attributed to the active surface area available for the CO reduction, which is higher with nanoparticles than with microparticles with the same catalyst loading. Besides that, the use of either microparticles or nanoparticles might also play a role in the mass transfer of the reactant (CO_2 or CO) through the catalyst layer, which might be first noticeable at high current densities.

Taking into account that the measurement of pH in the vicinity of the electrode during electrolysis was not possible in our set-up and that the pH value plays an important role in the conversion of the measured working electrode potential *vs.* Ag/AgCl to a reversible hydrogen electrode (RHE) scale ($V_{vs.\ \mathrm{RHE}} = V_{\mathrm{measured}\ vs.\ \mathrm{Ag/AgCl}} + 0.209 + 0.059 \cdot \mathrm{pH}$), we decided to show the working electrode potentials as collected with the Ag/AgCl reference electrode (Fig. 3.4d and 3.4h). Nevertheless, the pH value of the catholyte was measured before and after the electrolysis i.e. after the last step of the current density variation.

It was observed that at high current densities with the amount of electrolyte used (100 mL) and with CO_2 as the reactant, the pH value increased from 8 to 10 despite the use of a buffer electrolyte ($KHCO_3$). With CO as the reactant the pH raised from 8 to 13. This higher pH slope with the use of CO corresponds with the higher working electrode potential observed in Fig. 3.4h compared to Fig. 3.4d. However, the conversion of the measured working electrode potential to RHE e.g. for Cu <100 nm at −300 mA/cm^2 with CO_2 and CO and pH values of 10 and 13 results in −0.94 V *vs.* RHE and −0.91 V *vs.* RHE, respectively. Here it is important to notice that actually a slightly lower potential is needed with CO as reactant than with CO_2 when taking a pH independent scale for the comparison. Thus, it should be considered

that the differences in the potential shown in Fig. 3.4 also indicate the change of pH during the experiment. In the course of electrolysis with an aqueous electrolyte, H^+ can leave the catholyte either as H_2 as a result of HER or through the cation exchange membrane, while OH^- accumulates in the catholyte making the system alkaline. The lower pH change observed with CO_2 can be explained by the fact that CO_2 reacts with electrolyte transforming into species such as HCO_3^- and producing an additional buffer effect. On the contrary, CO does not react with the electrolyte, thus the accumulated OH^- can not be balanced and in consequence a pH raise is observed.

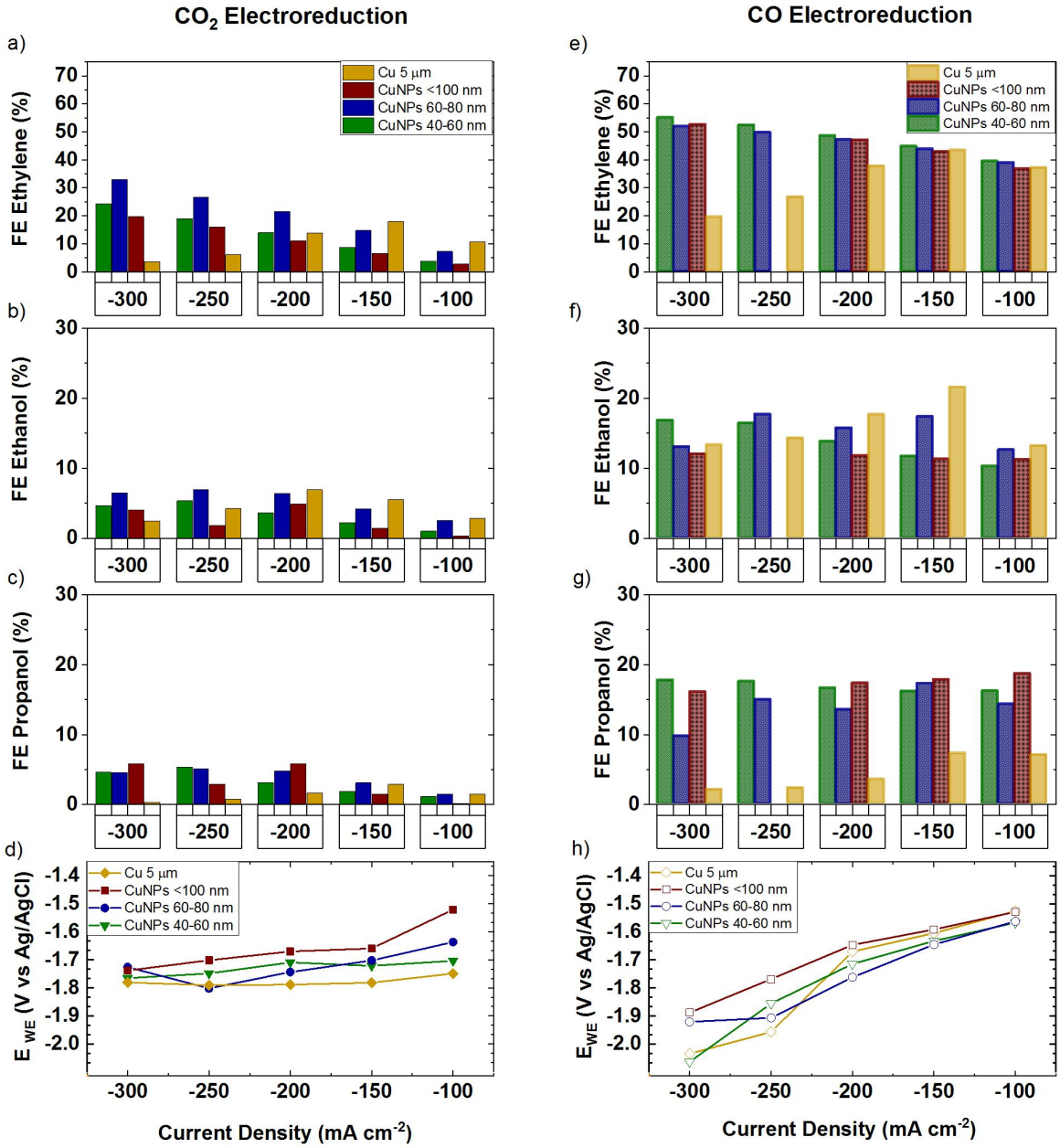

Figure 3.4: Faradaic efficiencies and resulting average working electrode potential of the current density variation for the CO_2 (a-d) and for CO (e-h) electrochemical reduction

Using CO as the reactant, the Faradaic efficiency for ethylene increased more than two-fold compared to the efficiencies achieved with CO_2. This is consistent with the potentiostatic experiments mentioned before. Furthermore, comparing micro- and nanoparticles for the production of ethylene during galvanostatic experiments, it can be observed that nanoparticles became, also in this case, more active at higher current densities delivering higher FE than microparticles. A maximum FE for Ethylene using the sample Cu 5 µm was observed at $-150\,mA/cm^2$, which corresponds with the limiting current density observed in the experiments with CO_2 as reactant. From the three nanoparticle samples investigated, CuNPs 40-60 nm nm shows the highest FE for ethylene, with $\sim$54 % at $-300\,mA/cm^2$. Reproducibility experiments show only slight measurement deviations of the obtained Faradaic efficiencies. These results can be found in the supporting information S.7.

We demonstrate that even in mild electrolytes such as 1 M $KHCO_3$, the use of CO as reactant leads to higher partial current densities for the formation of C2 and C3 products than with CO_2. The high current densities and moderated potentials reported in this work can be attributed to the use of a flow cell and gas diffusion electrodes, where gas and electrolyte are constantly circulating, improving the mass transport of both reactants and products. In a flow cell with gas and electrolyte compartments separated by a gas diffusion electrode, where the feed gas diffuses inside the electrode pores, a pronounced triple phase boundary is achieved allowing a high local presence of CO at the reaction interface. As suggested in previous works, the C-C bond as a result of the dimerization of two CO molecules is the intermediate in the formation of ethylene [41]. Thus, a high coverage together with the large number of active centers and lower intrinsic barriers to C-C coupling, accomplished by the deposition of Cu-nanoparticles with a $3\,mg/cm^2$ catalyst loading on a gas diffusion layer, leads to an increase of selectivity towards ethylene and suppression of hydrogen evolution reaction. Moreover, the remarkable increase in the production of *n*-propanol can be explained by the high local presence of CO and the high production of ethylene. As proposed by Hori et al. [129] and Ren et al. [51] high local concentration of CO and C_2H_4 (ads) together with a large surface area seems to be a key factor in the improvement of *n*-propanol production. Taking into account that *n*-propanol shows a high energy-mass density (30.94 kJ/kg), as well as a high octane number, and that a 99 % *n*-propanol separation from electrolyte using liquid-liquid extraction is feasible [51], the conversion of CO to *n*-propanol might become an interesting path to further investigate within the framework of a two-step CO_2 electrochemical reduction.

Apart form the effect of the local CO concentration, we suggest that the further reduction of CO to C2 and C3 products might also be hindered by competing reactions, which require less electrons when using CO_2 as the reactant. One of these competing reactions is the conversion of CO_2 to $HCOO^-$ ($2\,e^-$). On the other hand, when using CO as the reactant, the number of competing reactions is lower, along with the number of electrons required for the formation of ethylene ($8\,e^-$), ethanol ($8\,e^-$) and *n*-propanol ($12\,e^-$) as shown in Table 3.1.

3.4.4 Comparison to prior work

In comparison with previous works using nanoparticles supported on carbon substrates and $KHCO_3$ as electrolyte, we observed formation of ethylene at lower potentials than the ones reported by Baturina et al. [70]. The Faradaic efficiencies for ethylene, ethanol and n-propanol are comparable with the results reported by Kim et al. [52], who also investigated copper nanoparticle ensembles for the formation of C2 and C3 products and showed that a large catalyst loading can also improve the selectivity. Additionally, our results are consistent with the study conducted by Ma et al. [71], who also investigated CO_2 electrochemical reduction in a flow cell using Cu-nanoparticles deposited on gas diffusion layers. Specific information about catalyst, current densities, working electrode potentials and FE in each of the previous reports can be found in Table 3.2. Although Ma et al. [71] focused on alkaline electrolysis, they also conducted experiments with $KHCO_3$ for comparison. They observed at a working electrode potential of -1.05 V *vs.* RHE in 0.5 M $KHCO_3$ an ethylene FE around 20 %, while in our experiments 24.4 % FE ethylene was achieved at -0.97 V *vs.* RHE in 1 M $KHCO_3$ with the sample CuNPs 40-60 nm. The slightly higher Faradaic efficiency for ethylene in our results can be explained by the differences in the catalyst loading and by the CO_2 flow rate. Our catalyst loading was $\sim$3 mg/cm^2 , while in their experiments 1 mg/cm^2 was used. As described by Kim et al. [52] catalyst loading plays an important role in the selectivity for C2 and C3 products. Additionally, our CO_2 flow rate was 50 sccm, while Ma et al. used only 7 sccm CO_2 and as mentioned in previous publications, the CO_2 feed flow rate in a flow cell also has a significant effect on the Faradaic efficiency [85, 115].

Table 3.2: Previous reported performance of CO_2 electrochemical reduction to ethylene, ethanol and *n*-propanol in $KHCO_3$ using Cu-nanoparticles deposited onto carbon based support

		j	V_{WE}	% FE			
Electrode	**Electrolyte**	mA/cm^2	*vs.* RHE	**C_2H_4**	**EtOH**	**PrOH**	**Ref**
Cu NPs/carbon black	0.1 M $KHCO_3$	< –25	-1.4[a]	40	-	-	[70]
Cu NPs/carbon paper	0.1 M $KHCO_3$	< –20	-0.87	32	16	4	[52]
Cu NPs/N-doped graphene	0.1 M $KHCO_3$	-2	-0.87	-	63	-	[57]
Cu NPs/Gas diffusion layer	0.5 M $KHCO_3$	-	-1.05	20	6.5	-	[71]
Cu NPs/Gas diffusion layer	1 M KOH	-150	-0.8	25	12	-	[71]
Cu NPs/Gas diffusion layer	1 M $KHCO_3$	-300	-0.97[b]	24.4	4.6	4.6	this work

[a] Working electrode potential converted to RHE at pH=6.8

[b] Results with sample CuNPs 40-60 nm shown in Fig. 3.4. Working electrode potential converted to RHE at pH=10 (measured at the end of the electrolysis at -300 mA/cm^2)

Our results with CO as the reactant show an increase in the selectivity towards ethylene, ethanol and *n*-propanol higher than two-fold in comparison with direct CO_2 electroreduction. This remarkable increase in the selectivity has not been reported before to our knowledge up to date. In fact, CO electrochemical reduction has been scarcely investigated using gas diffusion

electrodes and flow cells. Han et al. [54] have recently reported CO electroreduction on Cu-gas diffusion electrodes using a batch cell where the electrolyte is stirred. They reported a partial current density for the ethylene formation of −50.8 mA/cm^2 at −0.85 V *vs.* RHE in 10 M KOH (−1.9 V *vs.* Ag/AgCl at pH = 14) with 17.8 % FE [54], while in the present work we observed 52.5 % ethylene FE, 12 % ethanol FE and 15.9 % *n*-propanol FE at a current density of −300 mA/cm^2 with a working electrode potential of −1.9 V *vs.* Ag/AgCl at a measured pH = 13 (−0.91 V *vs.* RHE) in 1 M $KHCO_3$ as shown in Fig. 3.4 for Cu<100 nm.

In some previous studies about CO electroreduction using Cu-oxide electrodes [121] and in-situ grown nano-dendritic Cu [120], it has been reported that a high presence of CO increases the formation of liquid products such as acetate and ethanol. On the one hand, our results are in agreement with the literature regarding the increase of acetate and ethanol. On the other hand, we achieved an increase in the selectivity for ethylene and *n*-propanol with CO as reactant at high current densities, which is not totally in agreement with previous studies. Schmid et al. [120] observed no significant increase in the Faradaic efficiency when using CO instead of CO_2 as reactant reaching around 40 % FE ethylene at a current density of −170 mA/cm^2 using in-situ grown nano-dendritic Cu on gas diffusion layers. On the contrary, we obtained a two-fold increase for ethylene with 55 % FE at a current density of −300 mA/cm^2 and a three-fold increase in n-propanol selectivity with 18 % FE with Cu-nanoparticles (40-60 nm). We assume that the difference lies in the mechanistic pathways to hydrocarbons using either in-situ grown nano-dendritic Cu or deposited Cu-nanoparticles. As explained by Schmid et al. [120] the mechanistic pathways to hydrocarbons using nano-dendritic Cu differ from the reaction pathways proposed by Ma et al. [71] on Cu-nanoparticles towards ethylene and ethanol. Keeping in mind that we used a similar type of electrode as Ma et al., we expect our experiments to follow their proposed mechanism. Additionally, we observed that Cu-nanoparticles deposited on gas diffusion layers can also lead to a high selectivity of *n*-propanol when sufficient CO is available at the three-phase reaction boundary.

3.4.5 Long term Experiments

Regarding durability, long-term experiments over 20 h were performed. Differently to the experiments shown in sections 3.4.1, 3.4.2 and 3.4.3, for long term analysis the circulating electrolytes (1 M $KHCO_3$) were mixed in one reservoir. A schematic of the modified set-up can be found in Fig. 3.12 of the supporting information. It is known that with cathode and anode compartments, separated by a cation exchange membrane such as Nafion, K^+ ions migrate during the electrolysis from the anolyte to the catholyte. Thus, after a certain time a depletion of cations in the anolyte leads to a very high cell voltage. The mixing of electrolytes is a solution to assure the migration of ions over a more extended period of time [131]. Since the mixing of

anolyte and catholyte may lead to inaccurate results for liquid products due to reoxidation, we focused in this case mainly on the formation of ethylene.

Fig. 3.5 shows the results for the gas products obtained using the samples CuNPs 40-60 nm and CuNPs <100 nm with both pure CO_2 and pure CO as reactants at −200 mA/cm^2. With CO_2 as the reactant, a high CO production right after the start of the experiment was observed in both cases, which decreases rapidly with the increase of ethylene. This suggests that presumably a high CO coverage and certain local pH might have been achieved after the first 3 h of the experiment. From that point an almost stable ethylene production was observed for both samples. The ethylene formation using CuNPs 40-60 nm slightly decreased from the maximum value of 29 %-23 % FE after 20 h, while with CuNPs <100 nm only a 2 % FE ethylene drop was observed with an almost constant value of 27 % FE. Reproducibility experiments can be found in the supporting information S.7. These results from a general perspective are comparable with Ma et al. [71], who showed that Cu-nanoparticles exhibit significant stability over 4 h electrolysis in KOH using commercial Cu-nanoparticles deposited on a gas diffu- sion layer. We obtained similar Faradaic efficiencies for ethylene between 20 % and 30 % using 1 M $KHCO_3$ as electrolyte.

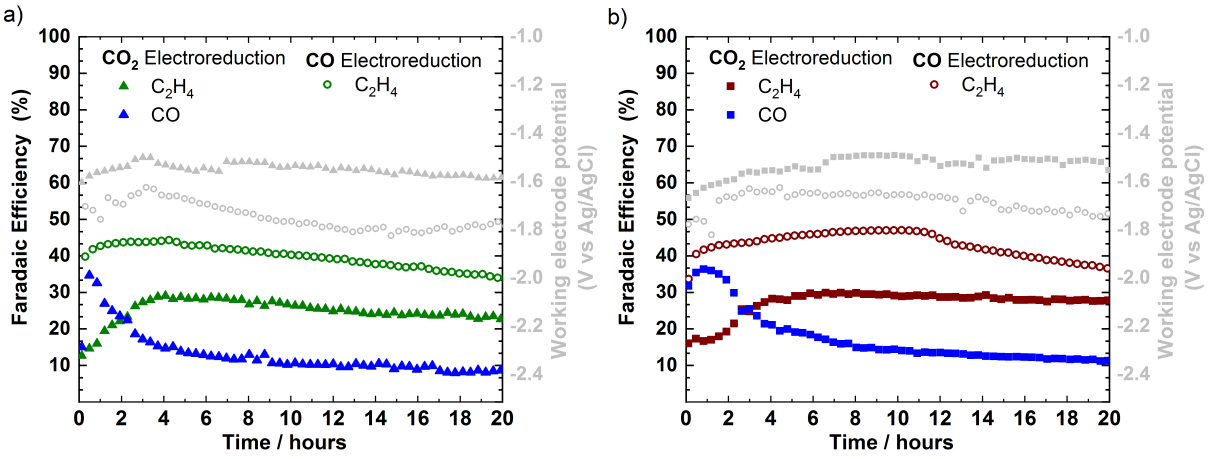

Figure 3.5: Faradaic efficiencies for gas products during long term experiments at −200 mA/cm^2 on a) Cu–NPs 40-60 nm and on b) Cu–NPs <100 nm with CO_2 or CO as the reactant

Using CO as the reactant, a high production of ethylene was observed right from the beginning of the experiment with a gradual increase during the first hours, followed by a steady decrease. For the sample with the smallest particle size, a maximum of 44 % FE for ethylene was achieved after the first 4 h, while with CuNPs <100 nm the highest Ethylene FE, 47 %, was achieved after 10 h. After that, the production of ethylene decreased to 37 % FE. In both cases, even with a drop on the selectivity, the production of ethylene after 20 h using CO as feed gas was still around 10 % higher than the one achieved with CO_2. The maximum Faradaic efficiency for

ethylene achieved was slightly higher than the one reported by Schmid et al. [120] (40 %) with CO as the reactant. They observed a sharp decrease to 10 % FE ethylene after the first 90 min of electrolysis. This decrease was attributed to a structural degradation of the active species formed during the in-situ deposition. With our preparation of the electrode using nanoparticles, only a gradual and slow degradation was observed after 20 h.

This gradual decrease can be explained by the loss of hydrophobicity of the gas diffusion layer during electrolysis. As reported by Dinh et al. [119] carbon gas diffusion electrodes turn from hydrophobic to hydrophilic when a negative potential is applied, so that during the electrolysis the electrode becomes soaked with electrolyte. With a flooded electrode, CO/CO_2 diffusion from the gas side to the catalyst is obstructed, decreasing the CO/CO_2 reduction rate and favoring the hydrogen evolution reaction. In addition, after long term experiments a slight change in the appearance of the membrane was observed. The transparent cation exchange membrane became slightly brown in some spots. This suggests that some Cu particles were stripped off of the catalyst and deposited onto the membrane. Thus, the gradual decrease in performance can also be attributed to catalyst delamination during electrolysis.

3.4.6 Characterization of Cu particles as powder and at GDL surface before and after electrolysis

Before deposition on the GDL, the Cu powders were microstructurally characterized: particle morphologies and size distributions were investigated by TEM or SEM. The constituent crystallographic phases and mean crystallite sizes were determined by XRD. Whereas nanoparticles depict some faceting and sharp edges, microparticles are mostly spherical as can be observed in Fig. 3.6. Particle size distribution determined by geometrical measurement on several micrographs confirm the supplier specifications as shown in Fig. 3.8 of the supporting information. All powders are polycrystalline, composed mainly of metallic Cu and a fraction of Cu_2O. Results for crystallite size, determined using the Scherer equation for the signals with the highest intensity, are also reported in Fig. 3.10 and Table 3.5 of the supporting information. For the nanopowders the mean crystallite size, determined by XRD, is similar to the particle size obtained by TEM. For the Cu-micro-powder the mean crystallite size determined by XRD amount to ∼30-80 nm indicating that each microparticle consists of several crystallites.

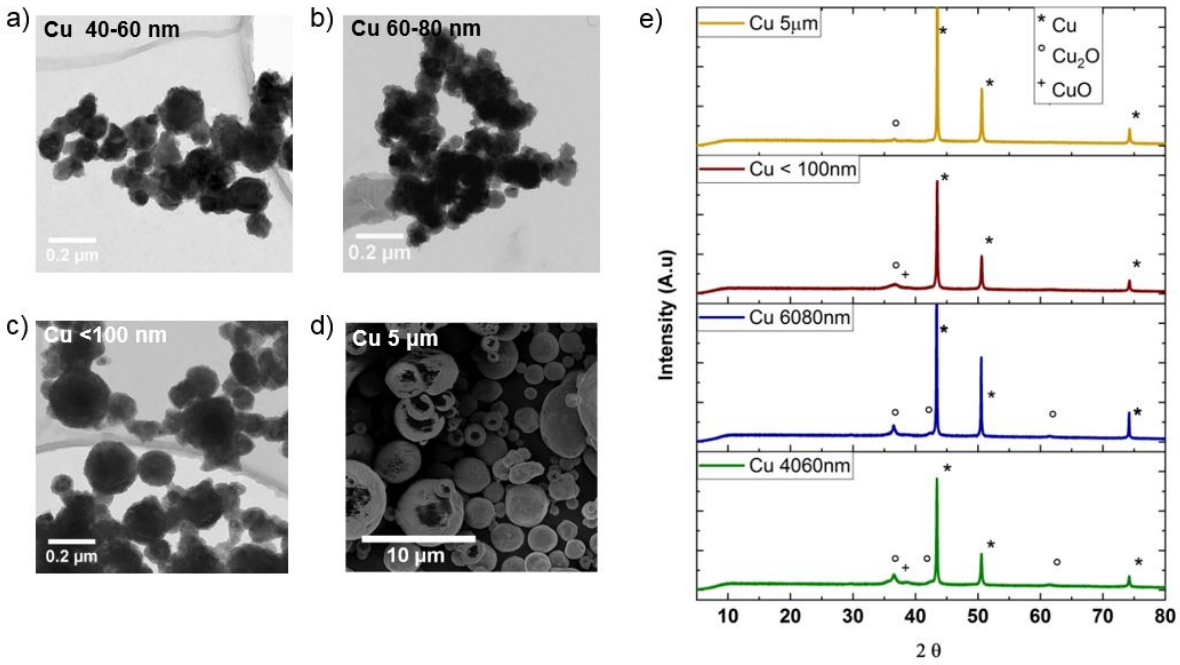

Figure 3.6: a) b) c) TEM micrographs of Cu-powders CuNPs 40-60 nm CuNPs 60-80 nm and CuNPs <100 nm; d) SEM micrograph of Cu powder 5 µm e) XRD patterns for the four commercial Cu-powders investigated

Particle size distribution after Cu deposition on the GDL was obtained by geometrical measurements on SEM micrographs. A significant change in the particle size distribution after deposition compared to the starting material is not discernible (see SEM images and corresponding histograms in Fig. 3.8 of the supporting information). Furthermore, the SEM micrographs after deposition show a difference between nanoparticles and microparticles regarding GDL coverage. Whereas using nanoparticles the GDL is completely covered, with microparticles the GDL coverage is incomplete for samples prepared with the same catalyst loading.

Electrodes used for long term experiments with CO_2 and CO as reactants were also characterized by SEM and XRD as shown in Fig. 3.7. After CO_2 electrolysis for the two investigated cases, a change in particle surface morphology is discernible: the initial grains appear to be overgrown by an even finer nanostructure in such a way that larger initially spherical grains turned into cauliflower shaped structures. After CO electrolysis cauliflower morphology is also observed. Additionally, differently from the CO_2 case, nanoaggregates depicting a cubic morphology are observed after CO electrolysis. These changes in particle surface morphology for both CO_2 and CO cases are not discernible by XRD: The XRD diffraction patterns only show the same crystallographic phase as before electrolysis (see Table 3.5 of the supporting information). A possible explanation for these differences in surface nano-aggregates after CO_2 and CO electrochemical reduction can be related to a local pH change during electrolysis. Although in both cases 1 M $KHCO_3$ was used as electrolyte, the pH value of the bulk electrolyte after electrolysis with CO changed from 8 to 10.5, while with CO_2 the pH only increased from

8 to 8.5, since the presence of CO_2 in the electrolyte has also a buffer effect. Here, it should be taken into account that all long experiments were performed with a mixed electrolyte. For this reason the pH changes before and after electrolysis are not as strong as in the experiments reported in section 3.4.3.

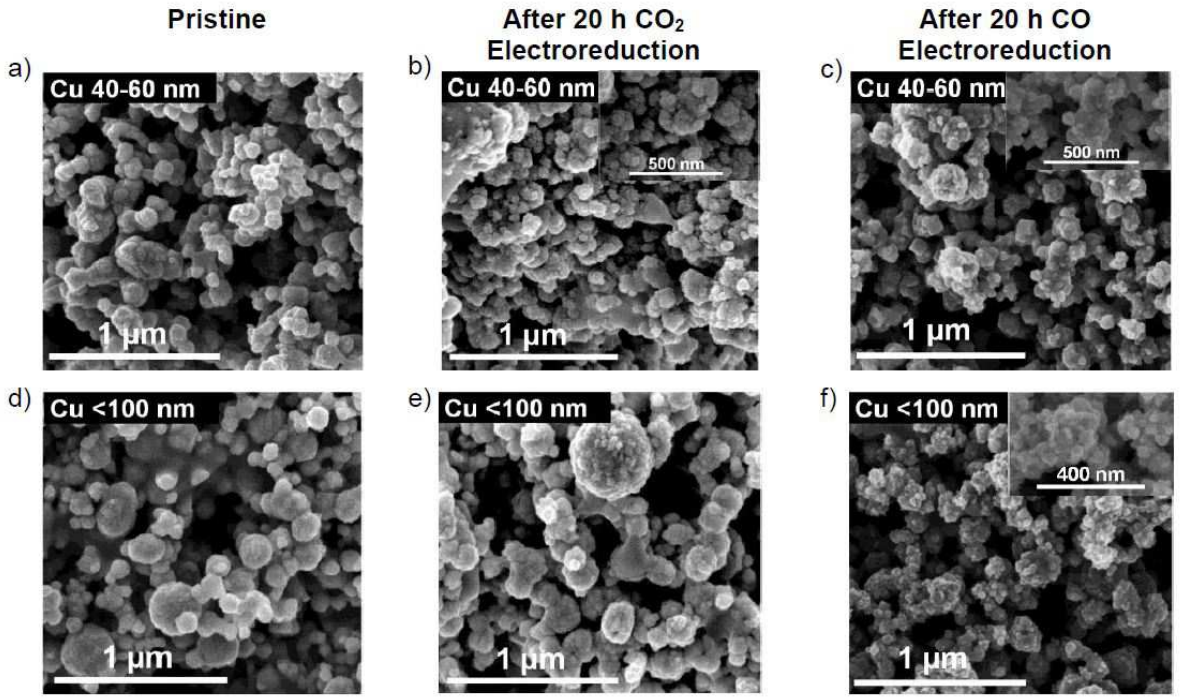

Figure 3.7: SEM micrographs of CuNPs 40-60 nm electrode: a) before, b) after CO_2, and c) after CO electrolysis. SEM micrographs of CuNPs <100 nm electrodes: d) before, e) after CO_2 and f) after CO electrolysis

We suggest that the higher selectivity for ethylene using CO as reactant is mainly the result of high CO coverage and improvement of the mass transport, but it might also be due to the morphological change of the Cu nanoparticles during electrolysis, rather than due to the amount of Cu surface oxide or the crystalline structure.

3.5 Conclusion

The electrochemical reduction of CO_2 and CO towards C1, C2, and C3 products is investigated. The focus lies on the production of ethylene, ethanol, and *n*-propanol using Cu-nanopowders deposited on gas diffusion layers as electrodes. This allows a fair comparison of the reactants, where neither solubility nor mass transport limits the reduction reaction. We report a remarkable increase in the selectivity towards ethylene, ethanol, and n-propanol of more than two-fold using CO as the reactant (cumulative 89 % FE at $-300\,mA/cm^2$) in comparison with the

direct CO_2 electroreduction (34 % FE cumulative at −300 mA/cm^2) in a mild electrolyte. The results also suggest that particle morphology and size, rather than oxidation state of Cu might play an important role in the preparation of electrodes for application at industrially relevant current densities. Nanoparticles (40-60 nm, 60-80 nm, >100 nm) become more selective with higher current densities, while the selectivity towards C2 and C3 products using microparticles (5 µm) decreases at current densities higher than −150 mA/cm^2. This can be attributed to the active surface area available for the CO reduction with nanoparticles, which is higher than with microparticles with the same catalyst loading. Furthermore, 20 h experiments show a relatively stable production of ethylene. These results demonstrate that a two-step electrochemical reduction of CO_2 can provide a more selective route to the production of ethylene, ethanol, and *n*-propanol than one step CO_2 electroreduction.

Acknowledgments

The Authors thank Prof. Eisenreich from the Technical University of Munich for his support with the NMR measurements; Dr. Ralf Krause and Dr. Christian Reller from Siemens AG for their support with the XRD characterization. N.S. Romero Cuellar would like to express her gratitude to the TUM Graduate School, to Riley Mather for language editing, and to her Siemens colleagues Dr. Erhard Magori, Dr. Remik Pastusiak, Dr. Angelika Tawil, Christian Scherer and Bernhard Schmid for the valuable discussions and support in the laboratory.

This research did not receive any specific grant from funding agencies in the public, commercial, or not-for-profit sectors.

3.6 Supporting Information

3.6.1 TEM and SEM Histograms

The starting materials as powder as well as the electrodes before electrolysis were analyzed with TEM and SEM in order to determine the particle size distribution of the four samples investigated.

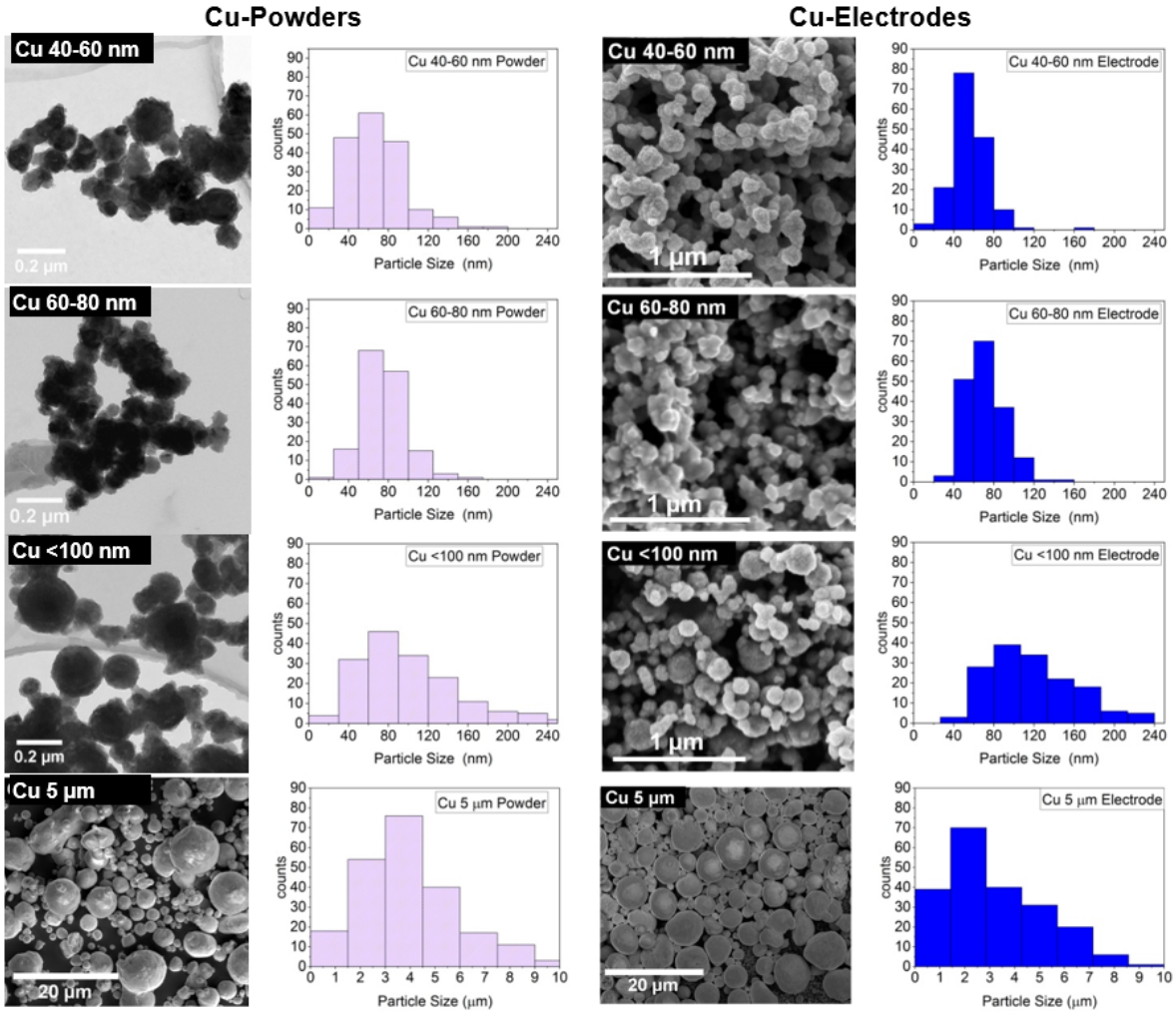

Figure 3.8: TEM micrographs and Histograms of Cu-powders CuNPs 40-60 nm, CuNPs 60 –80 nm, CuNPs <100 nm and SEM micrograph of Cu-powder 5 µm. SEM micrographs and histograms of the four Cu-electrodes investigated after deposition

3.6.2 SEM micrographs from a FIB cut of a GDL coated with copper nanoparticles

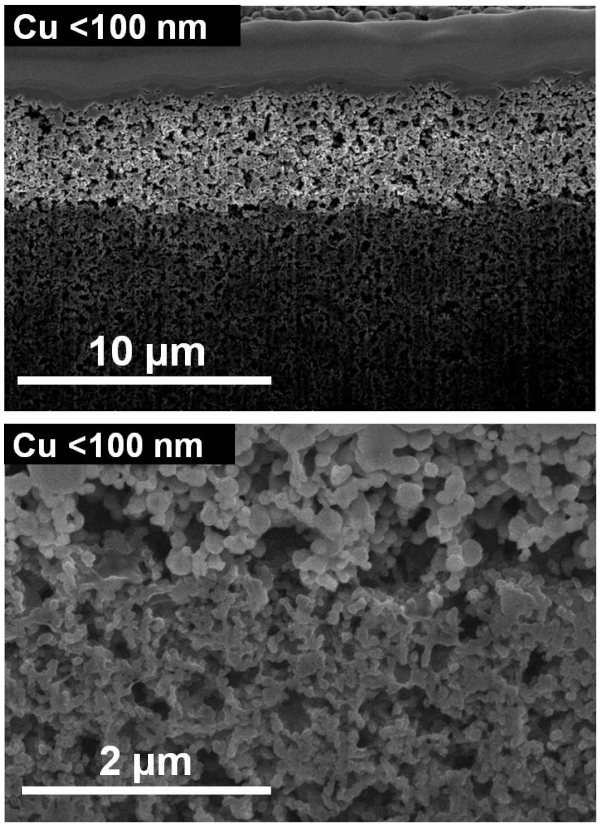

Figure 3.9: SEM micrographs from a FIB cut of a GDL after deposition of copper nanoparticles

3.6.3 XRD – Crystallite Size

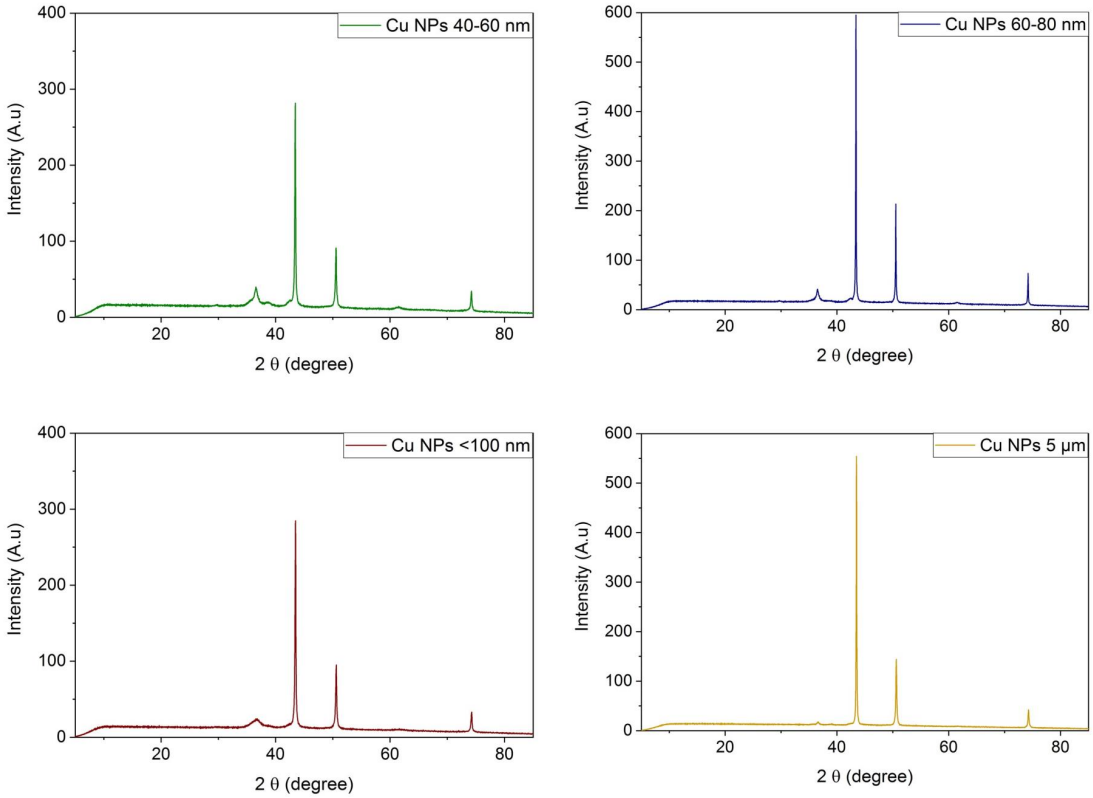

Figure 3.10: XRD patterns for the four Cu commercial powders investigated

Table 3.3: Crystallite Size calculated with the Scherer equation with $K = 0.9$ and $\lambda = 1,54$.

	2 Θ	FWHM	Crystallite Size (nm)
Cu 40-60 nm	43.5	0.16624	51.44
	50.6	0.24039	36.55
Cu 60-80 nm	43.5	0.09418	90.79
	50.6	0.10693	82.15
Cu <100 nm	43.5	0.16684	51.26
	50.6	0.22857	38.45
Cu 5 µm	43.5	0.11465	74.60
	50.6	0.19243	45.67

3.6.4 Experimental Set-up

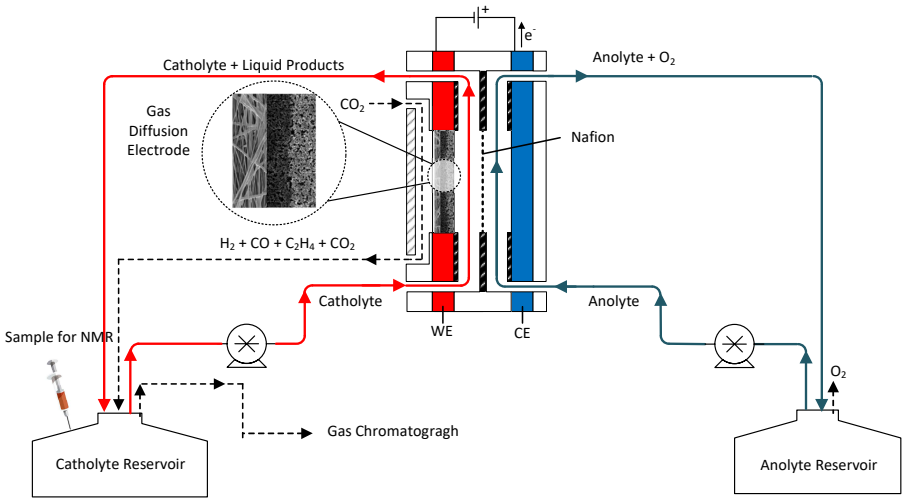

Figure 3.11: Schematic representation of the experimental set-up with separated anolyte and catholyte

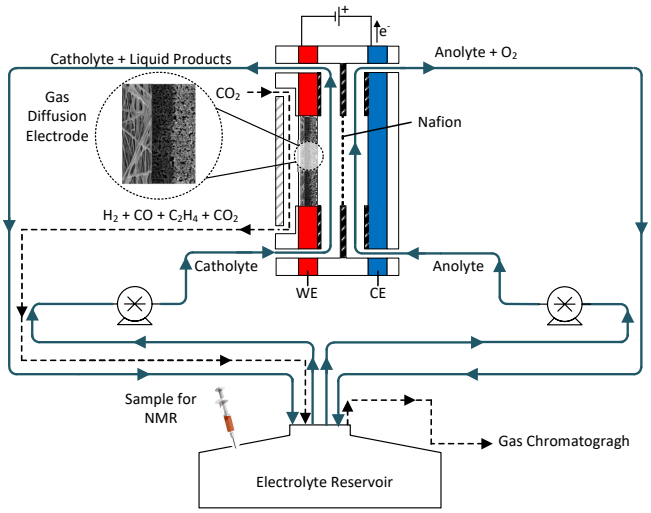

Figure 3.12: Schematic representation of the experimental set-up for long-term experiments with mixed electrolyte

3.6.5 Potentiostatic experiments with CO_2 and CO as reactant

Table 3.4: Faradaic efficiencies for the CO_2 electrochemical reduction by potential variation on Cu gas diffusion electrodes

Sample	WE	j	CO	CH_4	C_2H_4	PrOH	EtOH	Acetate	Acetone	MeOH	Ethylen-	Allyl-	Formate	H_2	Total
	V	*mA/cm²*									glycol	alcohol			
Cu 40-60 nm	-1.2	-10.70	14.56	0.00	0.00	0.00	4.08	1.65	0.00	0.00	1.34	0.00	7.32	79.53	108.48
	-1.3	-26.70	22.29	0.00	0.00	0.00	0.14	0.21	0.00	0.00	0.29	0.00	13.29	60.09	96.30
	-1.4	-67.16	35.07	0.00	6.17	2.28	2.18	0.12	0.00	0.00	0.32	0.00	17.68	34.81	98.63
	-1.5	-146.36	25.75	0.51	13.94	3.43	6.40	0.27	0.05	0.00	0.30	0.38	11.79	32.93	95.76
Cu 60-80 nm	-1.2	-12.18	28.44	0.00	0.00	0.00	0.00	3.83	0.00	1.50	0.00	0.00	6.89	76.63	117.30
	-1.3	-28.36	32.33	0.00	0.00	0.00	1.88	0.01	0.00	0.00	0.00	0.00	13.25	54.44	101.91
	-1.4	-50.96	40.02	0.00	5.27	2.05	1.28	0.00	0.05	0.00	0.52	0.00	22.69	40.18	112.05
	-1.5	-110.59	35.76	0.41	10.86	2.86	4.70	0.00	0.09	0.00	0.41	0.00	22.36	41.23	118.69
Cu <100 nm	-1.2	-10.08	28.44	0.00	0.00	0.00	0.00	0.00	0.00	0.00	1.33	0.00	4.57	70.82	105.15
	-1.3	-26.44	32.33	0.00	0.00	0.00	0.00	0.16	0.00	0.00	0.39	0.00	9.14	55.93	97.96
	-1.4	-56.83	40.02	0.00	3.55	1.77	1.78	0.05	0.00	0.00	0.18	0.17	14.90	35.65	98.05
	-1.5	-119.91	35.76	0.22	11.02	3.59	4.27	0.29	0.09	0.00	0.28	0.19	12.96	25.39	94.06
Cu 5 µm	-1.2	-9.87	26.17	0.00	0.00	0.00	0.00	4.16	0.00	0.00	0.00	0.00	14.69	78.44	123.45
	-1.3	-24.79	27.43	0.00	4.06	2.30	3.33	0.00	0.00	0.00	0.91	0.00	16.33	55.06	109.42
	-1.4	-51.56	21.05	1.09	8.40	2.27	3.34	0.03	0.11	0.00	0.24	0.00	11.51	61.79	109.83
	-1.5	-100.54	10.65	3.52	11.56	2.23	4.76	0.27	0.04	0.00	0.45	0.81	7.71	69.01	110.99

Table 3.5: Faradaic efficiencies for the CO electrochemical reduction by potential variation on Cu gas diffusion electrodes

Sample	WE	j	CH_4	C_2H_4	PrOH	EtOH	Acetate	Acetone	MeOH	Ethylen-	Allyl-	Formate	H_2	Total
	V	*mA/cm²*								glycol	alcohol			
Cu 40-60 nm	-1.2	-7.68	0.00	5.81	4.86	6.39	2.83	0.00	0.00	0.00	0.00	0.00	86.06	105.97
	-1.3	-18.22	0.00	10.77	9.59	4.75	1.16	0.42	0.00	1.52	0.00	0.00	63.08	91.29
	-1.4	-42.28	0.39	22.46	17.81	9.00	2.57	0.06	0.00	1.29	2.44	0.09	38.95	95.07
	-1.5	-68.20	0.35	27.63	23.62	13.46	4.20	0.04	0.08	0.80	2.80	0.13	28.55	101.67
Cu 60-80 nm	-1.2	-4.45	0.00	6.71	0.00	0.00	4.56	0.00	0.00	3.88	0.00	0.00	91.62	106.79
	-1.3	-10.34	0.00	7.02	6.66	8.35	0.71	1.28	0.00	0.66	0.00	0.00	72.10	96.78
	-1.4	-20.74	0.00	12.11	13.62	4.34	1.42	0.00	0.00	1.05	1.08	0.20	56.81	90.63
	-1.5	-42.02	0.40	21.45	20.03	10.08	2.82	0.00	0.00	1.38	2.64	0.08	37.66	96.53
Cu <100 nm	-1.2	-7.82	0.00	6.30	7.82	5.63	1.21	0.00	0.00	1.38	0.00	1.17	75.64	99.14
	-1.3	-17.96	0.00	9.79	13.76	7.23	2.41	0.00	0.00	1.16	0.00	0.35	54.16	88.86
	-1.4	-40.58	0.00	19.58	27.29	10.90	3.20	0.12	0.11	1.27	1.70	0.01	33.00	97.18
	-1.5	-104.03	0.00	29.35	28.06	14.14	4.28	0.00	0.00	0.35	1.81	0.14	17.42	95.53
Cu 5 µm	-1.2	-5.59	0.00	6.44	7.02	6.45	2.49	0.00	0.00	2.99	0.00	1.78	80.50	107.68
	-1.3	-14.80	0.79	10.49	7.62	6.86	1.24	0.00	0.00	0.83	2.04	0.21	54.21	84.29
	-1.4	-41.74	1.67	13.02	7.23	10.32	2.24	0.28	0.05	0.66	1.26	0.17	44.88	81.78
	-1.5	-107.83	0.99	14.11	3.85	10.70	4.74	0.07	0.00	0.95	1.05	0.11	45.70	82.26

3.6.6 Galvanostatic experiments with CO_2 and CO as reactant

Table 3.6: Faradaic efficiencies for the CO_2 electrochemical reduction by current density variation on Cu gas diffusion electrodes

j (mA/cm^2)	Sample	CO	Methane	Ethylene	PrOH	EtOH	Acetate	Acetone	MeOH	ETG	Allyl-alcohol	Formate	H_2	Total
-100	40-60 nm	47.30	0.00	3.89	1.17	1.02	0.08	1.00	0.01	2.62	0.00	15.05	32.71	104.84
-100	60-80 nm	51.54	0.00	7.25	1.52	2.52	0.14	0.04	0.00	0.01	0.00	14.38	24.96	102.36
-100	<100 nm	46.26	0.00	2.76	0.19	0.29	0.05	0.02	0.01	0.06	0.07	5.33	33.73	88.76
-100	5 µm	32.88	1.48	10.75	1.47	2.83	0.00	0.00	0.02	0.34	0.48	9.33	41.50	101.09
-150	40-60 nm	45.51	0.00	8.70	1.90	2.21	0.16	0.00	0.08	0.70	0.00	14.79	21.60	95.66
-150	60-80 nm	47.04	0.18	14.78	3.11	4.17	0.28	0.07	0.00	0.22	0.33	12.18	17.88	100.23
-150	<100 nm	47.39	0.00	6.64	1.47	1.44	0.00	0.04	0.01	0.09	0.63	14.84	21.78	94.32
-150	5 µm	15.04	5.11	18.08	2.90	5.53	0.11	0.20	0.00	0.00	0.49	6.71	48.22	102.40
-200	40-60 nm	41.25	0.00	13.97	3.17	3.63	0.25	0.98	0.00	0.00	0.29	15.09	17.67	96.30
-200	60-80 nm	40.14	0.15	21.49	4.77	6.39	0.40	0.10	0.00	0.24	0.48	10.16	16.56	100.89
-200	<100 nm	43.50	0.00	11.06	5.85	4.84	0.00	0.04	0.01	0.16	0.00	25.86	17.89	109.22
-200	5 µm	5.81	3.96	13.88	1.64	6.90	0.60	0.01	0.01	0.78	0.47	3.83	52.74	90.62
-250	40-60 nm	35.74	0.08	18.91	5.36	5.33	0.44	0.00	0.00	0.07	0.38	16.18	16.73	99.21
-250	60-80 nm	32.63	0.13	26.64	5.12	6.97	0.46	0.01	0.00	0.20	0.50	9.51	15.88	98.03
-250	<100 nm	39.26	0.00	16.00	2.93	1.78	0.00	0.06	0.00	0.06	0.00	5.99	17.12	83.20
-250	5 µm	2.20	1.83	6.09	0.80	4.23	0.50	0.00	0.03	0.41	0.14	1.25	64.79	82.26
-300	40-60 nm	31.08	0.07	24.37	4.63	4.64	0.32	0.00	0.00	0.13	0.25	8.95	17.46	91.90
-300	60-80 nm	26.75	0.12	33.04	4.53	6.50	0.40	0.03	0.00	0.19	0.50	5.04	16.56	93.68
-300	<100 nm	31.25	0.07	19.71	5.85	4.03	0.00	0.03	0.04	0.10	0.00	11.28	17.28	89.63
-300	5 µm	1.28	1.17	3.51	0.33	2.42	0.34	0.00	0.02	0.41	0.00	0.91	87.96	98.36

Table 3.7: Faradaic efficiencies for the CO electrochemical reduction by current density variation on Cu gas diffusion electrodes

j (mA/cm^2)	Sample	CH_4	C_2H_4	PrOH	EtOH	acetate	acetone	MeOH	ETG	allyl-alcohol	formate	H_2	Total
-100	40-60	0.92	39.42	16.13	10.22	4.00	0.10	0.03	0.85	2.09	0.11	32.61	106.48
-100	60-80	0.51	38.86	14.26	12.55	3.76	0.11	0.01	0.32	2.18	0.14	32.90	105.61
-100	<100	0.49	36.71	18.60	11.15	3.09	0.12	0.02	0.59	2.43	0.12	36.79	110.09
-100	5 um	3.51	37.14	7.02	13.16	4.08	0.14	0.00	1.09	1.65	0.12	39.56	107.48
-150	40-60	0.34	44.73	16.10	11.66	5.59	0.08	0.02	0.40	2.40	0.08	24.53	105.94
-150	60-80	0.23	43.79	17.22	17.30	5.92	0.04	0.03	0.86	2.73	0.17	24.33	112.63
-150	<100	0.27	42.84	17.77	11.24	4.07	0.04	0.07	0.22	2.33	0.09	25.81	104.75
-150	5 um	1.61	43.38	7.23	21.54	7.96	0.16	0.04	0.32	1.69	0.09	30.50	114.51
-200	40-60	0.14	48.51	16.53	13.73	7.27	0.07	0.01	0.27	2.34	0.08	19.12	108.06
-200	60-80	0.13	47.11	13.49	15.70	6.26	0.05	0.04	0.50	2.06	0.09	19.24	104.67
-200	<100	0.00	47.02	17.26	11.70	4.66	0.02	0.00	0.25	1.67	0.06	19.66	102.30
-200	5 um	1.65	37.78	3.51	17.63	8.23	0.02	0.02	0.00	0.80	0.05	43.07	112.74
-250	40-60	0.00	52.39	17.49	16.40	9.21	0.00	0.02	0.47	2.32	0.05	15.79	114.14
-250	60-80	0.10	49.68	14.91	17.63	7.87	0.00	0.01	0.39	2.26	0.12	16.09	109.05
-250	5 um	1.58	26.67	2.29	14.24	9.37	0.00	0.07	0.00	0.53	0.00	64.51	119.27
-300	40-60	0.00	54.99	17.66	16.79	10.19	0.00	0.03	0.11	1.92	0.55	11.18	113.42
-300	60-80	0.09	51.83	9.69	13.01	6.32	0.04	0.01	0.43	0.83	0.09	13.91	96.26
-300	<100	0.00	52.52	15.98	11.95	5.86	0.00	0.00	0.48	1.72	0.10	13.23	101.84
-300	5 um	1.64	19.53	2.06	13.27	10.30	0.00	0.01	0.00	0.75	0.03	81.26	128.85

3.6.7 Reproducibility measurements

The results shown above were reproduced obtaining only slight measurement deviations as shown in Figs. 3.13 and 3.14.

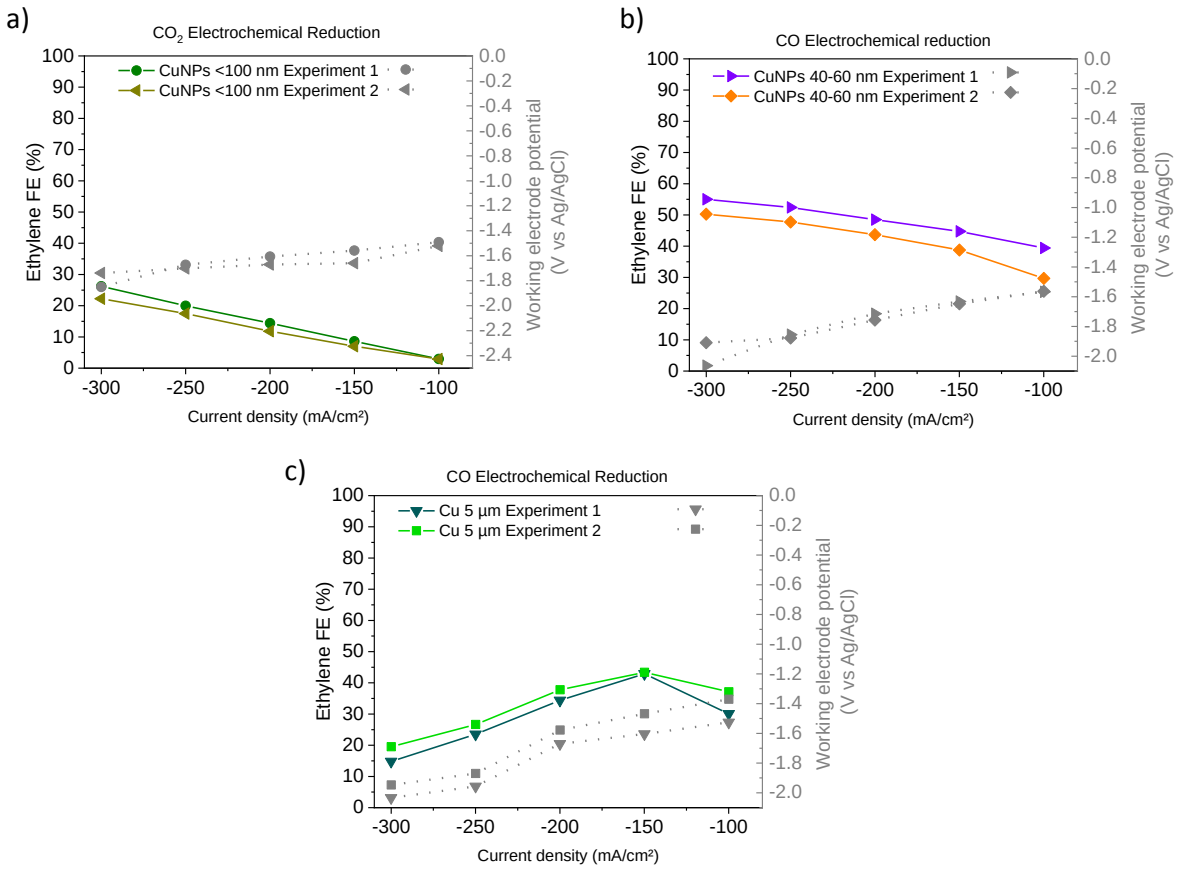

Figure 3.13: Reproducibility measurements of current density variation with: a) CO_2 as reactant and CuNPs<100 nm and b) CO as reactant and CuNPs 40-60 nm c) CO as reactant and Cu 5 µm

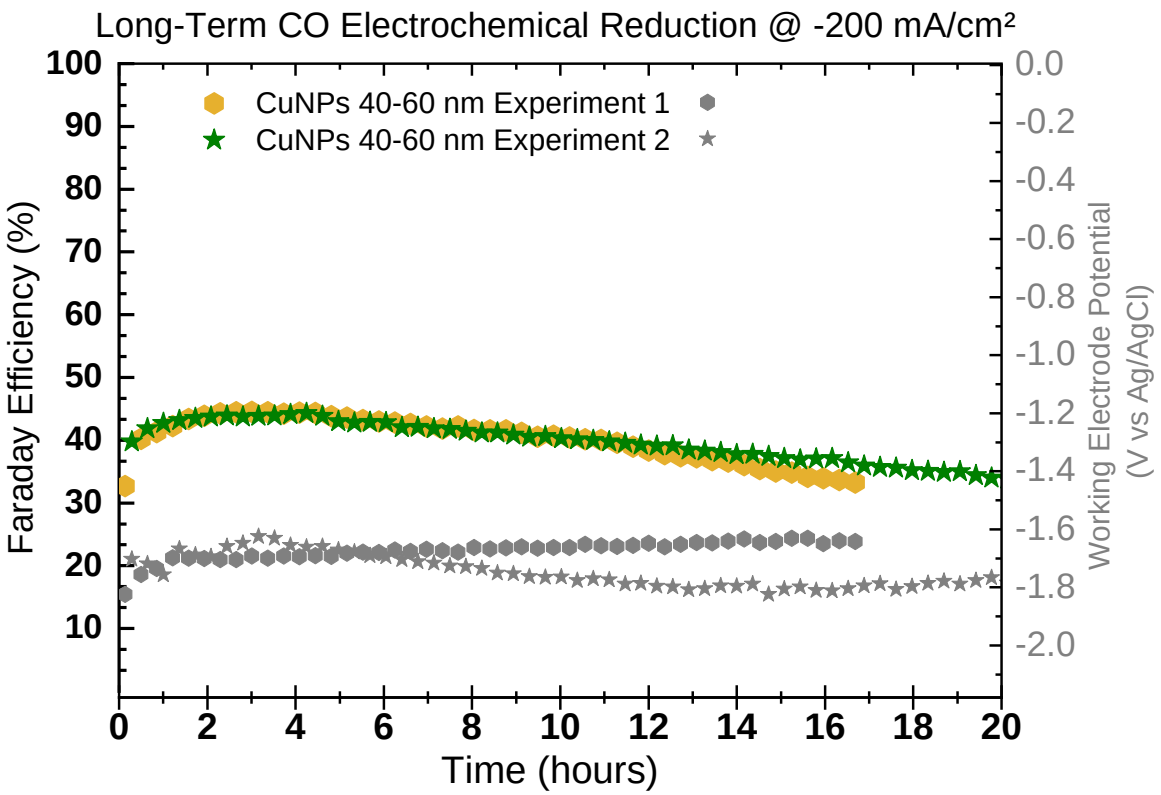

Figure 3.14: Reproducibility measurements of ethylene production at -200 mA/cm² using CO as reactant and CuNPs 40-60 nm

3.6.8 XRD before and after electrolysis

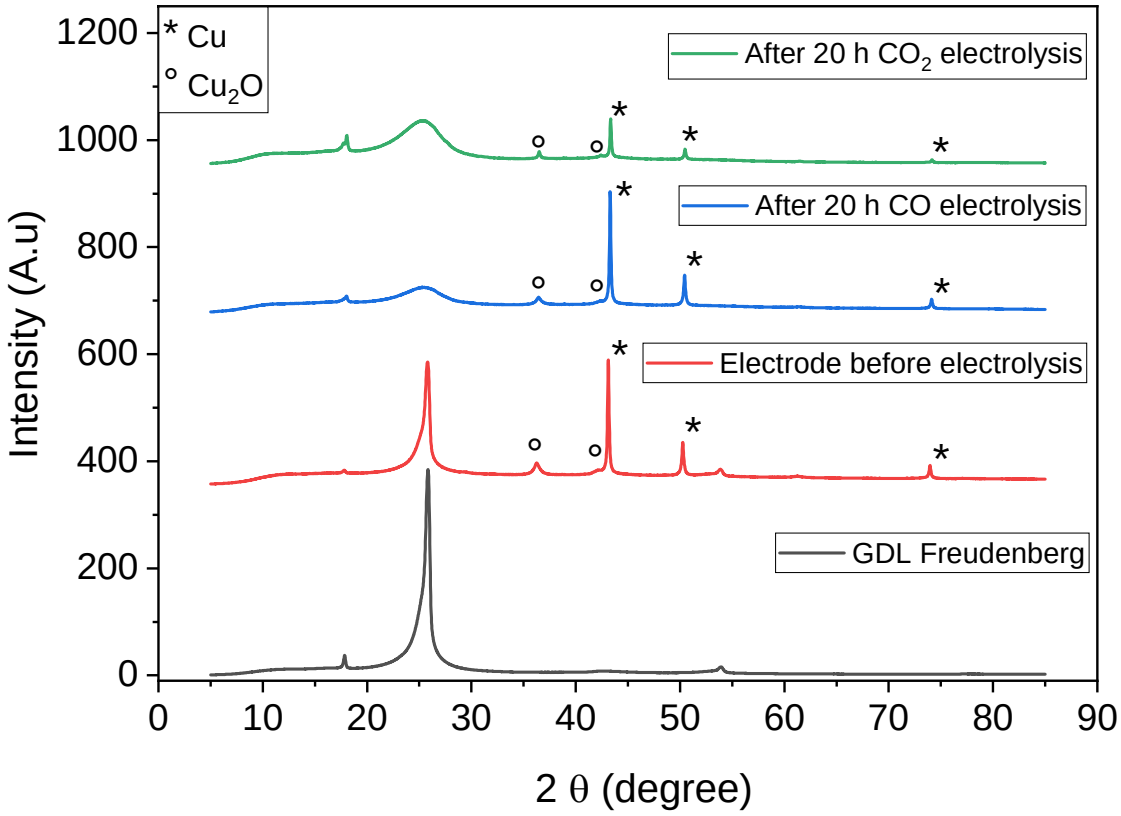

Figure 3.15: XRD pattern of a CuNPs 40-60 nm electrode before and after electrolysis

4 Two-step electrochemical reduction of CO_2 towards multi-carbon products at high current densities

This chapter is based on:

N. S. Romero Cuellar, C.Scherer, B. Kackar, W. Eisenreich, C. Huber, K. Wiesner-Fleischer, M. Fleischer, O. Hinrichsen, Two-step electrochemical reduction of CO_2 towards multi-carbon products at high current densities. Journal of CO_2 Utilization. 2019, 36, 263-275.
DOI: 10.1016/j.jcou.2019.10.016.

Author contributions:

N. S. Romero Cuellar prepared the Cu electrodes, performed the experiments, evaluated the results reported in sections 4.4.3, 4.4.4, and 4.4.5. N. S. Romero Cuellar also wrote the manuscript with input from all authors. C.Scherer and B. Kackar conducted the experiments and evaluated the results for the first electrolyzer reported in section 4.4.2. GC-MS analysis of isotopic gas and liquid samples was conducted by C. Huber. The quantification of the isotopic labeling experiments was performed by W. Eisenreich and C. Huber. The two-step electrochemical system was conceived by N. S. Romero Cuellar, C.Scherer and M. Fleischer. Two-step electrochemical experiments were conducted by N. S. Romero Cuellar, C.Scherer and B. Kackar. K. Wiesner-Fleischer, M. Fleischer and O. Hinrichsen supervised and guided all the findings of this work. All authors discussed the results and revised the manuscript.

4.1 Abstract

Two-step electrochemical reduction of CO_2 is considered as an alternative to increase selectivity towards C2 and C3 products. In this type of proposed cascade electrocatalytic operation, CO is produced in a first step and subsequently reduced to multi-carbon products in a second step with significantly higher Faradaic efficiencies compared to a one-step process. Research efforts have been focused on the feasibility of the isolated second step with pure CO as reactant, however the interdependencies of both steps need to be considered. Accordingly, two-step electrochemical reduction of CO_2 is studied in this work as an integrated system. Taking into account that the study of this technology at high current densities is crucial for industrial applicability, Gas Diffusion Electrodes and Flow-Cells were used for operation at current densities above $-200\,mA/cm^2$. An integrated two-cell electrolysis system was built and optimized. Firstly, each step was characterized separately, the first using a silver gas diffusion electrode to generate a mixture of humidified CO, H_2, and unreacted CO_2; the second step using copper nanoparticles on a carbon-based gas diffusion structure to obtain C2 and C3 products. This step was studied using synthetic mixtures of CO_2 and CO with different ratios. Furthermore, experiments with isotope labeled $^{13}CO_2$ and ^{13}CO were performed in order to obtain some insights on the (electrochemical) reaction path of gas mixtures containing CO_2 and CO. Subsequently, the two units were integrated into a system, where the full gas output of the first unit was directly fed to the second unit. The total Faradaic efficiency towards multi-carbon products of this initial system was limited to 20 % at total current density of $-470\,mA/cm^2$. These initial results together with the isotopic labeling studies indicate that the presence of significant amounts of unreacted CO_2 from the first step is detrimental for the second step. A significant improvement was achieved by introducing a CO_2 absorption column between the two units and after splitting the overall charge flow applied in each cell in accordance with the main reaction at each step. With this set-up a total Faradaic efficiency towards C2 and C3 products of 62 % at a total current density of $-300\,mA/cm^2$ was achieved. The results confirm the need for a gas separation technique between the two steps for a feasible two-step electrochemical reduction of CO_2.

4.2 Introduction

Within the context of the current energy system transformation, new technologies that allow a sustainable energy supply have gained special attention in the scientific community as well as in the industrial sector [3, 12, 13, 132]. Some of the decisive aspects for the development of these new technologies are the inclusion of renewable energies, the decentralization of the energy system, and a low carbon economy. The electrochemical reduction of CO_2 presents a potential solution for the integration of renewable energies into the value-added chain of

materials by transforming CO_2 into energy-intensive chemical products [28, 29, 34, 96, 115]. This electrochemical pathway, driven by renewable electricity sources, can provide more environmentally friendly chemicals and fuels than the traditional chemical processes driven by fossil energy [25]. However, an industrial application of the electrochemical conversion of CO_2 into multi-carbon products has still challenges to overcome, such as high overpotentials and rapid electrode degradation, as well as low efficiency and selectivity [28, 30, 96].

While the electrochemical reduction of CO_2 to C_1 products such as CO [85, 133–136] and HCOOH [117, 118, 137] have been reported to achieve high Faradaic efficiencies (FE) at high current densities, the electrochemical path of CO_2 to C2 and C3 products such as ethanol, ethylene, and *n*-propanol still has to deal with low selectivity and high overpotentials at industrially relevant current densities. The electrocatalytic conversion of CO_2 into multi-carbon products has been proven to be successful only with Cu as the electrocatalyst [33, 35, 38]. Thus, Cu electrocatalytic activity and its performance under different conditions have been widely studied [35, 40, 52, 53, 57, 70, 94, 122, 124, 125]. Although a significant progress has been made regarding the development of more selective and stable electrocatalysts [51, 52, 71, 72], an optimal approach for the production of hydrocarbons and oxygenates with high FE and at high current densities has still to be identified.

Some of the challenges when reducing CO_2 directly into C2 and C3 products are the high overpotentials and poor selectivity due to the multiple reactions that can take place simultaneously [35]. Nevertheless, the scientific community has already elucidated important aspects that should be taken into account in order to increase the selectivity to hydrocarbons and oxygenates. Studies about CO_2 conversion into multi-carbon products on Cu electrodes have reported CO to be the main intermediate [48, 93, 120]. Furthermore, experimental reports have shown that alkaline conditions lead to higher FE towards multi-carbon products [71, 72]. However, alkaline conditions for the direct reduction of CO_2 would lead to the formation of carbonates [54] and cause complication for up-scaling. On the other hand, direct CO electrochemical reduction has shown significant selectivity towards ethanol, acetate, and *n*-propanol at moderate overpotentials and high current densities [138, 139]. A direct CO supply allows a high CO surface coverage that enables C-C coupling [140], leading to high sensitivities of C2 and C3 products. With this in mind and the high efficiencies at high current densities achieved in electrochemical conversion of CO_2 to CO, a two-step electrochemical reduction of CO_2 becomes a worthy alternative to be explored. In this alternative approach, the complex reaction paths to C2 and C3 products will be split, where CO_2 is reduced to CO in the first step, and CO is subsequently converted into hydrocarbons and oxygenates in the second step.

Research efforts considering a two-step electrolysis as an alternative have been focused mainly on the investigation of the electrochemical reduction of pure CO as the second step. Many of the studies focused on the catalyst activity and have been performed in a batch type electrochemical

cell configuration, where the low solubility of CO causes mass transport limitations [54, 93, 94, 121, 127, 130, 141]. However, few studies have focused on a continuous flow operation mode, as well as the configuration of electrodes, which might determine the product spectrum and are of considerable importance for an energetic efficient transformation [81, 142]. Only few studies of CO electrolysis performed in flow cells with gas diffusion electrodes (GDE) have been reported [138, 139]. In a recent study, a cumulative Faradaic efficiency (FE) for C2 and C3 products of 89 % was achieved at $-300\,mA/cm^2$ by performing CO electrolysis in a flow cell using commercial Cu nanoparticles deposited onto gas diffusion layers [139]. This cumulative FE was two fold higher than what was achieved from CO_2 electrolysis. Furthermore, Jiao et al. [138] achieved a 91 % cumulative Faradaic efficiency for C2 products at $-630\,mA/cm^2$ using oxide-derived copper (OD-Cu) GDEs and a flow electrolyzer. Despite the investigation of the electrochemical reduction of pure CO, only one study about a heterogeneously catalyzed two-step cascade electrochemical reduction of CO_2 to ethanol has been reported to our knowledge up to date [128]. However, the cascade electrolysis was performed using batch type cells and planar electrodes, where mass transport limitations arise due to the low solubility of CO_2 and CO in the aqueous electrolytes used. Consequently, only low current densities were achieved (lower than $-5\,mA/cm^2$).

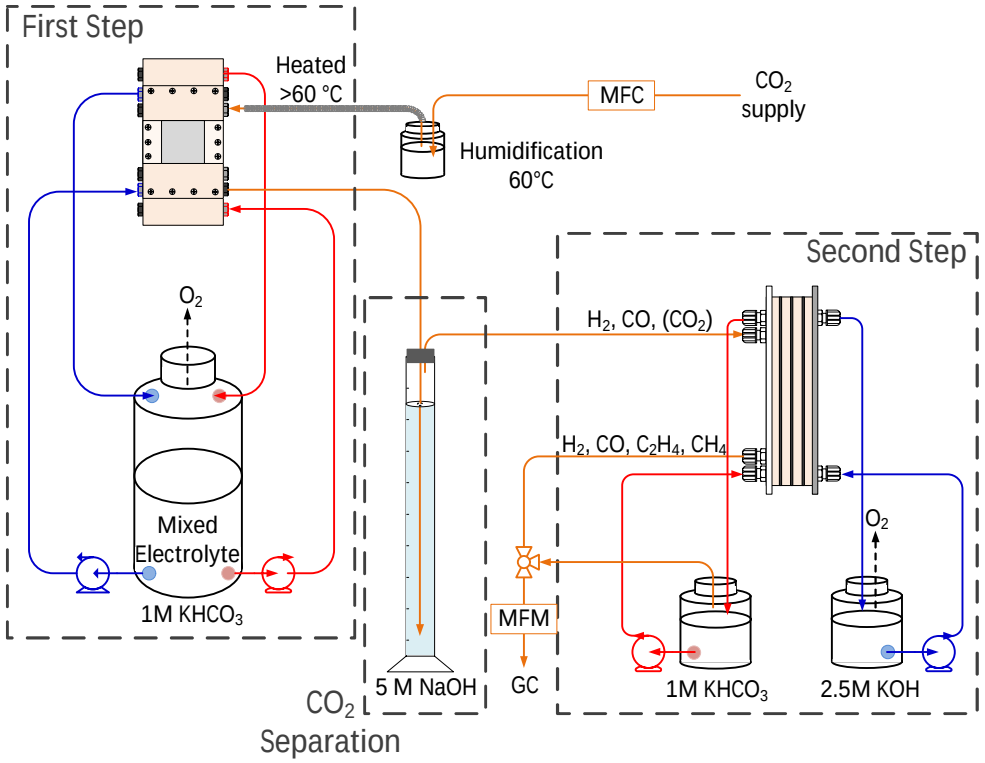

Figure 4.1: Schematic of the two-step CO_2 electrochemical reduction (Red lines for catholyte, blue lines for anolyte, yellow lines for gas)

In this work, we investigate the two-step electrochemical reduction of CO_2 as a single integrated system, using two flow cells with Ag and Cu gas diffusion electrodes, respectively. In this system, a large three phase boundary area between electrolyte, gas and electrode is achieved. Thus, the electrochemical reduction can be operated at industrially relevant current densities. Initially, each electrolyzer was investigated separately by performing linear sweep voltammetry and current density variation. For the analysis of the second electrolyzer, it was taken into account that the CO_2 supplied to the first reactor is not fully converted into CO. Thus, even with a high FE (>90 %) for CO, the product gas of the first step will be a mixture of both gases. For this reason, the electrochemical reduction of CO/CO_2 mixtures with different ratios was also investigated. As expected, the higher the amount of CO_2 the lower the efficiency for C2 and C3 products. For this reason, CO_2 absorption in NaOH was implemented before the second step as shown in Fig. 4.1, in order to increase the total Faradaic efficiency of the integrated system. Additionally, a simple calculation method for an optimal operation of the electrolyzer is proposed. With this a cumulative Faradaic efficiency towards C2 and C3 products of 62 % was obtained.

4.3 Experimental

4.3.1 Electrode preparation

For the first step, Ag-GDEs were prepared in a continuous process by casting silver particles and binder materials onto a reinforcement web as previously described [143]. For the second step, Cu-powder with a particle size range of 40-60 nm delivered by Sigma Aldrich was used for the preparation of Cu-GDEs. The electrode was prepared following a previously described method (section 3.3), in which a suspension with 60 mg of Cu-powder, 40 mg of 20 % Nafion® dispersion and 2 ml of iso-propanol was ultrasonicated and directly deposited onto a carbon-based gas diffusion layer (GDL) H23C2 from Freudenberg. This gas diffusion layer consists of two layers, namely a hydrophobic carbon fibers interface and a micro-porous layer. This procedure was repeated twice. Subsequently, the electrode was dried for at least 12 hours at room temperature under Ar atmosphere with a flow of 0.5 L/min. A catalyst loading of 3 mg/cm^2 was calculated from the weight difference of the GDL before and after deposition with a material loss in the order of 40 % within the entire preparation process. With this preparation method a three layers electrode is obtained, namely a carbon fibers interface, a diffusion layer, and a catalyst layer. While the preparation methods and resulting type of electrodes are different for Ag-GDE and Cu-GDE, in both cases the geometrical area used for the electrolysis is the same (10 cm^2).

4.3.2 First electrolyzer

An inhouse designed electrochemical flow cell was used as first electrolzyer. The cell is composed of three blocks in which channels have been machined. These blocks represent the 3-compartment setup of the flow cell: gas, catholyte, and anolyte compartment, and are made from polyether ether ketone (PEEK). A schematic cross section of the cell can be found in the supporting information (Fig. 4.9). A poly methyl methacrylate (PMMA) window is placed on the front side of the cell in order to see possible permeation of electrolyte through the GDE. O-rings in between the compartments ensure a leak free system. An IrOx coated electrode (Electrocell) with a geometrical surface area of 10 cm^2 was used as anode and a silver frame enabled the electrical contact of the Ag-GDE to the external current source. A Ag/AgCl (3 M NaCl, ALS Co.) was used as reference electrode.

As depicted in Fig. 4.1, the electrolytes where supplied to the cell from a single electrolyte reservoir. Compared to a setup where anolyte and catholyte are cycled separately, this configuration has the advantage of preventing the depletion of charge carriers in one of electrolytes [115]. The anolyte and catholyte compartment were separated by a ZrO_2 diaphragm. Two pressure pumps (MARCH PUMPEN GmbH) provided the continuous recirculation of the electrolyte through the compartments at a rate of 200 mL/min. The CO_2 feed gas (Linde 5.0) was controlled using a mass flow controller (Sensirion SFC4100). The flow rate was set to 72 sccm for single cell performance experiments and to 35 sccm for the two-step electrolysis setup. The lower CO_2 flow rate was used to reduce the amount of unreacted CO_2 in the first electrolyzer.

A fixed differential pressure of 20 mbar was set between the gas and catholyte side of the GDE. This differential pressure was sufficient to prevent the permeation of electrolyte to the gas side and low enough to inhibit a CO_2 flow through the GDE to the electrolyte side. As reported previously, at high current densities a high K^+ concentration is expected inside the pores of the Ag-GDE, which might cause K_2CO_3 precipitation [83]. Therefore, CO_2 was humidified at 60 °C by bubbling through a heated water flask, in order to avoid possible salt formation. Linear sweep voltammetry (LSV) and chronopotentiometry (CP) techniques were performed using a Bio-Logic VSP potentiostat with booster (VMP3) (Seyssinet-Pariset, France) and the corresponding EC-Lab® software. The IR-drop between the reference electrode and the Ag-GDE was determined using current interrupt technique.

4.3.3 Second electrolyzer

A micro flow cell® (Electrocell), consisting mainly of three compartments, i.e. gas, catholyte and anolyte with a geometric electrode area of 10 cm^2, was used for the second step. The

original cell was modified for the specific purpose as described previously (section 3.3.2). A schematic cross-section of the second electrolyzer is shown in the supporting information (Fig. 4.10). Cu-GDEs were used as cathode and prepared as aforementioned (3.3). These GDEs were contacted to a Ti-frame, that enables electrical contact to the electrical source. An IrOx coated electrode (Electrocell) and a Ag/AgCl (3 M NaCl) were used as anode and reference electrode, respectively. Catholyte (1 M $KHCO_3$) and anolyte (2.5 M KOH) were separated by a cation exchange membrane (Nafion® 117, DuPont). The electrolytes circulate trough the system by being pumped from each reservoir to the cell using a micro diaphragm liquid pump (NFB 25 KPDCB-4A, KNF) operated at a constant flow of 100 mL/min. For the gas supply CO/CO_2 mixtures were prepared with high purity CO_2 (Linde 5.0) and CO (Linde 4.7), which flow was controlled with mass flow controllers SFC5400 (Sensirion), that were calibrated for each gas. The performance of the second electrolyzer was investigated supplying gas mixtures with a total constant gas flow of 50 sccm. The catholyte outlet was delivered back to the cell, while the gas outlet of the cell together with the small gas outlet of the reservoir were measured with a flow meter before entering the gas chromatograph. Anolyte circulated constantly in a separated closed system between reservoir and anode, while the gas products of the anode left the system without being measured, as shown in Figure 4.1.

Electrochemical reduction of CO/CO_2 was also characterized by chronopotentiometry using a Bio-Logic VSP potentiostat, which was controlled by the EC-Lab® software. Current density variation experiments were performed by increasing the current −500 mA every 22 min in the range of −500 mA and −3000 mA. Current densities were calculated dividing the applied current by the geometrical electrode area (10 cm^2). The electrolysis was performed in a flow-by operation mode [85].

4.3.4 Two-step electrolysis

Two-step electrolysis was performed in the integrated set-up described in Fig 4.1. CO_2 was humidified and supplied to the first electrochemical cell, while electrolyte was pumped at a flow of 200 mL/min to the cathode and anode from one electrolyte reservoir containing 1 M $KHCO_3$. The first step is operated in a flow by operation mode, which is assured with a differential pressure between the gas and liquid compartment of 20 mbar. This differential pressure of the first step is hydrostatically controlled by the height of the gas outlet tubing placed inside the absorption column filled with 5 M NaOH. In this column unreacted CO_2 is separated from the produced CO and H_2. The gaseous product output from the absorption column is directed to the second electrolyzer, which operated with separated electrolytes each with a flow of 100 mL/min. In the second step CO is converted mainly to ethylene in the gas phase and ethanol and *n*-propanol in liquid phase. The total gas product outlet was measured with a mass flow meter (MFM) and subsequently injected into the gas chromatograph. The

electrochemical measurements were performed with two Bio-Logic VSP potentiostats using a galvanostatic mode, where a constant current density was set for each electrolyzer during a defined period of time.

4.3.5 Product analysis

Gas and liquid products were analyzed quantitatively by Gas Chromatography (GC) and ^{1}H Nuclear Magnetic Resonance (NMR), respectively. Gas analysis was performed in a calibrated gas chromatograph 7890B Agilent (Santa Clara, USA) with helium as carrier gas. 1 mL gas samples were automatically injected into the GC every 22 min during the electrolysis and analyzed as reported in a previous study [139]. The liquid products were analyzed taking aliquots of 1 mL from the catholyte compartment at the end of each current density step for subsequent analysis. ^{1}H NMR spectroscopy was performed using a 500 MHz AVANCE-III instrument (Bruker BioSpin, Karlsruhe, Germany) as described in a previous report [139].

Isotope profiling was performed using NMR spectroscopy for liquid products and gas chromatography mass spectroscopy (GC-MS) for both liquid and gaseous products. NMR-samples were prepared and analyzed as previously reported [139]. For GC-MS analysis of ethanol and *n*-propanol, 2 mL of the aqueous solution were heated in a closed 4 ml vial to 80 °C. The gaseous phase was transferred with a gas tight syringe into an evacuated 1.5 mL auto-sampler vial. Subsequently, 4 µL of the gaseous phase were analyzed using a GC-MS-QP 2010 Plus spectrometer (Shimadzu, Duisburg, Germany) equipped with an Equity TM-5, fused silica capillary column, 30 m x 0.25 mm and 0.25 µm film thickness (Supelco, Darmstadt, Germany). Interface and injector temperature were set to 260 °C and the column temperature was held at 30 °C. Column flow was 1.24 ml/min and the inlet pressure 62.6 kPa. The samples were analyzed three times as technical replicates in SIM mode (m/z 44-49 for ethanol, Rt: 2.15 min; m/z 58-65 for *n*-propanol, Rt: 2.80 min). Data were collected with LabSolution software (Shimadzu, Duisburg, Germany). The overall ^{13}C enrichment (mol-%) was calculated according to Lee et al. [144] and Ahmed et al. [145]. The software package is open source and can be downloaded by the following link: *http* : *//www.tr*34.*uni* – *wuerzburg.de/software_developments/isotopo/*. For the analysis of ethylene, 2 mL of the gaseous sample were transferred into an evacuated 1.5 ml autosampler vial. 8 µL of the sample were analyzed by GC-MS as described above on a CP-Volamine column, 30 m x 0.32 mm (Agilent, Santa Clara, CA 95051, United States). Injector temperature was set to 200 °C. For the SIM measurement m/z values 27 – 31 (Rt: 1.35 min) were used.

4.4 Results and Discussion

4.4.1 Electrode characterization

The electrochemical behavior of each cell was first evaluated independently by linear sweep voltammetry as shown in Fig. 4.2a. 1 M $KHCO_3$ was used as catholyte in both cells. While pure CO_2 was the inlet gas of the first cell, the second cell was supplied in this experiment with pure CO. The potentials, recorded with a Ag/AgCl reference electrode, were converted to the reversible hydrogen electrode (RHE) scale according to the Nernst equation ($V_{vs.\ \mathrm{RHE}} = V_{\mathrm{measured}\ vs.\ \mathrm{Ag/AgCl}} + 0.209 + 0.059 \cdot \mathrm{pH}$). The observed behavior of current density with the increase of potential in each cell, show that a higher potential is required for the electrochemical reaction of CO_2 on Ag electrodes than for the electroreduction of CO on Cu into multi-carbon products. The electrodes used in this work performed similar to what has been previously reported in the literature and showed moderated working electrode potentials [128, 138, 146].

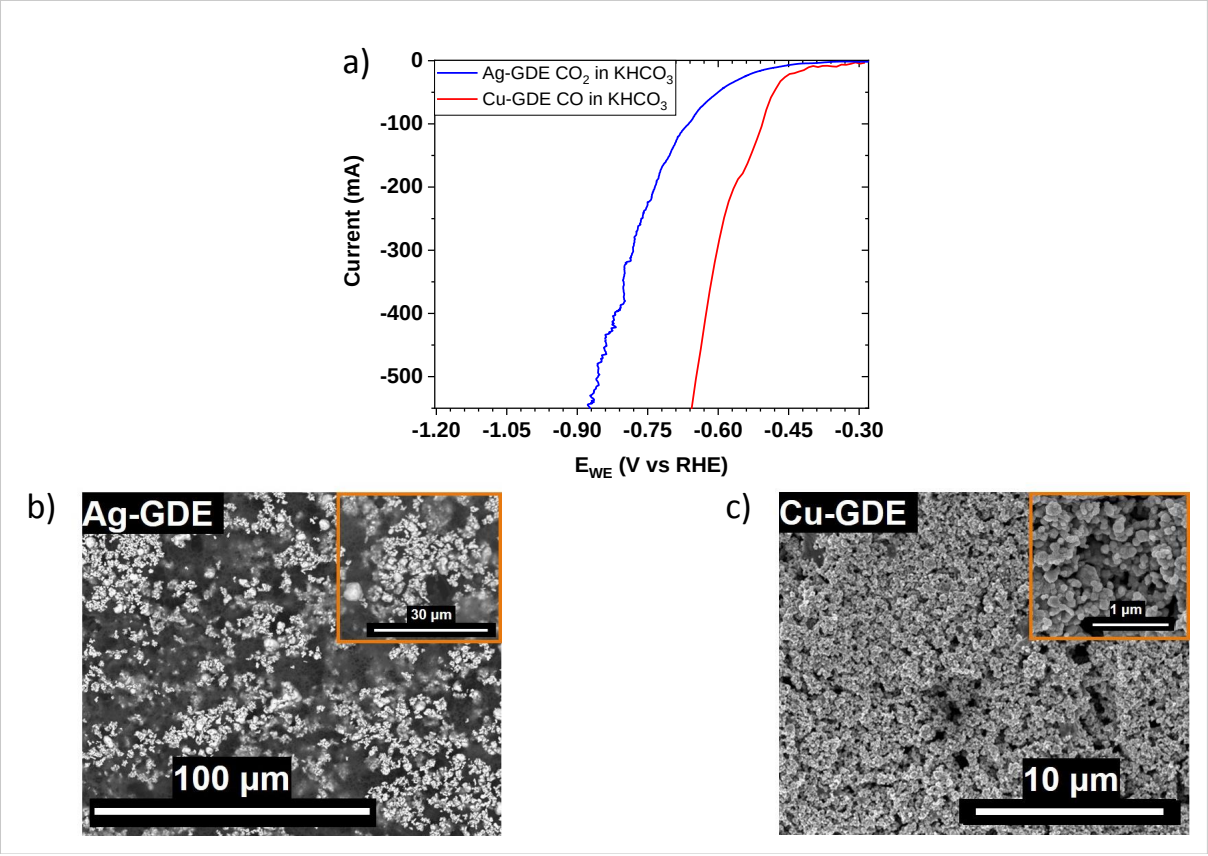

Figure 4.2: Characterization of each electrochemical reduction step a) linear voltammetry for the first step and for the second step electrolyzer. SEM micrographs of b) a Ag-GDE c) a Cu-GDE

SEM images reveal the surface differences between the type of electrodes used for each step. Fig. 4.2b shows the Ag-GDE electrode surface with bright particles being Ag, dark regions voids, and grey areas the polymeric binder. Ag-GDE presents diverse particle size with a non-defined particle shape. On the other hand, Fig. 4.2c confirms that in the preparation of the Cu-GDE, the GDL is completely covered with catalyst particles forming a catalyst layer that consists of spherical nanoparticles in the range of 40-60 nm. These observations are in accordance with the different preparation methods used for each type of electrode.

4.4.2 Individual performance: first step

In order to investigate the performance of the first electrolyzer, chronopotentiometric measurements with 72 sccm CO_2 inlet flow at three current densities, i.e. $-100\,mA/cm^2$, $-150\,mA/cm^2$, and $-200\,mA/cm^2$ were performed. Each current step was applied for 10 hours and subsequently increased. The accumulated liquid products in the electrolyte were analyzed after each current density step. Fig. 4.3 depicts the course of the Faradaic efficiency and working electrode potential over electrolysis time. At $-100\,mA/cm^2$ which corresponds to a working electrode potential of $-0.97\,V$ *vs.* RHE CO was the only product gas observed. With increasing current density the Faradaic efficiency of CO decreases slightly form 96 % at $-100\,mA/cm^2$ to 92 % at $-200\,mA/cm^2$. In contrast, the Faradaic efficiency of $HCOO^-$ increases with increasing overpotential from 2.3 % to 4.3 % which has previously been reported for metallic silver catalysts [147]. A maximum Faradaic efficiency of H_2 (2.4 %) is observed when the current density was increased to $-200\,mA/cm^2$. High CO Faradaic efficiency as well as stability of the Ag-GDE are crucial conditions to perform two-step electrolysis to C2 and C3 products. Furthermore, the feed gas composition for the second electrolyzer can have a significant impact on the product selectivity, as will be discussed in the next section. Thus, it is also important to evaluate the amount and composition of the outlet flow of the first electrolyzer.

After evaluation of the volumetric flow, a significant difference was observed between CO_2 feed flow and gas products flow. As depicted in Fig. 4.3b this difference increased with increasing current density. At $-100\,mA/cm^2$ a decrease in the gas flow of 6.5 sccm was observed whereas at $-200\,mA/cm^2$ double the amount was lost. This effect can be attributed to the direct interaction of CO_2 with hydroxide molecules. High current densities cause high local alkalinity [148] since two hydroxide ions are produced for every CO formed. The OH^- anions react with CO_2 forming carbonate species. At high alkalinity CO_3^{2-} is the predominant species, which leads to the overall reaction: $2\,CO_2 + 2\,e^- \rightleftharpoons CO + CO_3^{2-}$. Hence, in total two moles of CO_2 are required to produce one mole of CO. In fact, the measured amount of produced CO was in good approximation equal to the volumetric flow lost at each current density applied. For instance at $-100\,mA/cm^2$ a CO flow of 6.9 sccm was obtained, while the volumetric flow lost observed was 6.5 sccm.

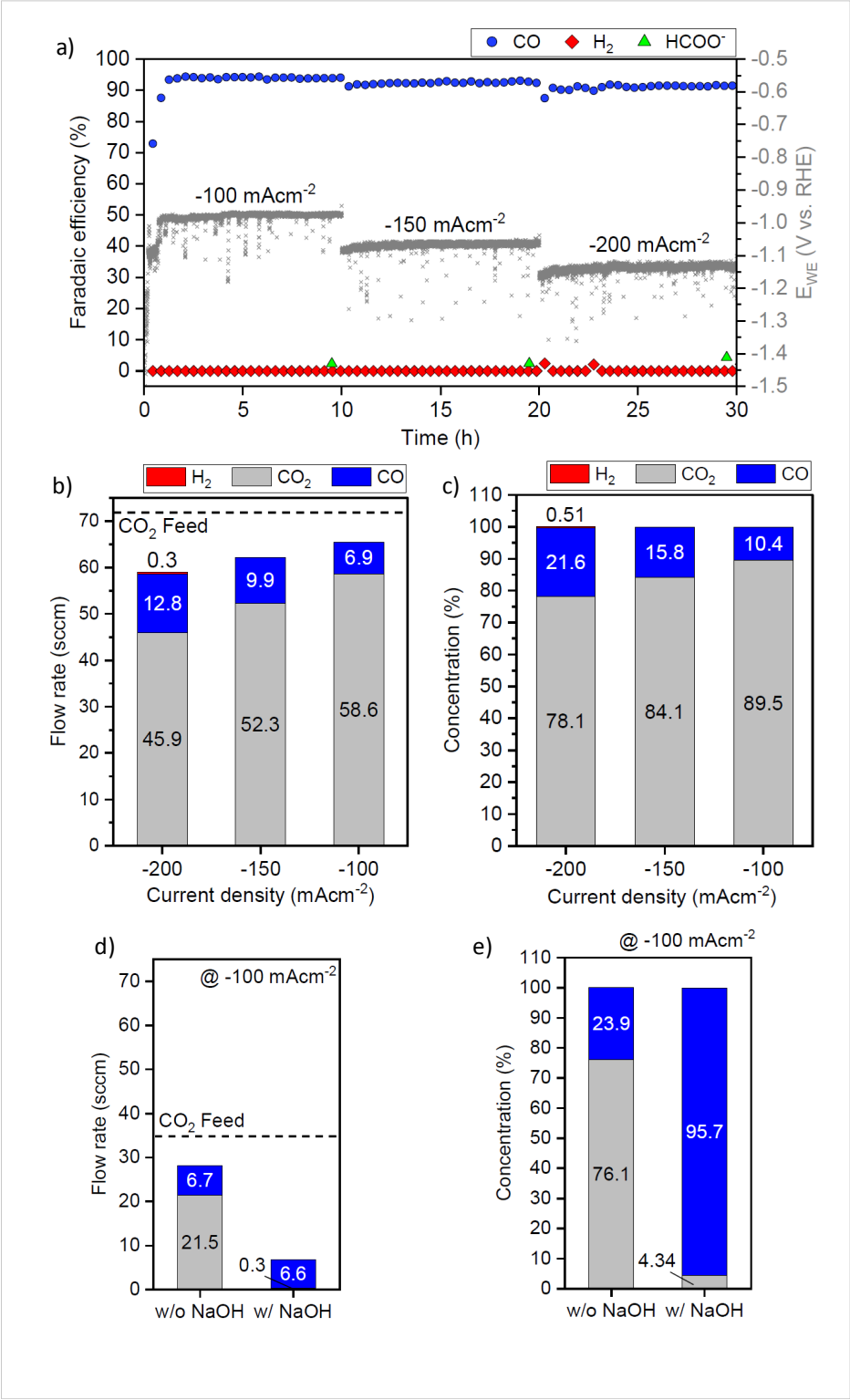

Figure 4.3: Characterization of the first electrochemical reduction step. a) Faradaic efficiencies of CO, H_2 and $HCOO^-$ over time at different current densities. b) Volumetric flow rates in standard cubic centimeter per minute (sccm) and c) concentration at the gas outlet of the first electrolyzer with 72 sccm CO_2 feed gas and different current densities. d) Volumetric flow rates and e) concentration at the gas outlet with 35 sccm CO_2 feed gas at $-100\,mA/cm^2$ with and without absorption of CO_2 using NaOH as absorber.

The loss of CO_2 is neither totally notable at low current densities, nor when focusing the evaluation of CO_2 electrolysis on the Faradaic efficiency. Although this effect has been recently discussed in the literature and some approaches regarding a catalyst-mediated abrupt reaction interface have been proposed [72], the structure of our Ag-GDE, with an uniform reaction interface over the entire thickness, does not prevent this reaction from occurring. Hence, some of the CO_2 supplied is lost in the electrolyte. Here it should be noted, that due to the use of 1 M $KHCO_3$ as catholyte and anolyte which are mixed after each cycle in one reservoir a stable pH and ion concentration is ensured. The oxidation of water in the anode compartment leads to the formation of H^+ which react with carbonate species to form CO_2. Thus, the CO_2 that is lost in the catholyte is evolved in the anode compartment (CO_2-cross over). With this configuration ion depletion does not take place and the system can be operated using the same electrolyte without limits.

A high volumetric feed rate of 72 sccm was initially used considering that a reactant excess ensures that CO_2 rather than protons populate the reaction surface [148]. However, this high CO_2 feed rate led to a high amount of unreacted CO_2 in the product gas of the first electrolyzer, which should be avoided in a two-step electrolysis system. As depicted in Fig. 4.3c at $-100\,mA/cm^2$ the fraction of unreacted CO_2 results in approximately 90 %. To reduce the amount of CO_2 which is fed into the second electrolyzer, we first reduced the CO_2 flow rate to 35 sccm. As shown in Fig. 4.3d-e, the reduced flow rate decreased the CO_2 concentration to 76 % maintaining a similar CO volumetric flow as before (6.7 sccm CO) without a loss in stability or Faradaic efficiency for CO over several hours of electrolysis (cf. Fig. 4.11). However, a much lower feed gas flow will lead to the production of H_2 and thus a decrease of the CO Faradaic efficiency. For this reason, the next alternative investigated, with the aim of achieving a high concentration of CO at the gas outlet of the first electrolyzer, was the incorporation of an absorption column with NaOH as absorbent. This increased the amount of CO to 96 % as shown in Fig. 4.3d-e.

4.4.3 Individual performance: second step

The performance of the second step was investigated considering that CO_2 is not fully converted into CO in the first step and also that Faradaic efficiencies >90 % are achieved, so that the concentration of H_2 in the gas outlet is lower than 1 % (see Fig. 4.3) and can be neglected. With this in mind, pure CO as well as mixtures of CO and CO_2 with a total flow of 50 sccm were electrochemically reduced at current densities between $-50\,mA/cm^2$ and $-300\,mA/cm^2$. The Faradaic efficiencies, for each products of the mixtures tested, were calculated with an average number of the electrons that would be needed for the reaction with CO and CO_2 depending on the CO/CO_2 ratio of the gas inlet. For instance, for a mixture containing 50 % CO + 50 % CO_2 the number of electrons estimated for the reduction to ethylene was $z_{ethylene}$ =

$0.5 \cdot 8\,e^- + 0.5 \cdot 12\,e^- = 10\,e^-$. A table with the average number for electrons for each product and each mixture investigated is given in the supporting information (Table 4.2).

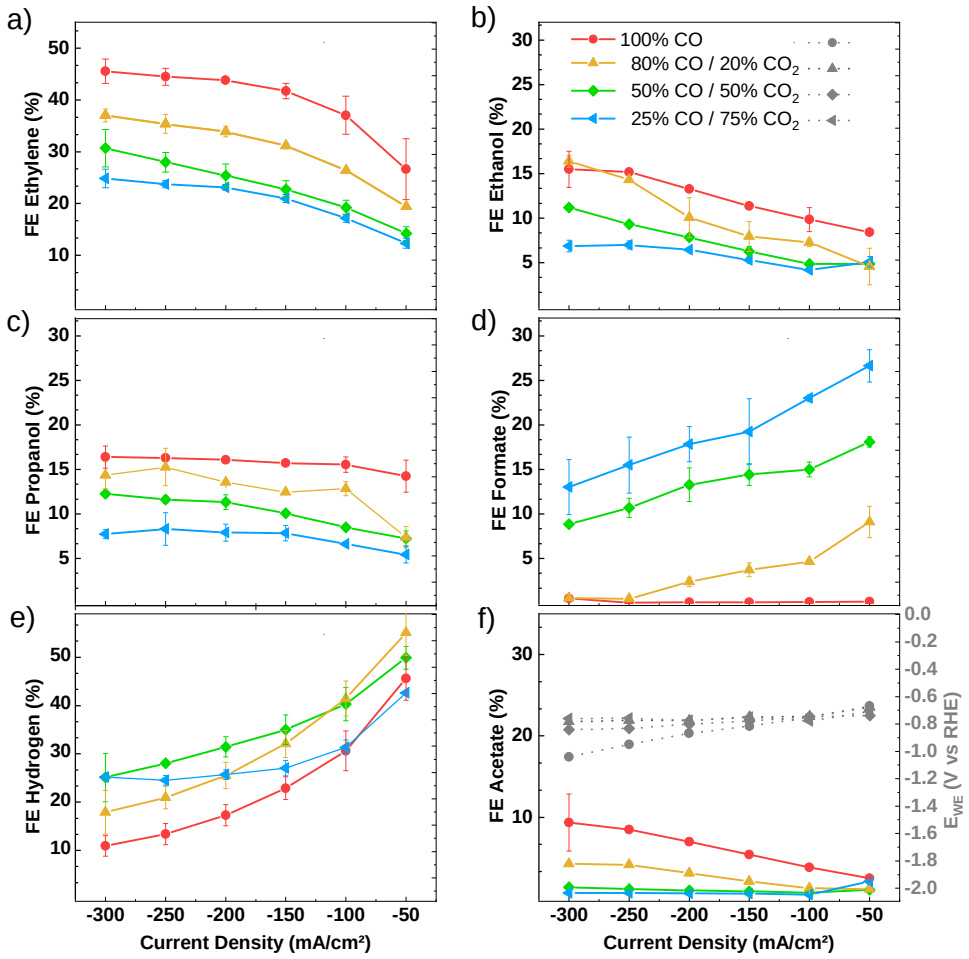

Figure 4.4: Current density variation for the electrochemical reduction of CO/CO_2 feed mixtures

Fig. 4.4 depicts the Faradaic efficiencies (FE) along with the working electrode potentials obtained during the current density variation for the electrochemical reduction of each CO/CO_2 mixture tested. It can be observed that the ratio of the two reactants has a clear effect on the selectivity to multi-carbons. A higher concentration of CO leads to higher FE of ethylene, ethanol, acetate and *n*-propanol, while the reduction reaction to formate and hydrogen is suppressed. Our results are in agreement with previous investigations that have shown the advantages of using pure CO rather than CO_2 [138, 139]. When reducing pure CO at $-300\,mA/cm^2$, 87 % of the FE corresponds to ethylene, ethanol, acetate and propanol, while with a high concentration of CO_2 (25 % CO / 75 % CO_2) only a cumulative FE of 41 % is achieved for C2 and C3 products. In this case competing reactions such as the formation of formate take place rather than the

reaction to multi-carbons. Here it should also be taken into account that CO is not only an intermediate but also a final product of the electrochemical reduction of CO_2 when using Cu as electrocatalyst. Thus, part of the current applied is used for the formation of CO when having a mixture of the two gases as feed. However, the quantification of which percentage of the detected CO in the gas outlet was unreacted CO or the product of CO_2 reduction was not an easily accomplished task. For this reason, CO Faradaic efficiencies are not included in Fig. 4.4. The depicted results suggest that the presence of non-converted CO_2 in the second step of a two-step electrolysis needs to be avoided in order to optimize the selectivity towards C2 and C3 products. Additionally, the increase of current density leads to a decrease of formate and hydrogen and an increase in multi-carbon products for all gas mixtures studied. In fact, it can also be observed that concentrations of CO_2 close to 20 % are manageable if the electrochemical reduction is operated at current densities over $-200\,mA/cm^2$. As shown in Fig. 4.4 for the 80 % CO / 20 % CO_2 mixture, formate production was suppressed to FE lower than 1 %, while the formation of ethanol and *n*-propanol surged to values close to the Faradaic efficiencies achieved with pure CO as reactant. Faradaic efficiencies for the overall product spectrum as well as the average ethylene flow obtained with each mixture at each current density are shown in the supporting information (Table 4.3 and Fig. 4.12).

4.4.4 Isotopic labeling studies for the electrolysis of CO and CO_2 mixtures

As mentioned in section 4.4.3, when performing electrolysis of a mixture consisting of CO and CO_2, both gases might be reactants towards multi-carbon products. However, it has not been elucidated if CO and CO_2 in a mixture react in the same proportion as they are supplied to the cell. It is known that the amount of electrons needed for the conversion to multi-carbon products with each reactant is different. Hence, for an accurate evaluation of the Faradaic efficiency, it is worthwhile to get some insights into the eletrochemical behavior of the mixture CO and CO_2. For this reason, electrochemical reduction of a 1:1 mixture with either labeled $^{13}CO_2$ or with labeled ^{13}CO was performed. The electrolysis was conducted for one hour at $-200\,mA/cm^2$ with a gas inlet flow of 50 sccm and an electrolyte flow of 100 mL/min. Liquid samples were taken from the reservoir at the end of the experiment and were analyzed using proton nuclear magnetic resonance (^1H NMR). Gas products were collected in gas sampling bags every 20 min and a gas chromatography-mass spectrometry (GC-MS) system was used for their analysis.

In a usual ^1H NMR spectrum, the observed peaks for each product are the result of hydrogens connected to ^{12}C. Here, scalar couplings can only arise between hydrogen atoms that are neighbored (typically via 3JHH). However, with the presence of ^{13}C, additional couplings occur between the hydrogen atoms connected to ^{13}C nucleus (via 1JCH). These couplings result in

^{13}C coupled satellites of the respective ^{1}H NMR signals. Fig. 4.5 depicts the obtained spectra for the liquid products after electrolysis of CO_2 and CO mixtures. The results for a non-isotope mixture of 50 % CO and 50 % CO_2 are shown in green. The spectrum in red depicts the liquid products from electrolysis of a mixture with labeled $^{13}CO_2$ and the blue spectrum shows the results for the sample with labeled ^{13}CO. The three experiments were performed using the same gas inlet flow and composition at the same conditions.

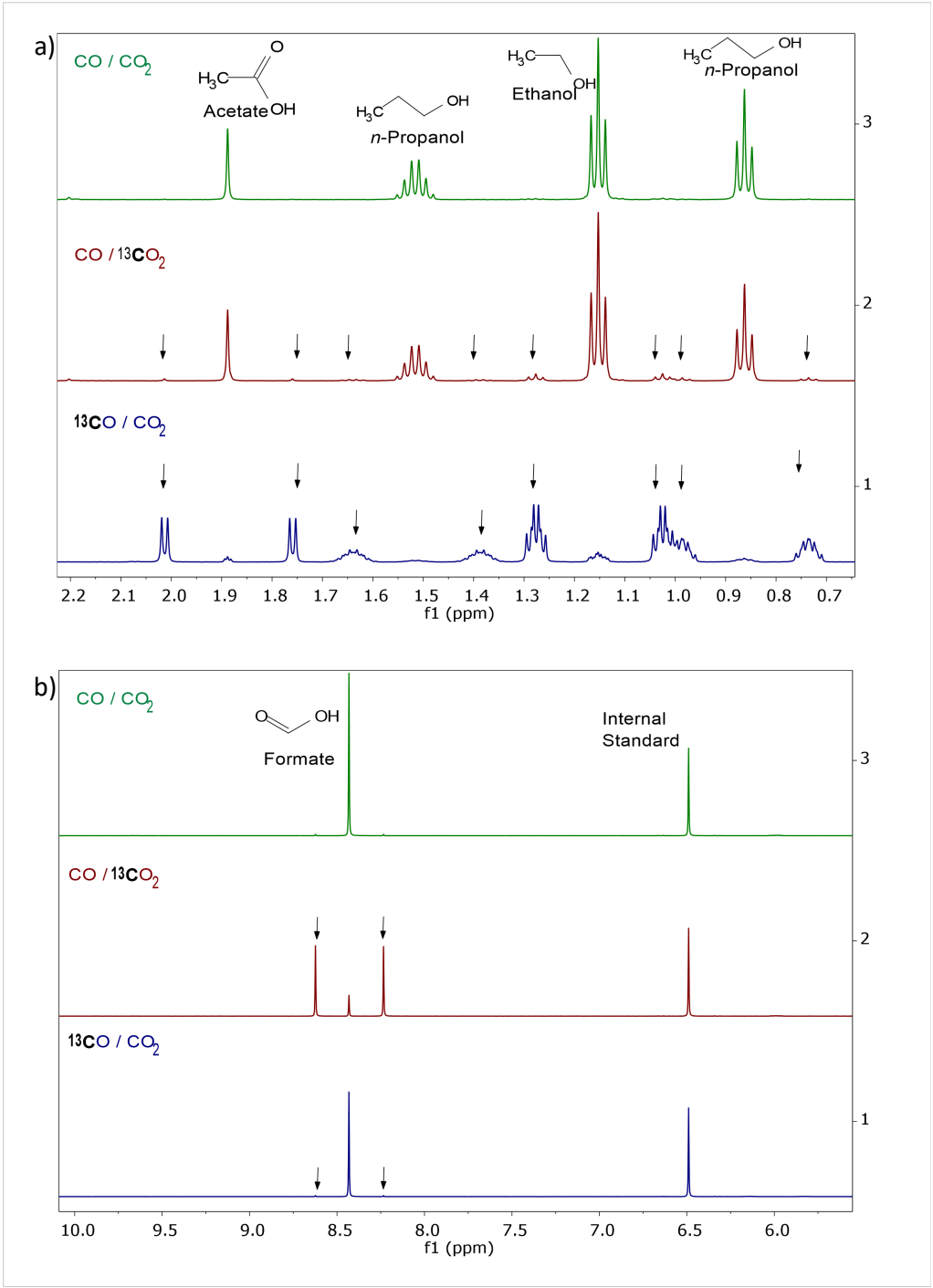

Figure 4.5: Partial ^{1}H NMR spectra of the liquid products obtained from the electrochemical reduction of 1:1 mixtures of CO and CO_2. Green: non-isotope labeled mixture. Red: mixture with labeled $^{13}CO_2$. Blue: mixture with labeled ^{13}CO.

Fig. 4.5a shows the results for the methyl signals of acetate, *n*-propanol, and ethanol as well as the methylene signal of C2 of *n*-propanol. Fig. 4.5b depicts the signals of formate and the internal standard. In the green spectrum, carbon satellites are barely seen, since the natural abundance of ^{13}C of all natural carbon in earth is about 1 %. In the red spectrum, small satellites are observed for acetate (5.6 %), ethanol (10.7 %), and *n*-propanol (7.4 %); while large carbon satellites are visible for formate (87.0 %). On the contrary, in the blue spectrum large satellites are observed for multi-carbon products (acetate 94.5 %, ethanol 91.0 % and *n*-propanol 92.8 %), while the satellites of the formate peak are barely visible.

Table 4.1 summarizes the relative integrals of the satellites. These results were confirmed using GC-MS analysis as shown in the supporting information Table 4.5. On this basis, it became clear that approximately 90 % of the obtained liquid multi-carbon products are mainly derived from CO although 50 % of the gas supplied to the cell was CO_2. This indicates that in a 1:1 mixture CO_2 and CO do not react to liquid products in the same proportion as they are supplied to the cell. CO_2 is preferably reduced to formate (87 %), while CO is converted to acetate, *n*-propanol, and ethanol. Additionally, the results suggest that not all the formate is obtained from a gaseous carbon source. A small percentage seems to be the result of the bicarbonates present in the electrolyte. Because of the carbonate equilibrium reaction, a 1 M $KHCO_3$ solution contains approximately 10 mM aqueous CO_2. This CO_2 can be reduced to formate, which explains the proton-carbon coupling obtained after electrolysis of the mixture CO/$^{13}CO_2$. When the mixture $^{13}CO/CO_2$ is used as feed gas, the natural abundance of ^{13}C in CO_2 should also be taken into account, which as mentioned before is close to 1 %.

Table 4.1: Quantification of the ^{13}C enrichment for liquid products found after electrochemical reduction of 1:1 CO / CO_2 mixtures with isotope labeled $^{13}CO_2$ and ^{13}CO

Liquid products	**^{13}C Enrichment**	
	CO / $^{13}CO_2$	^{13}CO / CO_2
Propanol	7.40%	92.80%
Ethanol	10.70%	91.00%
Acetate	5.60%	94.50%
Formate	87%	1.90%

Fig. 4.6 shows the spectra obtained after GC-MS analysis of the collected gas products. With the column available, CO_2 and ethylene present different retention times with slightly overlapping signals. Moreover, the elution of $CO/N_2/O_2$ occurs at the same time. Nevertheless, with a reference gas spectrum and the obtained spectra, it was possible to calculate the overall ^{13}C enrichment (mol-%) according to Lee et al. [144] and Ahmed et al. [145]. The quantification indicates that from the total ethylene detected, 46.28 % would be produced from ^{13}CO ($^{13}CH_2$=$^{13}CH_2$, m/z=30), 36.91 % would come from CO_2 (CH_2=CH_2, m/z=28) and 16.81 % from ^{13}CO and CO_2 ($^{13}CH_2$=CH_2, m/z=29). From the total ethylene obtained a slightly higher amount is derived from CO than from CO_2. Thus CO_2 and CO do not react towards ethylene in the same proportion as they are supplied to the cell (50 % CO/50 %CO_2). The lower amount of

ethylene resulting from CO_2 might be due to the carbonate formation, which as mention before is a competing reaction. However, in order to obtain more conclusive mechanistic insights, future work is required to improve the GC-MS analysis. Additionally, it would be worthwhile to investigate the electrolysis of isotopic labeled mixtures with different CO/CO_2 concentrations.

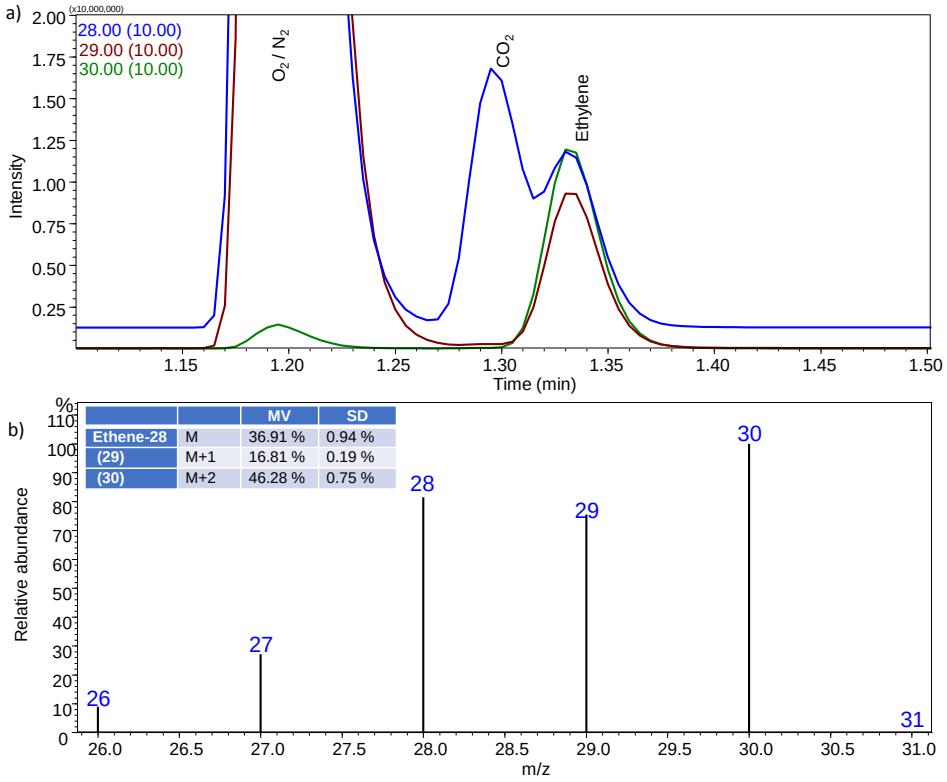

Figure 4.6: GC-MS analysis of the gas products obtained from the electrochemical reduction of 1:1 mixtures of ^{13}CO and CO_2. a) GC-MS spectrum for m/z 26-31 of the gas products obtained after electrolysis of a 1:1 $^{13}CO/CO_2$ mixture. b) Mass spectrum for the signal with retention time between 1.31-1.36 min, which corresponds to ethylene, m/z=28: $CH_2{=}CH_2$, m/z=29: $^{13}CH_2{=}CH_2$, m/z=30: $^{13}CH_2{=}^{13}CH_2$.

4.4.5 Full experimental demonstration of two-step electrochemical reduction

An initial two-step electrolysis experiment was performed, connecting the gas outlet of the first electrolyzer directly to the second step without a separation process in between and using 1 M $KHCO_3$ as electrolyte. Taking the CO_2 lost due to high local alkalinity into account, the first electrolyzer was operated at a current density of $-270\,mA/cm^2$ with a gas flow of 72 sccm. With these conditions, a flow of 51 sccm at the gas outlet was obtained with a concentration of 27 % CO. Thus, a high volumetric flow of CO (14 sccm) was ensured. The second electrolyzer was operated at $-200\,mA/cm^2$. Hence, a total current density of $-470\,mA/cm^2$ was applied to

the complete system. As depicted in Fig. 4.7b, this initial approach led to a low production of multi-carbon products.

Considering the lessons learned from section 4.4.3 regarding the presence of CO_2 in the second electrolyzer, an absorption step after the first electrolyzer was incorporated to the system using 5 M NaOH as absorbent (cf. Fig. 4.1). It is known that depending on the concentration of the absorber and the volume of the column, the absorption rate could decrease during the experiment. For this reason, prior to performance of two-step electrolysis, the gas outlet of the first electrolyzer was analyzed before and after the incorporation of the absorption column. As shown in Fig. 4.7a, the initial gas flow of 51 sccm obtained at the end of the first electrolyzer drops to 17.5 sccm after CO_2 was absorbed by NaOH, increasing the concentration of CO from 26 % to 83 %. With this configuration, it was also ensured that a relatively stable flow and concentration was supplied to the second electrolyzer over a time period of at least 6 hours. Subsequently, two-step electrolysis was performed with an absorption step between the first and second electrolyzer. The results in Fig. 4.7b demonstrate how the incorporation of CO_2 absorption to the overall system led to a twofold increase in the Faradaic efficiency for multi-carbon products. However, a high concentration of unreacted CO was still obtained, which suggests that the system could be further optimized.

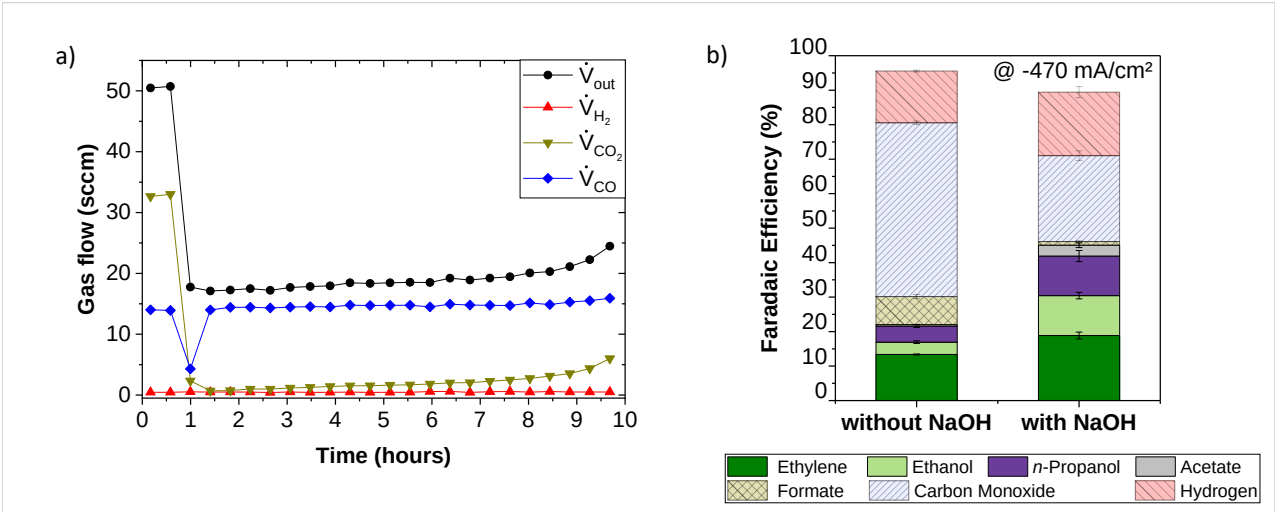

Figure 4.7: a) Gas flow before and after incorporation of the CO_2 absorption column. b) Faradaic efficiency for multi-carbon products after two-step electrochemical reduction at a total current density of −470 mA/cm^2 without and with CO_2 absorption using NaOH as absorber.

Consequently, it was taken into account that the overall charge flow applied to the system should be split in accordance with the reactions that are expected to occur in each step. Thus, the number of electrons (z_n) needed for the ideal main reaction, the area of the electrolyzer (A_i), and the stoichiometric coefficients of the reactants (ν_r) were considered for the calculation as follows:

$$\frac{j_1 \cdot A_1 \cdot v_1}{z_1} \geq \frac{j_2 \cdot A_2 \cdot v_2}{z_2} \tag{4.1}$$

If the main reaction of the first electrolyzer is the conversion of CO_2 to CO

$$CO_2 + H_2O + 2\,e^- \rightleftharpoons CO + 2\,OH^- \tag{4.2}$$

and for an ideal case, the main reaction of the second electrolyzer should be the conversion of CO to a C2 product such as ethanol:

$$2\,CO + 7\,H_2O + 8\,e^- \rightleftharpoons C_2H_5OH + 8\,OH^- \tag{4.3}$$

when operating the first electrolyzer at a current density of $-100\,mA/cm^2$, the second electrolysis should be carried out at a current density of:

$$j_{2,max} = j_1 \cdot \frac{z_{COtoC_2H_4}}{z_{CO_2toCO}} \cdot \frac{v_{CO_2}}{v_{CO}} \cdot \frac{A_2}{A_1} = -100\,\frac{mA}{cm^2} \cdot \frac{8}{2} \cdot \frac{1}{2} \cdot \frac{10\,cm^2}{10\,cm^2} = -200\,\frac{mA}{cm^2} \tag{4.4}$$

The full integrated system was assembled and measured as shown in Fig.4.1. The gas flow of the first electrolyzer was adjusted to 35 sccm in order to obtain a CO concentration in the gas outlet close to 25 %, with a CO FE of >90 % at a current density of $-100\,mA/cm^2$. The gas product of the first electrolyzer was directed to the absorption column before feeding the second electrolyzer with approximately 7 sccm and a CO concentration of 95 %. The second step was then operated at $-200\,mA/cm^2$. Two-step electrolysis was accomplished over 2.5 hours using independent potentiostats for each electrolyzer and monitoring the working electrode potential behavior at each current density applied. The overall process was evaluated with a total current density of $-300\,mA/cm^2$. Liquid products were analyzed after the first and second hour of experiment. Fig. 4.8a depicts the performance of the optimized two-step electrolysis regarding FE towards multi-carbons and working electrode potential for each step. A cumulative Faradaic efficiency of 62 % was obtained for the multi-carbon products analyzed after the first hour of experiment. The FE for ethylene slightly decreased after two hours, while the efficiency towards ethanol and *n*-propanol remained stable.

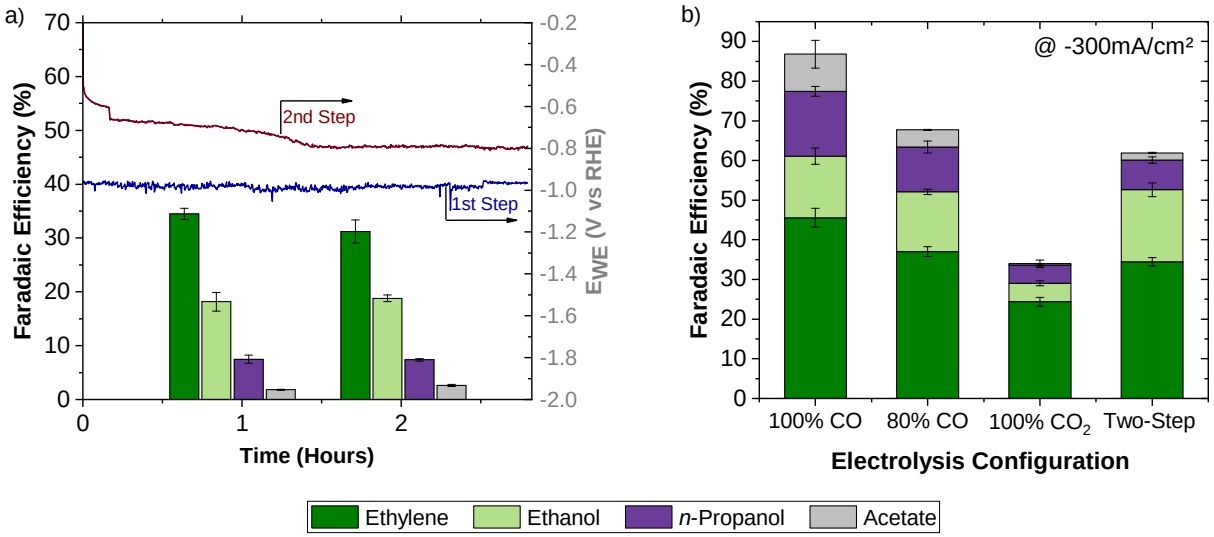

Figure 4.8: Performance of two-step electrochemical reduction of CO_2 a) Faradaic efficiencies for multi-carbon products after the first and second hour of electrolysis at a total current density of $-300\,mA/cm^2$ and working electrode potential for the first and second step, b) Cumulative Faradaic efficiency obtained after the first hour of electrolysis at a total current density of $-300\,mA/cm^2$ from a single-step electrolysis with pure CO, a mixture of 80 % CO / 20 % CO_2, and pure CO_2 compared to a two-step electrolysis system.

In Fig. 4.8b, the performance of two-step electrochemical reduction of CO_2 is compared to single-step electrolysis of pure CO_2, pure CO and a mixture of 80 % CO / 20 % CO_2 using the same kind of Cu-GDE at $-300\,mA/cm^2$. It can be observed that the cumulative Faradaic efficiency is nearly twofold higher with a two-step electrolysis configuration than with a single-step electrochemical reduction of pure CO_2. On the other hand, the yield of multi-carbon products from two-step electrolysis is not as high as from direct reduction of pure CO. In fact, the yield of two-step electrolysis is 5 % lower than the one-step electrolysis of the mixture with 80 % CO. Here it is important to note that with the incorporation of the absorption step, the gas flow rate directed to the second electrolyzer was expected to be approximately 7 sccm, while the single-step electrolysis of pure CO and of the mixture with 80 % CO was performed with a volumetric flow rate of 50 sccm. Thus, the lower cumulative Faradaic efficiency of two-step electrolysis compared to the direct electrolysis of CO can be explained by the lower gas feed in the second electrolyzer. This suggests that the introduction of a CO_2 separation process needs to be carefully conducted; on one hand, it leads to an increase of the CO concentration. On the other hand, it causes a decrease in the flow rate that will be supplied to the second electrolyzer. Thus, a compromise should be found in order to optimize the overall process.

Two-step electrolysis systems show a high potential for further optimization due to the versatility to vary conditions separately. In this study, $KHCO_3$ was used as the catholyte in both steps in order to assure a direct comparison to the separate analysis of the second step with

gas mixtures. However, the process can be improved by using KOH as electrolyte in the second electrolyzer. As shown by Jouny et al. [138], when using KOH at high concentrations, the active area of the triple-phase boundary might be improved by the increase in electrolyte conductivity and higher pH should favour C-C coupling. Hence, higher Faradaic efficiencies towards multi-carbon products as well as a reduction in hydrogen evolution reaction and cell potential is expected, when operating the second electrolyer with KOH. Apart from the introduction of a more conductive electrolyte, the second step can also be improved by using a more selective electrocatalyst, for instance, an oxide-derived nanocrystalline copper [121, 128, 138].

While the required gas separation process could be understood as disadvantage, it has been shown from a technoeconomical view that its cost would be likely minor relative to the total system economics [149]. Additionally, the lower working electrode potential required for the reduction of CO to multi-carbon products in the second step implies an improvement in energy efficiency compared to a one-step electrolysis of CO_2 [138, 139]. Despite the potential improvements in selectivity and energy efficiency, further investigation is necessary to find assertive ways for the engineering of the system. As an alternative, the absorption of CO_2 that was performed in this work in an absorption column, might be coupled with the reservoir of the second electrolyzer, which will reduce the number of apparatus in the system. Furthermore, the absorbed CO_2 can be regenerated and recycled to the gas supply of the first step. With all of this, the up-scaling of a two-step electrolysis of CO_2 seems to be a feasible alternative to obtain high efficiencies for multi-carbon products at high current densities.

The obtained results demonstrate that two-step electrolysis, even using a mild electrolyte in the second step, leads to higher Faradaic efficiencies for multi-carbon products than what can be achieved with a single-step electrolysis of CO_2 at the same total current density. While a two-step electrolysis cannot completely solve the discussed problem of carbonate formation in the first step, the overall loss of CO_2 due to a non-electrochemical reaction will be lower than in an alkaline one-step electrolysis. Here it should also be considered that 2 OH^- are produced for each CO_2 that reacts to CO in the first step of a two-step electrolysis, which leads to a high local alkalinity in the reaction boundary layer and to the formation of carbonates as discussed in section 4.4.2. If the second step is fed with pure CO, no loss of reactant due to non-electrochemical reactions is expected in the second electrolyzer. On the other hand, in the direct one-step electrolysis to ethylene, 6 OH^- will be produced for each CO_2 fed ($2\,CO_2 + 8\,H_2O + 12\,e^- \rightleftharpoons C_2H_4 + 12\,OH^-$). Thus, a higher CO_2 loss would be expected. Moreover, the amount of CO_2 that reacts to carbonate increases at higher current densities as shown in section 4.4.2. In the two-step electrolysis proposed in this work, the charge for the overall process is split in two. Hence, both electrolysis steps would be operated at a lower current. In fact, the first step is operated at half of the current applied in the second step. Thus, as long as it can be assured that the feed to the second step is CO with a high purity, the CO_2

loss, due to a local high alkalinity at the reaction boundary layer, can be expected to be a third of what it might be in a single-step electrolysis.

4.4.6 Comparison of the present results with literature

Our results for the separate analysis of the first and second electrolyzer are in agreement with the literature [115, 138]. Regarding two-step electrochemical reduction of CO_2 as an integrated system, to our knowledge, only Theaker et al. [128] have reported a low current two-step cascade system for the electrochemical reduction of CO to ethanol, which was performed in conventional cells with Ag-NC and OD-Cu foil electrodes. Theaker et al. reported 11 % FE for ethanol at a current density close to $-3\,mA/cm^2$. Since the electrode of the second electrolyzer they used was specially tailored for the formation of ethanol, only low efficiencies for other products were achieved. With our approach, a Faradaic efficiency of 18 % for ethanol was gained at a total current density of $-300\,mA/cm^2$. In addition, 34.5 % FE ethylene, 7.5 % FE *n*-propanol, and 1.8 % FE acetate were obtained. The different results regarding FE and current densities can be explained by the differences in the set-up, which are not only related to the type of cell and electrodes, but also to the design of the overall process. In the experiments performed by Theaker et al. [128] CO_2 was passed through an absorption column with 0.1 M $KHCO_3$, which was subsequently used as the electrolyte of the first reactor. Since only dissolved CO_2 is supplied to the electrolyzer, the gas outlet of the first step is expected to be mainly CO and H_2. The mixture of CO and H_2 is then directed to the second electrolyzer and reduced to ethanol. While their proposed system might be an innovative way to circumvent the undesired presence of CO_2 in the second electrolyzer, up-scaling of this set-up would be rather challenging for an industrial application. On the other hand, with the integrated system presented in this work, high current densities can be achieved and the system can be scaled up to an industrial application due to the use of gas diffusion electrodes and flow-cells.

4.5 Conclusion

Two-step electrochemical reduction of CO_2 is investigated using flow cells with gas diffusion electrodes at current densities up to $-300\,mA/cm^2$. The initial analysis of each step separately allows the definition of parameters that have to be taken into account for the design of two-step electrolysis. It was confirmed that the presence of CO_2 in the gas inlet of the second electrolyzer lowers the Faradaic efficiency towards multi-carbon products, since its presence introduces competing reactions such as the electrochemical reduction of CO_2 to formate and the formation of carbonates. Thus, a separation process for the purification of carbon monoxide

plays an important role in the performance of the overal system. Furthermore, it was shown that the total applied current density should be weighted by the expected reactions in each step in order to have an effective conversion of CO in the second electrolyzer. A cumulative Faradaic efficiency for multi-carbon products of 62 % was achieved at a total applied current density of $-300\,\mathrm{mA/cm^2}$, which is 30 % higher compared to the efficiency achieved in single-step electrolysis at the same current density. The obtained results demonstrate that two-step electrolysis is a feasible alternative to obtain high Faradaic efficiencies for multi-carbon products at high current densities.

Acknowledgments

The authors thank Dr. Andreas Rucki and Martin Hansen from Siemens AG for their support with the SEM characterization of the electrodes. N.S. Romero Cuellar would like to express her gratitude to the TUM Graduate School, to Riley Mather for language editing, and to her Siemens colleagues Dr. Erhard Magori, Dr. Remik Pastusiak, and Dr. Angelika Tawil for the valuable discussions and support in the laboratory.

4.6 Supporting Information

4.6.1 Electrolyzers

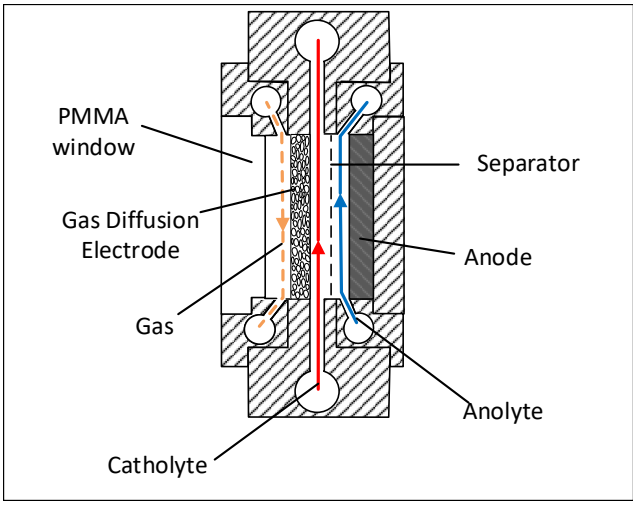

Figure 4.9: Schematic cross-section of the first electrolyzer

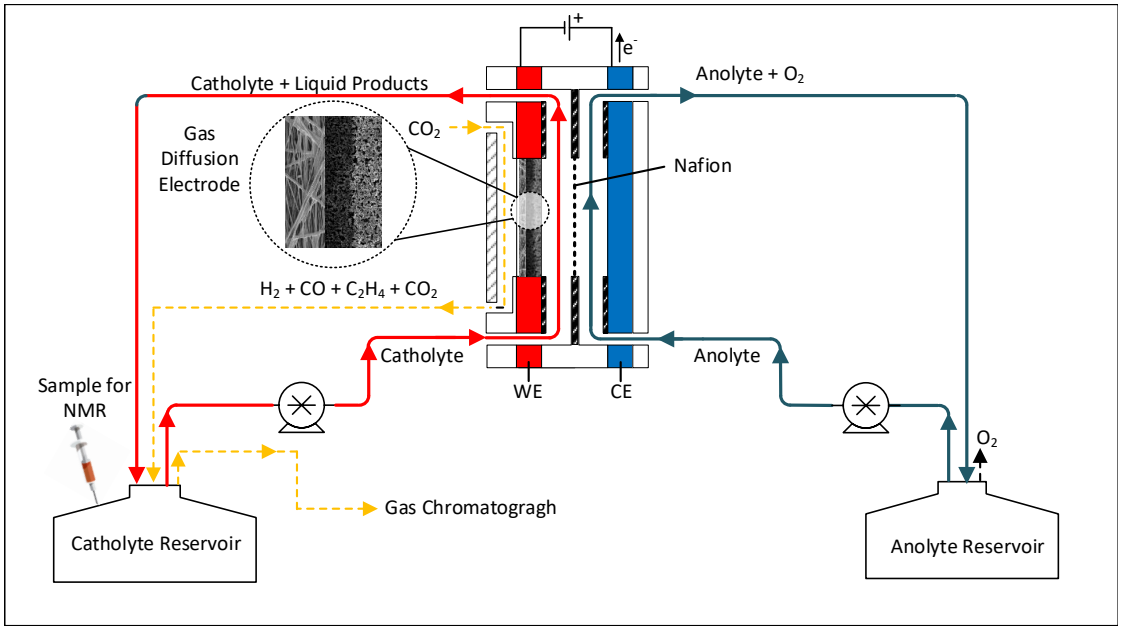

Figure 4.10: Schematic cross-section of the second electrolyzer along with gas and electrolyte flow representation.

4.6.2 Long term experiments for the first step

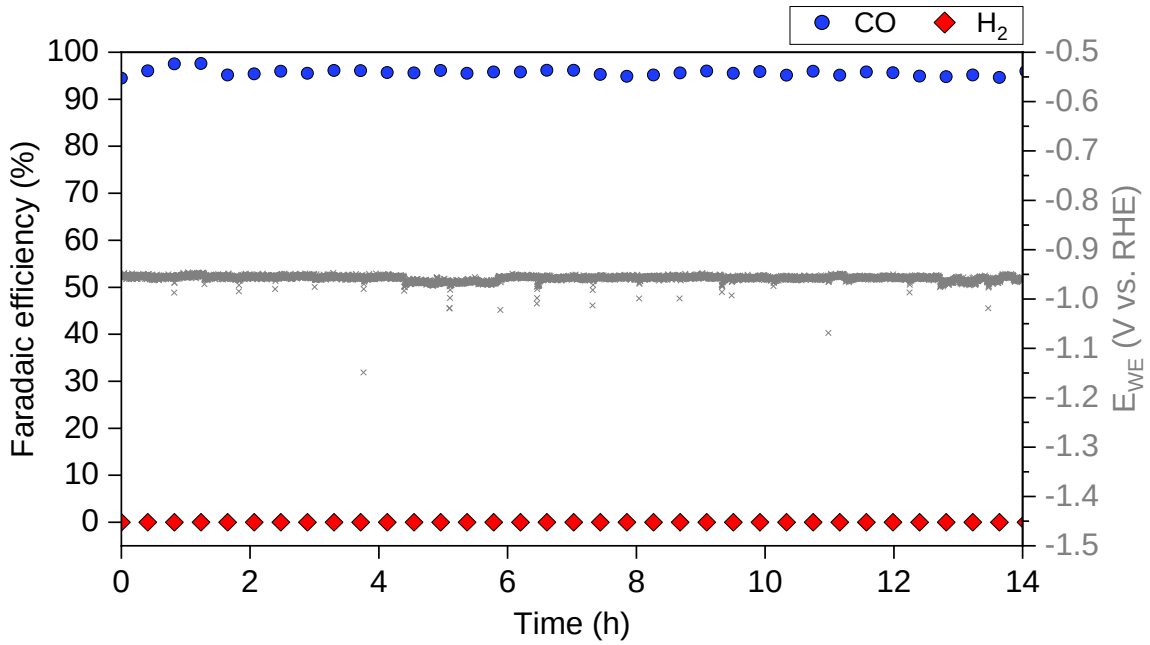

Figure 4.11: Faradaic efficiencies and working electrode potential over electrolysis time. A lower feed gas flow rate of 35 sccm CO_2 was used. No decrease in stability was observed within 15 hours of electrolysis.

4.6.3 Electrochemical reduction of CO/CO_2 mixtures

Table 4.2: Average number of electrons for the electrochemical reduction of CO/CO_2 mixtures.

Mix		Electrons, z							
CO2	CO	Propanol	Ethanol	Ethylene	Acetate	Methanol	Acetone	Methane	Formate
1	0	18	12	12	8	6	16	8	2
0	1	12	8	8	4	4	10	6	2
0,2	0,8	13,2	8,8	8,8	4,8	4,4	11,2	6,4	2
0,5	0,5	15	10	10	6	5	13	7	2
0,75	0,25	16,5	11	11	7	5,5	14,5	7,5	2

Table 4.3: Faradaic efficiencies for the electrochemical reduction of CO/CO_2 mixtures. Current density variation on Cu gas diffusion electrodes

Gas Mixture	j (mA/cm^2)	Faradaic Efficiency (%)							
		Propanol	Ethanol	Ethylene	Acetate	Formate	CH_4	H_2	Total
100 %CO	**50**	14,23	8,40	26,64	2,50	0,13	0,74	45,61	98,26
	100	15,53	9,83	37,03	3,84	0,11	0,86	30,63	97,84
	150	15,73	11,36	41,72	5,43	0,08	0,32	22,88	97,53
	200	16,06	13,28	43,84	7,00	0,07	0,12	17,28	97,66
	250	16,28	15,16	44,46	8,48	0,05	0,00	13,40	97,84
	300	16,38	15,49	45,57	9,35	0,50	0,00	10,92	98,21
80 %CO/ 20 %CO_2	**50**	9,79	8,66	19,42	1,19	9,09	2,59	55,09	105,84
	100	11,27	8,16	26,39	1,29	4,63	1,66	41,44	94,85
	150	12,19	11,27	31,13	2,13	3,71	1,20	32,06	93,69
	200	13,57	14,55	33,86	3,14	2,36	0,72	25,51	93,71
	250	11,05	14,82	35,35	4,15	0,46	0,52	20,95	87,31
	300	11,35	15,07	37,00	4,30	0,54	0,40	17,92	86,58
50 %CO/ 50 %CO_2	**50**	7,22	4,84	14,20	1,12	18,10	0,00	49,90	95,38
	100	8,47	4,87	19,24	0,75	15,00	1,23	40,29	89,84
	150	10,05	6,25	22,77	0,91	14,41	0,79	34,99	90,18
	200	11,33	7,84	25,38	1,03	13,28	0,55	31,45	90,87
	250	11,60	9,32	27,98	1,17	10,67	0,42	28,03	89,20
	300	12,27	11,19	30,71	1,41	8,84	0,34	25,11	89,87
25 %CO/ 75 %CO_2	**50**	5,44	5,08	12,32	2,11	26,63	0,00	42,65	94,23
	100	6,63	4,16	17,16	0,50	22,99	1,33	31,37	84,15
	150	7,83	5,29	20,97	0,63	19,24	0,88	27,04	81,88
	200	7,90	6,45	23,11	0,66	17,84	0,75	25,71	82,41
	250	8,30	6,99	23,73	0,72	15,48	0,67	24,53	80,41
	300	7,73	6,87	24,84	0,71	13,03	0,62	25,20	78,99

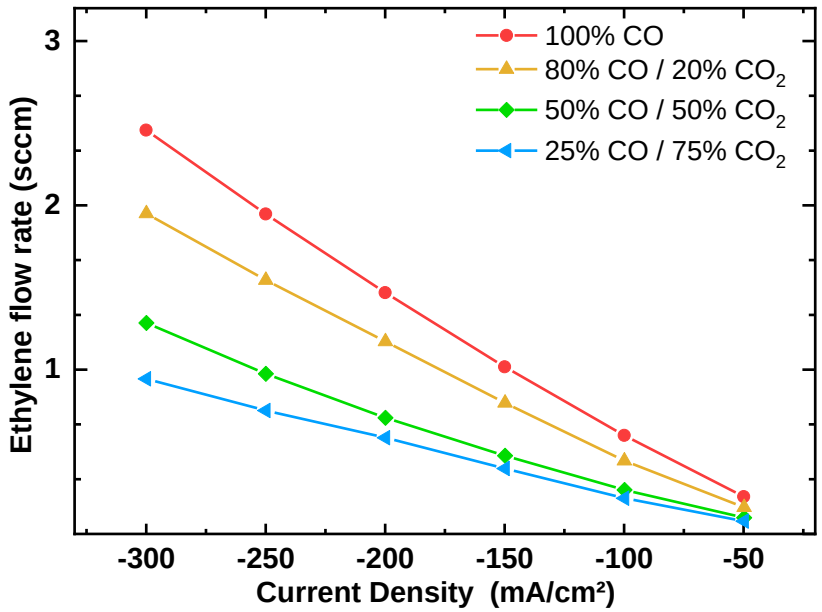

Figure 4.12: Volumetric gas flow rates in standard cubic centimeter per minute (sccm) for ethylene by the electrochemical reaction of CO/CO_2 feed mixtures

4.6.4 Comparison of one-step and two-step electrolysis configurations

Table 4.4: Faradaic efficiencies for the electrochemical reduction at $-300\,mA/cm^2$. Average values after one hour electrolysis

Configuration	Faradaic Efficiency (%)								
	Propanol	Ethanol	Ethylene	Acetate	Formate	CH_4	CO	H_2	Total
100% CO (one-step)	16,38	15,49	44,89	7,17	0,08	0,13	0	17,69	101,83
80 / 20 (one-step)	11,35	15,07	37,00	4,30	0,54	0,40	-	17,92	86,58
100% CO_2 (one-step)	4,63	4,64	24,37	0,32	8,95	0,07	31,1	17,46	91,53
Two-step	7,48	18,17	34,46	1,82	0,05	0,18	8,14	24,96	95,25

4.6.5 ^{13}C enrichment validation experiments

Table 4.5: ^{13}C enrichment for ethanol and *n*-propanol obtained from the electrochemical reduction of a mixture with labeled 50 % CO and 50 % $^{13}CO_2$ measured by GC-MS and calculated according to Lee et al. [144] and Ahmed et al. [145].

		Mean Value	SD
EtOH-45	M	88,39%	0,37%
	M+1	9,87%	0,40%
	M+2	1,74%	0,16%
PrOH-59	M	88,07%	0,95%
	M+1	10,70%	0,51%
	M+2	0,56%	0,52%
	M+3	0,66%	0,11%

5 Summary and Outlook

The electrochemical reduction of CO_2 ($ERCO_2$) is a technology receiving increasing interest and relevance on the way to a sustainable energy system. While it has been proven to be a promising technology, there is still much work to be done before it can be up-scaled for industrial application. In this thesis, the electrochemical reduction of CO_2 was investigated, focusing on the cathodic reaction, in which CO_2 can be reduced to multi-carbon products. Initially, a material screening was performed in a simple batch system in order to obtain a better understanding of the phenomena that take place during electrolysis. Furthermore, this screening was used to characterize possible products and selectivity using non-metallic and metallic electrodes. The results of Chapter 2 provide the basis for the following development of a more suitable electrochemical system, as presented in Chapters 3 and 4. As a result, the selectivity towards ethylene, ethanol and *n*-propanol was improved at industrially-relevant current densities.

In Chapter 2, boron doped diamond (BDD) and transition metal electrodes were studied as electrocatalysts by performing galvanostatic and potentiostatic experiments in batch cells, as well as ex-situ surface analysis. The study of BDD electrodes was motivated by their mechanical and chemical stability, as proven in other electrochemical applications. The activity of BDD was demonstrated using electrolytes with different buffer capacities. The main products obtained were CO and HCOOH. It was confirmed that the BDD activity is enhanced by the electrolyte without buffer ability. In this type of electrolyte, the CO_2 reduction should occur at a local alkaline pH, thereby suppressing the hydrogen evolution reaction (HER) and promoting the formation of carbonaceous products. However, the Faradaic efficiency (FE) for CO_2 reduction products was low due to the poor activity of BDD and the inherent mass transport limitations of the batch cell used for this study. Furthermore, the modification of BDD by Ag electro-deposition led to the increase of CO FE, while neither compromising the stability of the electrode nor decreasing the production of HCOOH in the liquid phase. This was confirmed by performing galvanostatic measurements at $-10\,mA/cm^2$ over 10 hours. While stability was confirmed, the activity of BDD electrodes remains lower compared to metallic electrocatalyst. This suggests that transition metal deposition on boron doped diamond could, for instance, be a viable alternative to deal with some of the durability challenges in the CO_2 electrochemical reduction.

Due to the scarce information regarding the characteristics of boron doped diamond used for CO_2 reduction, the effect of BDD growth parameters on the electrochemical reduction of CO_2 was selected for further study in this thesis. Two main variables were investigated, namely the methane concentration and the B/C ratio in the feed gas used for nanocrystalline (NC) BDD growth. The methane concentration was varied from 0.5 % to 1.5 % CH_4 maintaining the B/C content (boron content) constant at 1.0 %. Then, the B/C ratio was modified from 1.0 % to 2.0 % with a constant methane concentration of 1.0 %. The results demonstrate that methane concentration (carbon source) plays an important role in the ability of the electrode to electrochemically reduce CO_2. Higher Faradaic efficiencies for CO and HCOOH were achieved with the sample prepared with the lowest methane concentration. Besides the methane concentration, the B/C ratio was also investigated by characterizing two samples with 1.0 % and 2.0 % B/C content. Although no significant difference was observed in the performance of these two samples, further investigation would help to completely understand the role of the boron concentration on NC BDD films at B/C ratios lower than 1.0 %. Comparing the results obtained with the microcrystalline (MC) samples supplied by Einaga Group and the nanocrystalline (NC) samples supplied by Haenen Group, it was found that NC BDD electrodes are more selective towards CO than MC BDD electrodes having the same boron content. In order to establish more conclusive trends, it would be worthwhile to investigate NC and MC BDD samples prepared in the same reactor with similar CH_4 and B/C content. Additionally, it might be worthwhile to investigate the performance of BDD as a gas diffusion electrode (GDE). While this might require the development of a very complex growth method, it could be an alternative to the current electrochemical reduction systems for improving durability.

Subsequently, transition metals were investigated for the electrochemical reduction of both CO_2 and CO. While all metals tested showed activity for MeOH and HCOOH, Cu was confirmed to be the only electrocatalyst able to reduce CO into multi-carbon products. Nevertheless, the formation of methanol seems to be more favorable in Ni than in Cu, suggesting that the formation of methanol might require a stronger CO binding than the intermediate binding energy that occurs with Cu. It was experimentally demonstrated that not only the CO binding energy plays a role in the activity towards carbonaceous products, but also the activity of the metals for HER. Ni, Fe, and Co are highly active for hydrogen formation at lower potentials than Cu, which makes the competition between HER and $ERCO_2$ challenging. This leads to higher efficiencies for HER than to CO_2 or CO reduction products. In general, the lower solubility of CO compared to CO_2 in water, which causes further mass transfer limitations, makes the comparison of the two reactants difficult in this kind of set-up. Nevertheless, it was found that the presence of CO can suppress the hydrogen evolution reaction, which leads to higher onset potentials for HER. This was more evident for the metals with a stronger CO binding energy (Ni and Fe). On this regard, it would be interesting to further investigate, if the presence of CO would lead to the same observed HER suppressing effect in Ni, when using GDEs and flow cells.

However, since the focus of this thesis is the CO/ CO_2 electroreduction towards multi-carbon products, Cu was selected as the metal for further study.

In Chapter 3 the electrochemical reduction towards multi-carbon products was investigated using Cu-GDEs in a flow cell and comparing CO_2 and CO as the reactant. The aim was to improve the production of ethylene, ethanol, and *n*-propanol using Cu-powders deposited on gas diffusion layers as electrodes. Since mass transport limitations were circumvented by using Cu-GDEs, a direct comparison of CO_2 and CO as the reactant was possible. A remarkable increase in the selectivity towards ethylene, ethanol, and *n*-propanol of more than two-fold was achieved using CO as the reactant (cumulative 89 % FE at $-300\,mA/cm^2$) in comparison with the direct CO_2 electroreduction (cumulative 34 % FE at $-300\,mA/cm^2$) in a mild electrolyte. The results also demonstrate that particle morphology and size, play an important role in the preparation of electrodes for application at industrially relevant current densities. Nanoparticles (40-60 nm, 60-80 nm, >100 nm) became more selective with higher current densities, while the selectivity towards C2 and C3 products using microparticles (5 µm) decreased at current densities higher than $-150\,mA/cm^2$. This was attributed to the active surface area available for the CO reduction with nanoparticles, which is higher than with microparticles with the same catalyst loading. For future work, it would be worthwhile to investigate the intrinsic activity of the Cu powders by determining the electrochemically active surface area of the prepared electrodes and make it a constant parameter to compare Cu catalyst materials. Regarding durability, 20 h experiments showed a relatively stable production of ethylene. However, further investigation could be done by testing, for instance, different kind of ionomers, membranes (anion exchange, cation exchange), carbon layers and electrode assembly. It is still necessary to address the loss of hydrophobicity of the carbon layer during electrolysis. Overall the results of Chapter 3 suggests that a two-step electrochemical reduction of CO_2 might provide a more selective route to the production of ethylene, ethanol, and *n*-propanol than one step CO_2 electroreduction.

In Chapter 4 a cascade electrochemical reduction system was built up and investigated using flow cells and GDEs for the first time to the best of my knowledge up to date. With this, the feasibility of a two-step CO_2 electrolysis system was demonstrated at current densities up to $-300\,mA/cm^2$. The initial analysis of each step separately allowed the definition of relevant parameters for the design of an integrated two-step electrolysis system. It was demonstrated that the presence of CO_2 in the gas inlet of the second electrolyzer is detrimental for the formation of multi-carbon products. The presence of CO_2 in the second step introduces competing reactions such as the electrochemical reduction of CO_2 to formate and the formation of carbonates. Thus, a separation process for the purification of carbon monoxide is crucial to achieve high selectivity towards ethylene, ethanol and *n*-propanol. Furthermore, it was demonstrated that the total applied current density should be weighted by the expected reactions in each step in order to have an effective conversion of CO in the second electrolyzer. A cumulative Faradaic efficiency for multi-carbon products of 62 % was achieved at a total applied current density of

$-300\,mA/cm^2$, which is 30 % higher compared to the efficiency achieved in a single-step electrolysis at the same current density. The obtained results demonstrate that two-step electrolysis is a feasible alternative to improve the Faradaic efficiency for multi-carbon products at high current densities.

While important insights are provided in this thesis, a two-step electrolysis system has still a high potential for further optimization due to the versatility to vary conditions separately. For the present study, $KHCO_3$ was used as the catholyte in both steps to assure a direct comparison to the separate analysis of the second step with gas mixtures. However, the process can be improved by using KOH as the electrolyte in the second electrolyzer. The higher conductivity of KOH compared to $KHCO_3$ should reduce the charge transfer resistance at the triple phase boundary and thus improve the CORR. Additionally, higher pH should favour C-C coupling. Hence, higher Faradaic efficiencies towards multi-carbon products as well as a reduction in hydrogen evolution reaction and cell potential would be expected. Furthermore, it might be worthwhile to study the effect of electrolyte flow rate on the efficiency towards liquid multi-carbon products. Apart from a deeper investigation of the electrolyte effects, the second step can also be improved by using a more selective electrocatalyst. The development of a mechanically and chemically durable Cu-GDE remains a challenge to address. Despite the potential improvements in selectivity and energy efficiency, further investigation is necessary to find assertive ways for the engineering of the system to make it economically feasible. As an alternative, the absorption of CO_2 between first and second step that was performed in this work in an absorption column, might be coupled with the reservoir of the second electrolyzer, which will reduce the number of apparatus in the system. Additionally, the absorbed CO_2 can be regenerated and recycled to the gas supply of the first step. In general, this thesis provides insights into the feasibility of a two-step CO_2 electrolysis system for the improvement of selectivity towards multi-carbon products at application-relevant current densities.

6 Bibliography

[1] N. S. Lewis, D. G. Nocera, *Proceedings of the National Academy of Sciences* **2006**, *103*, 15729–15735.

[2] J. Dangerman, H. J. Schellnhuber, *Proceedings of the National Academy of Sciences of the United States of America* **2013**, *110*, E549–58.

[3] S. Chu, A. Majumdar, *Nature* **2012**, *488*, 294–303.

[4] United Nations, Department of Economic and Social Affairs, Population Division, World Urbanization Prospects: The 2014 Revision, Highlights: (ST/ESA/SER.A/352), **2014**.

[5] International Energy Agency, *Global Energy and CO_2 Status Report: The latest trend in energy and emissions in 2018*, (Ed.: IEA Publications), **2019**.

[6] M. Meinshausen, N. Meinshausen, W. Hare, S. C. B. Raper, K. Frieler, R. Knutti, D. J. Frame, M. R. Allen, *Nature* **2009**, *458*, 1158–1163.

[7] T. R. Anderson, E. Hawkins, P. D. Jones, *Endeavour* **2016**, *40*, 178–187.

[8] R. P. Core Writing Team, L. Meyer, Eds., Climate Change 2014: Synthesis Report, Intergovernmental Panel on Climate Change, **2014**, http://www.ipcc.ch/site/assets/uploads/2018/05/SYR_AR5_FINAL_full_wcover.pdf (visited on 05/16/2019).

[9] T. L. Root, J. T. Price, K. R. Hall, S. H. Schneider, C. Rosenzweigk, J. A. Pounds, *Nature* **2003**, *421*, 57–60.

[10] C. Streck, The Paris Agreement Summary, Climate Focus, **2015**, http://www.climatefocus.com/publications/cop21-paris-2015-climate-focus-overall-summary-and-client-briefs (visited on 06/03/2019).

[11] E. Schmid, B. Knopf, A. Pechan, *Energy Research & Social Science* **2016**, *11*, 263–275.

[12] F. Ausfelder, C. Beilmann, M. Bertau, S. Braeuninger, A. Heinzel, R. Hoer, W. Koch, F. Mahlendorf, A. Metzelthin, M. Peuckert, L. Plass, *ChemBioEng* **2017**, 144–210.

[13] A. Tremel, *Electricity-based Fuels*, Springer International Publishing, **2018**.

[14] *Roadmap des Kopernikus-Projektes "Power-to-X": Flexible Nutzung Erneuerbarer Ressourcen (P2X). Optionen für ein nachhaltiges Energiesystem mit Power to X Technologien*, (Eds.: F. Ausfelder, H. E. Dura), DECHEMA Gesellschaft für Chemische Technik und Biotechnologie e.V., **2018**.

[15] P. D. B. Burger, Ed., Stromerzeugung in Deutschland im ersten Halbjahr 2018, Fraunhofer-Institut für Solare Energysyteme ISE, **2018**, https://www.ise.fraunhofer.de/content/dam/ise/de/documents/publications/studies/daten-zu-erneuerbaren-energien/ISE_Stromerzeugung_2018_Halbjahr.pdf (visited on 06/03/2019).

[16] R. Perez, M. Perez, *IEA-SHCP-Newsletter* **2015**, *62*, 1–3.

[17] V. Masson-Delmotte, P. Zhai, H.-O. Pörtner, D. Roberts, J. Skea, P.R. Shukla, A. Pirani, W. Moufouma-Okia, C. Péan, R. Pidcock, S. Connors, J.B.R. Matthews, Y. Chen, X. Zhou, M.I. Gomis, E. Lonnoy, Maycock, M. Tignor, and T. Waterfield, Ed., Global Warming of 1.5°C. An IPCC Special Report, Intergovernmental Panel on Climate Change, **2018**, http://www.ipcc.ch/sr15/ (visited on 06/02/2019).

[18] R. M. Cuéllar-Franca, A. Azapagic, *Journal of CO_2 Utilization* **2015**, *9*, 82–102.

[19] E. S. Sanz-Pérez, C. R. Murdock, S. A. Didas, C. W. Jones, *Chemical Reviews* **2016**, *116*, 11840–11876.

[20] S. Evans, The Swiss company hoping to capture 1% of global CO_2 emissions by 2025, Carbon Brief, **2017**, https://www.carbonbrief.org/swiss-company-hoping-capture-1-global-co2-emissions-2025 (visited on 05/28/2019).

[21] What is carbon dioxide removal and why is it important?, Climeworks AG, **2019**, https://www.climeworks.com/co2-removal/ (visited on 05/28/2019).

[22] K. Appunn, Sector coupling - Shaping an integrated renewable energy system, Clean Energy Wire, **2018**, https://www.climeworks.com/co2-removal/ (visited on 05/30/2019).

[23] M. Fleischer, P. Jeanty, K. Wiesner-Fleischer, O. Hinrichsen in *Zukünftige Kraftstoffe*, (Ed.: W. Maus), Springer Verlag, **2019**, pp. 224–250.

[24] IRENA, International Renewable Energy Agency, Renewable Power Generation Costs in 2018, Abu Dhabi, **2019**.

[25] S. Gu, B. Xu, Y. Yan, *Annual Review of Chemical and Biomolecular Engineering* **2014**, *5*, 429–454.

[26] V. Molkov in *Comprehensive Renewable Energy*, (Ed.: A. Sayigh), Elsevier, **2012**, pp. 97–129.

[27] M. Sterner, Dissertation, Kassel University, Kassel, **2009**.

[28] O. S. Bushuyev, P. de Luna, C. T. Dinh, L. Tao, G. Saur, J. van de Lagemaat, S. O. Kelley, E. H. Sargent, *Joule* **2018**, *2*, 825–832.

[29] H.-R. M. Jhong, S. Ma, P. J. A. Kenis, *Current Opinion in Chemical Engineering* **2013**, *2*, 191–199.

[30] A. J. Martín, G. O. Larrazábal, J. Pérez-Ramírez, *Green Chemistry* **2015**, *17*, 5114–5130.

[31] M. Jouny, W. Luc, F. Jiao, *Industrial and Engineering Chemistry Research* **2018**, *57*, 2165–2177.

[32] Y. Hori, K. Kikuchi, S. Suzuki, *Chemistry Letters* **1985**, *14*, 1695–1698.

[33] Y. Hori in *Modern Aspects of Electrochemistry*, (Eds.: C. G. Vayenas, R. E. White, M. E. Gamboa-Aldeco), Springer New York, New York, NY, **2008**, pp. 89–189.

[34] D. T. Whipple, P. J. A. Kenis, *Journal of Physical Chemistry Letters* **2010**, *1*, 3451–3458.

[35] K. P. Kuhl, E. R. Cave, D. N. Abram, T. F. Jaramillo, *Energy und Environmental Science* **2012**, *5*, 7050–7059.

[36] J.-P. Jones, G. K. S. Prakash, G. A. Olah, *Israel Journal of Chemistry* **2014**, *54*, 1451–1466.

[37] R. Kortlever, J. Shen, K. J. P. Schouten, F. Calle-Vallejo, M. T. M. Koper, *Journal of Physical Chemistry Letters* **2015**, *6*, 4073–4082.

[38] A. A. Peterson, F. Abild-Pedersen, F. Studt, J. Rossmeisl, J. K. Nørskov, *Energy and Environmental Science* **2010**, *3*, 1311–1315.

[39] M. Ma, Dissertation, Delft University of Technology, Delft, The Netherlands, **2017**.

[40] M. Gattrell, N. Gupta, A. Co, *Journal of Electroanalytical Chemistry* **2006**, *594*, 1–19.

[41] K. J. P. Schouten, Y. Kwon, C. J. M. van der Ham, Z. Qin, M. T. M. Koper, *Chemical Science* **2011**, *2*, 1902–1909.

[42] R. J. Lim, M. Xie, M. A. Sk, J.-M. Lee, A. Fisher, X. Wang, K. H. Lim, *Catalysis Today* **2014**, *233*, 169–180.

[43] Y. Hori, A. Murata, R. Takahashi, *J. Chem. Soc. Faraday Trans. 1* **1989**, *85*, 2309–2326.

[44] M. Azuma, K. Hashimoto, M. Hiramoto, M. Watanabe, T. Sakata, *Journal of The Electrochemical Society* **1990**, *137*, 1772–1778.

[45] K. P. Kuhl, T. Hatsukade, E. R. Cave, D. N. Abram, J. Kibsgaard, T. F. Jaramillo, *Journal of the American Chemical Society* **2014**, *136*, 14107–14113.

[46] W. Tang, A. Peterson, A. S. Varela, Z. Jovanov, L. Bech, W. Durand, S. Dahl, J. Nørskov, I. Chorkendorff, *Phys. Chem. Chem. Phys.* **2012**, *14*, 76–81.

[47] C. Shi, K. Chan, J. S. Yoo, J. K. Nørskov, *Organic Process Research & Development* **2016**, *20*, 1424–1430.

[48] X. Liu, J. Xiao, H. Peng, X. Hong, K. Chan, J. K. Nørskov, *Nature Communications* **2017**, *8*, 15438.

[49] C. Hahn, T. Hatsukade, Y.-G. Kim, A. Vailionis, J. H. Baricuatro, D. C. Higgins, S. A. Nitopi, M. P. Soriaga, T. F. Jaramillo, *Proceedings of the National Academy of Sciences of the United States of America* **2017**, *114*, 5918–5923.

[50] K. Youn-Geun, J. Alnald, J. Baricuatro, M. Soriaga, *Electrocatalysis* **2016**, *7*, 391–399.

[51] D. Ren, N. T. Wong, A. D. Handoko, Y. Huang, B. S. Yeo, *Journal of Physical Chemistry Letters* **2016**, *7*, 20–24.

[52] D. Kim, C. S. Kley, Y. Li, P. Yang, *Proceedings of the National Academy of Sciences of the United States of America* **2017**, *114*, 10560–10565.

[53] C. Reller, R. Krause, E. Volkova, B. Schmid, S. Neubauer, A. Rucki, M. Schuster, G. Schmid, *Advanced Energy Materials* **2017**, *7*, 1602114.

[54] L. Han, W. Zhou, C. Xiang, *ACS Energy Letters* **2018**, *3*, 855–860.

[55] Y.-X. Duan, F.-L. Meng, K.-H. Liu, S.-S. Yi, S.-J. Li, J.-M. Yan, Q. Jiang, *Advanced Materials* **2018**, *30*, 1706194.

[56] D. Ren, B. S.-H. Ang, B. S. Yeo, *ACS Catalysis* **2016**, *6*, 8239–8247.

[57] Y. Song, R. Peng, D. K. Hensley, P. V. Bonnesen, L. Liang, Z. Wu, H. M. Meyer, M. Chi, C. Ma, B. G. Sumpter, A. J. Rondinone, *ChemistrySelect* **2016**, *1*, 6055–6061.

[58] A. Williams, E. Lightowlers, A. Collins, *Journal of Physics C: Solid State Physics* **1970**, *3*, 1727–1735.

[59] N. Yang, S. R. Waldvogel, X. Jiang, *ACS Applied Materials & Interfaces* **2016**, *8*, 28357–28371.

[60] J. V. Macpherson, *Physical Chemistry Chemical Physics* **2015**, *17*, 2935–2949.

[61] J. Xu, K. Natsui, S. Naoi, K. Nakata, Y. Einaga, *Diamond and Related Materials* **2018**, *86*, 167–172.

[62] K. Nakata, T. Ozaki, C. Terashima, A. Fujishima, Y. Einaga, *Angewandte Chemie* **2014**, *53*, 871–874.

[63] P. K. Jiwanti, K. Natsui, K. Nakata, Y. Einaga, *RSC Advances* **2016**, *6*, 102214–102217.

[64] N. Ikemiya, K. Natsui, K. Nakata, Y. Einaga, *RSC Advances* **2017**, *7*, 22510–22514.

[65] Y. Y. Birdja, M. T. M. Koper, *Journal of the American Chemical Society* **2017**, *139*, 2030–2034.

[66] Q. Lu, J. Rosen, F. Jiao, *ChemCatChem* **2015**, *7*, 38–47.

[67] J. Rosen, G. Hutchings, Q. Lu, S. Rivera, Y. Zhou, D. Vlachos, F. Jiao, *ACS Catalysis* **2015**, *5*, 4293–4299.

[68] R. Reske, H. Mistry, F. Behafarid, B. Roldan Cuenya, P. Strasser, *Journal of the American Chemical Society* **2014**, *136*, 6978–6986.

[69] K. Manthiram, B. Beberwyck, P. Alivisatos, *Journal of the American Chemical Society* **2014**, *136*, 13319–13325.

[70] O. A. Baturina, Q. Lu, M. A. Padilla, Le Xin, W. Li, A. Serov, K. Artyushkova, P. Atanassov, F. Xu, A. Epshteyn, T. Brintlinger, M. Schuette, G. E. Collins, *ACS Catalysis* **2014**, *4*, 3682–3695.

[71] S. Ma, M. Sadakiyo, R. Luo, M. Heima, M. Yamauchi, P. J. Kenis, *Journal of Power Sources* **2016**, *301*, 219–228.

[72] C.-T. Dinh, T. Burdyny, M. G. Kibria, A. Seifitokaldani, C. M. Gabardo, F. P. García de Arquer, A. Kiani, J. P. Edwards, P. De Luna, O. S. Bushuyev, et al., *Science* **2018**, *360*, 783–787.

[73] A. Murata, Y. Hori, *Bulletin of the Chemical Society of Japan* **1991**, *64*, 123–127.

[74] M. Thorson, K. Siil, P. Kenis, *Journal of the Electrochemical Society* **2013**, *160*, F69–F74.

[75] H. Mistry, A. S. Varela, S. Kühl, P. Strasser, B. Roldan Cuenya, *Nature Reviews* **2016**, *1*, 16009.

[76] P. De Luna, R. Quintero-Bermudez, C.-T. Dinh, M. B. Ross, O. S. Bushuyev, P. Todorović, T. Regier, S. O. Kelley, P. Yang, E. H. Sargent, *Nature Catalysis* **2018**, *1*, 103–110.

[77] S. Verma, X. Lu, S. Ma, R. Masel, P. J. A. Kenis, *Physical Chemistry Chemical Physics* **2016**, *18*, 7075–7084.

[78] C.-T. Dinh, F. P. G. de Arquer, D. Sinton, E. Sargent, *ACS Energy Letters* **2018**, *3*, 2835–2840.

[79] P. Jeanty, Dissertation, Technische Universität München, München, **2018**.

[80] T. Burdyny, S. Wilson, *Energy and Environmental Science* **2019**, *12*, 1442–1453.

[81] B. Endrődi, G. Bencsik, F Darvas, R Jones, K Rajeshwar, C. Janáky, *Progress in Energy and Combustion Science* **2017**, *62*, 133–154.

[82] Z. Sun, T. Ma, H. Tao, Q. Fan, B. Han, *Chem* **2017**, *3*, 560–587.

[83] L.-C. Weng, A. T. Bell, A. Z. Weber, *Physical Chemistry Chemical Physics* **2018**, *20*, 16973–16984.

[84] C. Scherer, Masterarbeit, Technische Universität München, München, **2015**.

[85] P. Jeanty, C. Scherer, E. Magori, K. Wiesner-Fleischer, O. Hinrichsen, M. Fleischer, *Journal of CO_2 Utilization* **2018**, *24*, 454–462.

[86] R. L. Cook, R. C. MacDuff, A. F. Sammells, *Journal of the Electrochemical Society* **1990**, *137*, 607–608.

[87] M. Jouny, W. Luc, F. Jiao, *Industrial & Engineering Chemistry Research* **2018**, *57*, 2165–2177.

[88] M. Bernstein, qNMR: quantitative NMR, Mestrelab Research S.L., **2012**, `https://resources.mestrelab.com/what-is-qnmr/` (visited on 05/30/2016).

[89] N. Amin, T. Clarige, Quantitative NMR Spectroscopy, University of Oxford, **2017**, `http://nmrweb.chem.ox.ac.uk/Data/Sites/70/userfiles/pdfs/quantitative-nmr.pdf` (visited on 03/30/2017).

[90] P. De Luna, C. Hahn, D. Higgins, S. A. Jaffer, T. F. Jaramillo, E. H. Sargent, *Science* **2019**, *364*, 350.

[91] M. Balat, H. Balat, *Applied Energy* **2009**, *86*, 2273–2282.

[92] H. T. Luk, C. Mondelli, D. C. Ferré, J. Stewart, J. Perez-Ramirez, *Chemical Society Reviews* **2017**, *46*, 1358–1426.

[93] Y. Hori, A. Murata, R. Takahashi, S. Suzuki, *Journal of the American Chemical Society* **1987**, *109*, 5022–5023.

[94] F. S. Roberts, K. P. Kuhl, A. Nilsson, *ChemCatChem* **2016**, *8*, 1119–1124.

[95] D. S. Ripatti, T. R. Veltman, M. Kanan, *Joule* **2019**, *3*, 240–256.

[96] K. Malik, S. Singh, S. Basu, A. Verma, *Wiley Interdisciplinary Reviews: Energy and Environment* **2017**, *6*, e244.

[97] X. Mao, T. A. Hatton, *Industrial & Engineering Chemistry Research* **2015**, *54*, 4033–4042.

[98] Y. Hori, H. Wakebe, T. Tsukamoto, O. Koga, *Electrochimica Acta* **1994**, *39*, 1833–1839.

[99] M. R. Singh, Y. Kwon, Y. Lum, J. W. Ager, A. T. Bell, *Journal of the American Chemical Society* **2016**, *138*, 13006–13012.

[100] A. Kaifer, M. Gómez-Kaifer, *Supramolecular Electrochemistry*, Wiley-VCH Verlag GmbH, **2007**, Chapter 4, pp. 32–44.

[101] Y.-J. Zhang, V. Sethuraman, R. Michalsky, A. A. Peterson, *ACS Catalysis* **2014**, *4*, 3742–3748.

[102] J. March, *Advanced Organic Chemistry: Reactions, Mechanisms, and Structure*, Sixth edition, John Wiley and Sons, **1992**.

[103] Z. Wang in *Comprehensive Organic Name Reactions and Reagents*, John Wiley & Sons, Inc., **2010**.

[104] N. Hoshi, M. Kato, Y. Hori, *Journal of Electroanalytical Chemistry* **1997**, *440*, 283–286.

[105] Y. Hori, H. Ito, K. Okano, K. Nagasu, S. Sato, *Electrochimica Acta* **2003**, *48*, 2651–2657.

[106] F. Goodridge, K. Scott, *Electrochemical Process Engineering: A Guide to the Design of Electrolytic Plant*, Springer US, **2013**.

[107] T. A. Ivandini, Y. Einaga, *Chemical Communications* **2017**, *53*, 1338–1347.

[108] S. Smits, Masterarbeit, Technische Universität München, München, **2018**.

[109] S. D. Janssens, P. Pobedinskas, J. Vacik, V. Petráková, B. Ruttens, J. D'Haen, M. Nesládek, K. Haenen, P. Wagner, *New Journal of Physics* **2011**, *13*, 083008.

[110] M. Gajdos, A. Eichler, J. Hafner, *Journal of Physics: Condensed Matter* **2008**, *16*, 1141.

[111] E. R. Cave, C. Shi, K. P. Kuhl, T. Hatsukade, D. N. Abram, C. Hahn, K. Chan, T. F. Jaramillo, *ACS Catalysis* **2018**, *8*, 3035–3040.

[112] Lazard's Levelized Cost of Energy Analysis - Version 11.0, Lazard, **2017**, `http://www.lazard.com/media/450337/lazard-levelized-cost-of-energy-version-110.pdf` (visited on 10/13/2018).

[113] W. Zhang, Y. Hu, L. Ma, G. Zhu, Y. Wang, X. Xue, R. Chen, S. Yang, Z. Jin, *Advanced Science* **2018**, *5*, 1700275.

[114] B. Endrődi, G. Bencsik, F. Darvas, R. Jones, K. Rajeshwar, C. Janáky, *Progress in Energy and Combustion Science* **2017**, *62*, 133–154.

[115] T. Haas, R. Krause, R. Weber, M. Demler, G. Schmid, *Nature Catalysis* **2018**, *1*, 32.

[116] S. Verma, Y. Hamasaki, C. Kim, W. Huang, S. Lu, H.-R. M. Jhong, A. A. Gewirth, T. Fujigaya, N. Nakashima, P. J. Kenis, *ACS Energy Letters* **2017**, *3*, 193–198.

[117] C. Oloman, H. Li, *ChemSusChem* **2008**, *1*, 385–391.

[118] D. Kopljar, A. Inan, P. Vindayer, N. Wagner, E. Klemm, *Journal of Applied Electrochemistry* **2014**, *44*, 1107–1116.

[119] C.-T. Dinh, T. Burdyny, M. G. Kibria, A. Seifitokaldani, C. M. Gabardo, F. P. G. de Arquer, A. Kiani, J. P. Edwards, P. De Luna, O. S. Bushuyev, et al., *Science* **2018**, *360*, 783–787.

[120] B. Schmid, C. Reller, S. Neubauer, M. Fleischer, R. Dorta, G. Schmid, *Catalysts* **2017**, *7*, 161.

[121] C. W. Li, J. Ciston, M. W. Kanan, *Nature* **2014**, *508*, 504–507.

[122] D. Ren, J. Fong, B. S. Yeo, *Nature Communications* **2018**, *9*, 925.

[123] D. Ren, Y. Deng, A. D. Handoko, C. S. Chen, S. Malkhandi, B. S. Yeo, *ACS Catalysis* **2015**, *5*, 2814–2821.

[124] R. Kas, K. K. Hummadi, R. Kortlever, P. de Wit, A. Milbrat, M. W. J. Luiten-Olieman, N. E. Benes, M. T. M. Koper, G. Mul, *Nature Communications* **2016**, *7*, 10748.

[125] P. de Luna, R. Quintero-Bermudez, C.-T. Dinh, M. B. Ross, O. S. Bushuyev, P. Todorović, T. Regier, S. O. Kelley, P. Yang, E. H. Sargent, *Nature Catalysis* **2018**, *1*, 103–110.

[126] K. G. Schulz, U. Riebesell, B. Rost, S. Thoms, R. E. Zeebe, *Marine Chemistry* **2006**, *100*, 53–65.

[127] A. Verdaguer-Casadevall, C. W. Li, T. P. Johansson, S. B. Scott, J. T. McKeown, M. Kumar, I. E. L. Stephens, M. W. Kanan, I. Chorkendorff, *Journal of the American Chemical Society* **2015**, *137*, 9808–9811.

[128] N. Theaker, J. M. Strain, B. Kumar, J. P. Brian, S. Kumari, J. M. Spurgeon, *Electrochimica Acta* **2018**, *274*, 1–8.

[129] Y. Hori, Y. Takahashi Ryutaro Yoshinami, Murata Akira, *Journal of Physical Chemistry B* **1997**, *101*, 7075–7081.

[130] L. Wang, S. A. Nitopi, E. Bertheussen, M. Orazov, C. G. Morales-Guio, X. Liu, D. C. Higgins, K. Chan, J. K. Nørskov, C. Hahn, T. F. Jaramillo, *ACS Catalysis* **2018**, *8*, 7445–7454.

[131] M. Fleischer, P. Jeanty, R. Krause, E. Magori, N. S. Romero Cuéllar, B. Schmid, G. Schmid, K. Wiesner-Fleischer, *pat.*, US020180179649A1, **2018**.

[132] A. T. C. J. Dangerman, H. J. Schellnhuber, *Proceedings of the National Academy of Sciences of the United States of America* **2013**, *110*, E549–58.

[133] C. Delacourt, P. L. Ridway, J. B. Kerr, J. Newman, *Journal of the Electrochemical Society* **2008**, *155*, B42–B49.

[134] B. Kim, S. Ma, H.-R. M. Jhong, P. J. Kenis, *Electrochimica Acta* **2015**, *166*, 271–276.

[135] M. Liu, Y. Pang, B. Zhang, P. de Luna, O. Voznyy, J. Xu, X. Zheng, C. T. Dinh, F. Fan, C. Cao, F. P. G. de Arquer, T. S. Safaei, A. Mepham, A. Klinkova, E. Kumacheva, T. Filleter, D. Sinton, S. O. Kelley, E. H. Sargent, *Nature* **2016**, *537*, 382–386.

[136] S. Verma, Y. Hamasaki, C. Kim, W. Huang, S. Lu, H.-R. M. Jhong, A. A. Gewirth, T. Fujigaya, N. Nakashima, P. J. A. Kenis, *ACS Energy Letters* **2018**, *3*, 193–198.

[137] W. Ma, S. Xie, X.-G. Zhang, F. Sun, J. Kang, Z. Jiang, Q. Zhang, D.-Y. Wu, Y. Wang, *Nature Communications* **2019**, *10*, 892.

[138] M. Jouny, W. Luc, F. Jiao, *Nature Catalysis* **2018**, *1*, 748–755.

[139] N. S. Romero Cuellar, K. Wiesner-Fleischer, M. Fleischer, A. Rucki, O. Hinrichsen, *Electrochimica Acta* **2019**, *307*, 164–175.

[140] J. H. Montoya, C. Shi, K. Chan, J. K. Nørskov, *Journal of Physical Chemistry Letters* **2015**, *6*, 2032–2037.

[141] Y. Pang, J. Li, Z. Wang, C.-S. Tan, P.-L. Hsieh, T.-T. Zhuang, Z.-Q. Liang, C. Zou, X. Wang, P. de Luna, J. P. Edwards, Y. Xu, F. Li, C.-T. Dinh, M. Zhong, Y. Lou, D. Wu, L.-J. Chen, E. H. Sargent, D. Sinton, *Nature Catalysis* **2019**, *2*, 251–258.

[142] J.-B. Vennekoetter, R. Sengpiel, M. Wessling, *Chemical Engineering Journal* **2019**, *364*, 89–101.

[143] M. Hansen, K. Therkildsen, Method for Producing a Gas Diffusion Electrode and Gas Diffusion Electrode. International Patent No. WO/2018/233843, Siemens Aktiengesellschaft, **2018**.

[144] W. Lee, L. Byerley, E. Bergner, J. Edmond, *Biological Mass Spectrometry* **1991**, *20*, 451–458.

[145] Z. Ahmed, S. Zeeshan, H. C., M. Hensel, D. Schomburg, R. Münch, E. Eylert, W. Eisenreich, T. Dandekar, *Database (Oxford)* **2014**, *bau*, 077.

[146] Q. Lu, J. Rosen, Y. Zhou, G. Hutchings, Y. Kimmel, J. Chen, F. Jiao, *Nature Communications* **2014**, *5*, DOI 10.1038/ncomms4242.

[147] T. Hatsukade, K. P. Kuhl, E. R. Cave, D. N. Abram, T. F. Jaramillo, *Physical Chemistry Chemical Physics* **2014**, *16*, 13814–13819.

[148] T. Burdyny, W. A. Smith, *Energy & Environmental Science* **2019**, DOI 10.1039/c8ee03134g.

[149] J. M. Spurgeon, B. Kumar, *Energy & Environmental Science* **2018**, *11*, 1536–1551.

List of Figures

List of Tables

Nomenclature

Latin Symbols

A	geometrical area	m^2
A_i	integral area of a product peak	m^2
$A_{Standard}$	integral area of a standard peak	m^2
c	concentration	mol/L
e	elementary charge	C
E	potential	V
F	Faradic constant	C/mol
FE	Faradic efficiency	%
I	total applied current	A
j	current density	mA/cm^2
n_i	amount of substance of an specific product	mol
$\dot{n}_i$	molar flow of an specific product	mol/L
N_a	Avogadro number	1/mol
p	pressure	atm
P	number of protons	-
Q	applied charge	A s
R	gas constant	L·atm/K·mol
t	time	s
T	temperature	K
V	volume	L
$\dot{V}$	volumetric gas flow	L/s
y	gas fraction	-
z_i	number of electrones	-

Greek Symbols

ν	stoichiometric coefficient of the reactants	-

Subscript

aq	aqueous
g	gaseous
i	specific product
l	liquid
theo	theoretical
out	outlet
WE	working electrode

Abbreviations

AG	Aktiengesellschaft (stock company)
AM	Alkali-metal cations
AMOH	Alkaline solutions
BDD	Boron Doped Diamond
B/C	Boron (TMB) / Carbon (CH_4) ratio
CVD	Chemical Vapor Deposition
C2	Carbonaceous Compound with Two Carbons
C3	Carbonaceous Compound with Three Carbons
CORR	Carbon Monoxide Reduction Reaction
CO_2RR	Carbon Dioxide Reduction Reaction
CuNPs	Copper Nanoparticles
DFT	Density functional theory
DM	Diffusion Medium
ERCO	Electrochemical Reduction of Carbon Monoxide
ERCO_2	Electrochemical Reduction of Carbon Dioxide
EtOH	Ethanol
ETG	Ethylene glycol
FE	Faradaic Efficiency
FEG-SEM	Field Emission Gun Scanning Electron Microscope
GC	Gas Chromathography
GC-MS	Gas Chromathography-Mass Spectroscopy
GDE	Gas Diffusion Electrode
GDL	Gas Diffusion Layer
HF-CVD	Hot Filament Chemical Vapor Deposition
HER	Hydrogen Evolution Reaction
IEA	International Energy Agency
IPCC	Intergovernmental Panel of Climate Change
IRENA	International Renewable Energy Agency

LSV	Linear Sweep Voltammetry
MC	Microcrystalline
MeOH	Methanol
MFC	Mass Flow Controller
MFM	Mass Flow Meter
ML	Microporous Layer
MWP-CVD	Microwave Plasma Chemical Vapor Deposition
NC	Nanocrystalline
NDC	Non-Diamond-Carbon
NMR	Nuclear Magnetic Resonance
P2X	Power to X
PEEK	Polyether Ether Ketone
PMMA	Poly Methyl Methacrylate
PTFE	Polytetrafluoroethylene
PrOH	Propanol
RHE	Reversible Hydrogen Electrode
SEM	Scanning Electron Microscopy
SD	Standard Deviation
SCCM	Standad Cubic Centimeter per Minute
TEM	Transmission Electron Microscopy
TMB	Trimethylborane
UCN	Ultracrystalline
XPS	X-ray Photoelectron Spectroscopy
XRD	X-ray Diffraction

Chemical Compounds

Ag	Silver
AgCl	Silver chloride
$AgNO_3$	Silver nitrate
Au	Gold
B	Boron
Cd	Cadmium
Co	Cobalt
CO	Carbon monoxide
CO_2	Carbon dioxide
CO_3^{2-}	Carbonate
CH_3OH	Methanol
CH_4	Methane
C_2H_4	Ethylene

C_2H_5OH	Ethanol
C_3H_7OH	*n*-Propanol
Cu	Copper
Fe	Iron
Ga	Gallium
H_2	Hydrogen
HCHO	Formaldehyde
$HCOO^-$	Formate
HCO_3^-	Bicarbonate
HCOOH	Formic acid
He	Helium
Hg	Mercury
In	Indium
K_2CO_3	Potassium carbonate
$KHCO_3$	Potassium bicarbonate
KOH	Potassium hydroxide
K_2SO_4	Potassium sulfate
NaOH	Sodium hydroxide
N_2	Nitrogen
Ni	Nickel
Pb	Lead
Pd	Palladium
Pt	Platinum
Sn	Tin
Zn	Zinc

Reprint Permissions

John Wiley and Sons copyright clearance

JOHN WILEY AND SONS LICENSE
TERMS AND CONDITIONS

Jun 22, 2019

This Agreement between Ms. Nayra Sofia Romero Cuellar ("You") and John Wiley and Sons ("John Wiley and Sons") consists of your license details and the terms and conditions provided by John Wiley and Sons and Copyright Clearance Center.

License Number	4614160995232
License date	Jun 22, 2019
Licensed Content Publisher	John Wiley and Sons
Licensed Content Publication	ChemistrySelect
Licensed Content Title	Electrochemical Reduction of CO2 in Water-Based Electrolytes KHCO3 and K2SO4 Using Boron Doped Diamond Electrodes
Licensed Content Author	Maximilian Fleischer, Olaf Hinrichsen, Kerstin Wiesner-Fleischer, et al
Licensed Content Date	Mar 30, 2018
Licensed Content Volume	3
Licensed Content Issue	13
Licensed Content Pages	5
Type of Use	Dissertation/Thesis
Requestor type	Author of this Wiley article
Format	Print and electronic
Portion	Full article
Will you be translating?	No
Title of your thesis / dissertation	Electrochemical Reduction of Carbon Dioxide and Carbon Monoxide towards Value-Added Chemicals
Expected completion date	Jul 2019
Expected size (number of pages)	110
Requestor Location	Ms. Nayra Sofia Romero Cuellar Rosenheimerstr. 214 Munich, 81669 Germany Attn: Ms. Nayra Sofia Romero Cuellar
Publisher Tax ID	EU826007151
Total	0.00 USD
Terms and Conditions	

TERMS AND CONDITIONS

This copyrighted material is owned by or exclusively licensed to John Wiley & Sons, Inc. or one of its group companies (each a"Wiley Company") or handled on behalf of a society with which a Wiley Company has exclusive publishing rights in relation to a particular work (collectively "WILEY"). By clicking "accept" in connection with completing this licensing transaction, you agree that the following terms and conditions apply to this transaction (along with the billing and payment terms and conditions established by the Copyright Clearance Center Inc., ("CCC's Billing and Payment terms and conditions"), at the time that you opened your RightsLink account (these are available at any time at http://myaccount.copyright.com).

Terms and Conditions

- The materials you have requested permission to reproduce or reuse (the "Wiley Materials") are protected by copyright.
- You are hereby granted a personal, non-exclusive, non-sub licensable (on a stand-alone basis), non-transferable, worldwide, limited license to reproduce the Wiley Materials for the purpose specified in the licensing process. This license, and any CONTENT (PDF or image file) purchased as part of your order, is for a one-time use only and limited to any maximum distribution number specified in the license. The first instance of republication or reuse granted by this license must be completed within two years of the date of the grant of this license (although copies prepared before the end date may be distributed thereafter). The Wiley Materials shall not be used in any other manner or for any other purpose, beyond what is granted in the license. Permission is granted subject to an appropriate acknowledgement given to the author, title of the material/book/journal and the publisher. You shall also duplicate the copyright notice that appears in the Wiley publication in your use of the Wiley Material. Permission is also granted on the understanding that nowhere in the text is a previously published source acknowledged for all or part of this Wiley Material. Any third party content is expressly excluded from this permission.
- With respect to the Wiley Materials, all rights are reserved. Except as expressly granted by the terms of the license, no part of the Wiley Materials may be copied, modified, adapted (except for minor reformatting required by the new Publication), translated, reproduced, transferred or distributed, in any form or by any means, and no derivative works may be made based on the Wiley Materials without the prior permission of the respective copyright owner.For STM Signatory Publishers clearing permission under the terms of the STM Permissions Guidelines only, the terms of the license are extended to include subsequent editions and for editions in other languages, provided such editions are for the work as a whole in situ and does not involve the separate exploitation of the permitted figures or extracts, You may not alter, remove or suppress in any manner any copyright, trademark or other notices displayed by the Wiley Materials. You may not license, rent, sell, loan, lease, pledge, offer as security, transfer or assign the Wiley Materials on a stand-alone basis, or any of the rights granted to you hereunder to any other person.
- The Wiley Materials and all of the intellectual property rights therein shall at all times remain the exclusive property of John Wiley & Sons Inc, the Wiley Companies, or their respective licensors, and your interest therein is only that of having possession of and the right to reproduce the Wiley Materials pursuant to Section 2 herein during the continuance of this Agreement. You agree that you own no right, title or interest in or to the Wiley Materials or any of the intellectual property rights therein. You shall have no rights hereunder other than the license as provided for above in Section 2. No right, license or interest to any trademark, trade name, service mark or other branding ("Marks") of WILEY or its licensors is granted hereunder, and you agree that you shall not assert any such right, license or interest with respect thereto
- NEITHER WILEY NOR ITS LICENSORS MAKES ANY WARRANTY OR REPRESENTATION OF ANY KIND TO YOU OR ANY THIRD PARTY, EXPRESS, IMPLIED OR STATUTORY, WITH RESPECT TO THE MATERIALS OR THE ACCURACY OF ANY INFORMATION CONTAINED IN THE MATERIALS, INCLUDING, WITHOUT LIMITATION, ANY IMPLIED WARRANTY OF MERCHANTABILITY, ACCURACY, SATISFACTORY QUALITY, FITNESS FOR A PARTICULAR PURPOSE, USABILITY, INTEGRATION OR NON-INFRINGEMENT AND ALL SUCH WARRANTIES ARE HEREBY EXCLUDED BY WILEY AND ITS LICENSORS AND WAIVED BY YOU.
- WILEY shall have the right to terminate this Agreement immediately upon breach of this Agreement by you.
- You shall indemnify, defend and hold harmless WILEY, its Licensors and their respective directors, officers, agents and employees, from and against any actual or threatened claims, demands, causes of action or proceedings arising from any breach of this Agreement by you.
- IN NO EVENT SHALL WILEY OR ITS LICENSORS BE LIABLE TO YOU OR ANY OTHER PARTY OR ANY OTHER PERSON OR ENTITY FOR ANY SPECIAL, CONSEQUENTIAL, INCIDENTAL, INDIRECT, EXEMPLARY OR PUNITIVE DAMAGES, HOWEVER CAUSED, ARISING OUT OF OR IN CONNECTION WITH THE DOWNLOADING, PROVISIONING, VIEWING OR USE OF THE MATERIALS REGARDLESS OF THE FORM OF ACTION, WHETHER FOR BREACH OF CONTRACT, BREACH OF WARRANTY, TORT, NEGLIGENCE, INFRINGEMENT OR OTHERWISE (INCLUDING, WITHOUT LIMITATION, DAMAGES BASED ON LOSS OF PROFITS, DATA, FILES, USE, BUSINESS OPPORTUNITY OR CLAIMS OF THIRD PARTIES), AND WHETHER OR NOT THE PARTY HAS BEEN ADVISED OF THE POSSIBILITY OF SUCH DAMAGES. THIS LIMITATION SHALL APPLY NOTWITHSTANDING ANY FAILURE OF ESSENTIAL PURPOSE OF ANY LIMITED REMEDY PROVIDED HEREIN.
- Should any provision of this Agreement be held by a court of competent jurisdiction to be illegal, invalid, or unenforceable, that provision shall be deemed amended to achieve as nearly as possible the same economic effect as the original provision, and the legality, validity and enforceability of the remaining provisions of this Agreement shall not be affected or

impaired thereby.

- The failure of either party to enforce any term or condition of this Agreement shall not constitute a waiver of either party's right to enforce each and every term and condition of this Agreement. No breach under this agreement shall be deemed waived or excused by either party unless such waiver or consent is in writing signed by the party granting such waiver or consent. The waiver by or consent of a party to a breach of any provision of this Agreement shall not operate or be construed as a waiver of or consent to any other or subsequent breach by such other party.
- This Agreement may not be assigned (including by operation of law or otherwise) by you without WILEY's prior written consent.
- Any fee required for this permission shall be non-refundable after thirty (30) days from receipt by the CCC.
- These terms and conditions together with CCC's Billing and Payment terms and conditions (which are incorporated herein) form the entire agreement between you and WILEY concerning this licensing transaction and (in the absence of fraud) supersedes all prior agreements and representations of the parties, oral or written. This Agreement may not be amended except in writing signed by both parties. This Agreement shall be binding upon and inure to the benefit of the parties' successors, legal representatives, and authorized assigns.
- In the event of any conflict between your obligations established by these terms and conditions and those established by CCC's Billing and Payment terms and conditions, these terms and conditions shall prevail.
- WILEY expressly reserves all rights not specifically granted in the combination of (i) the license details provided by you and accepted in the course of this licensing transaction, (ii) these terms and conditions and (iii) CCC's Billing and Payment terms and conditions.
- This Agreement will be void if the Type of Use, Format, Circulation, or Requestor Type was misrepresented during the licensing process.
- This Agreement shall be governed by and construed in accordance with the laws of the State of New York, USA, without regards to such state's conflict of law rules. Any legal action, suit or proceeding arising out of or relating to these Terms and Conditions or the breach thereof shall be instituted in a court of competent jurisdiction in New York County in the State of New York in the United States of America and each party hereby consents and submits to the personal jurisdiction of such court, waives any objection to venue in such court and consents to service of process by registered or certified mail, return receipt requested, at the last known address of such party.

WILEY OPEN ACCESS TERMS AND CONDITIONS
Wiley Publishes Open Access Articles in fully Open Access Journals and in Subscription journals offering Online Open. Although most of the fully Open Access journals publish open access articles under the terms of the Creative Commons Attribution (CC BY) License only, the subscription journals and a few of the Open Access Journals offer a choice of Creative Commons Licenses. The license type is clearly identified on the article.
The Creative Commons Attribution License
The Creative Commons Attribution License (CC-BY) allows users to copy, distribute and transmit an article, adapt the article and make commercial use of the article. The CC-BY license permits commercial and non-
Creative Commons Attribution Non-Commercial License
The Creative Commons Attribution Non-Commercial (CC-BY-NC)License permits use, distribution and reproduction in any medium, provided the original work is properly cited and is not used for commercial purposes.(see below)

Creative Commons Attribution-Non-Commercial-NoDerivs License
The Creative Commons Attribution Non-Commercial-NoDerivs License (CC-BY-NC-ND) permits use, distribution and reproduction in any medium, provided the original work is properly cited, is not used for commercial purposes and no modifications or adaptations are made. (see below)
Use by commercial "for-profit" organizations
Use of Wiley Open Access articles for commercial, promotional, or marketing purposes requires further explicit permission from Wiley and will be subject to a fee.
Further details can be found on Wiley Online Library http://olabout.wiley.com/WileyCDA/Section/id-410895.html

Other Terms and Conditions:

v1.10 Last updated September 2015

Questions? customercare@copyright.com or +1-855-239-3415 (toll free in the US) or +1-978-646-2777.

Elsevier copyright clearance

Two-step electrochemical reduction of CO2 towards multi-carbon products at high current densities

Author:
N.S. Romero Cuellar,C. Scherer,B. Kaçkar,W. Eisenreich,C. Huber,K. Wiesner-Fleischer,M. Fleischer,O. Hinrichsen

Publication: Journal of CO2 Utilization

Publisher: Elsevier

Date: February 2020

List of Publications

Papers

- N. S. Romero Cuellar, C. Scherer, B. Kackar, K. Wiesner-Fleischer, M. Fleischer, O. Hinrichsen. *Two-Step Electrochemical Reduction towards Multi-Carbon Products at High Current Densities*. Journal of CO_2Utilization. Journal of CO_2 Utilization. 2019, 36, 263-275. DOI:10.1016/j.jcou.2019.10.016.

- N. S. Romero Cuellar, K. Wiesner-Fleischer, O. Hinrichsen, M. Fleischer. *Advantages of CO over CO_2 as reactant for Electrochemical Reduction to Ethylene, Ethanol and n-Propanol on Gas Diffusion Electrodes at High Current Densities*. Electrochimica Acta, 307 (C):164-175; 2019. DOI:10.1016/j.electacta.2019.03.142

- N. S. Romero Cuellar, K. Wiesner-Fleischer, O. Hinrichsen, M. Fleischer. *Electrochemical Reduction of CO_2 in Water-Based Electrolytes $KHCO_3$ and K_2SO_4 Using Boron Doped Diamond Electrodes*. ChemistrySelect, Volume 3 Number 13; 2018. DOI: 10.1002/slct.201702414

Conferences

- N. S. Romero Cuéllar, K. Wiesner-Fleischer, M. Fleischer, C. Reller, A. Rucki, O. Hinrichsen. *Electrochemical Conversion of Carbon Monoxide at High Current densities* (Poster). 69th Annual Meeting of the International Society of Electrochemistry. September 2-7 2018, Bologna, Italy.

- N. S. Romero Cuéllar. *Electrochemical Reduction of CO_2 and CO to Value-Added Chemicals* (Presentation). 4th Siemens Young Researcher Forum. July 3th 2018 Nürnberg, Germany.

- G. Schmid, C. Reller, L. Astudillo, N. Martic, N. S. Romero Cuéllar, D. Rainisch, C. Scherer, B. Schmid. *CO_2-Rohstoff für die Industrie - Die elektrokatalytische Reduktion von CO_2* (Presentation). Die Lange Nacht der Wissenschaften. October 21th 2017, Erlangen, Germany.

- N. S. Romero Cuéllar, K. Wiesner, W. Eisenreich, O. Hinrichsen, Y. Einaga, K. Nakata. *Electrochemical Reduction of CO_2 Using Boron Doped Diamond Electrodes in Aqueous Electrolytes $KHCO_3$ and K_2SO_4* (Presentation). 11th European Symposium on Electrochemical Engineering. June 4-8 2017, Prague, Czech Republic.

- P. Jeanty, C. Scherer, N. S. Romero Cuéllar, E. Magori, K. Wiesner, G. Schmid, O. Hinrichsen, M. Fleischer, *Investigation on long-term stability of electrochemical conversion of CO_2 to CO at a silver gas diffusion electrode*, Future Energy Conference, 2016, Sydney (Australien)

Patents

- C. Scherer, N. S. Romero Cuéllar, M. Fleischer. *Auslegung kaskadierter CO_2 Elektrolyseure*, Patent Application 2019P13331 DE (registration date: 27.05.2019)

- C. Scherer, N. S. Romero Cuéllar, M. Fleischer, K. Wiesner-Fleischer, E. Magori. *Aufreinigung des Zwischenproduktes bei kaskadierten CO_2-Elektrolyseuren*, Patent Application 2019P13331 DE (registration date: 27.05.2019)

- M. Fleischer, P. Jeanty, R. Krause, E. Magori, N. S. Romero Cuéllar, B. Schmid, G. Schmid, K. Wiesner-Fleischer. *Reduction Method And Electrolysis System For Electrochemical Carbon Dioxide Utilizatio*n, US 20180179649 (28.06.2018)

- P. Jeanty, M. Fleischer, R. Krause, E. Magori, N. S. Romero Cuéllar, B. Schmid, D. Schmid, K. Wiesner. *Reduktionsverfahren und Elektrolysesystem zur elektrochemischen Kohlenstoffdioxid-Verwertung*, Patent DE 10 2015 212 503 (5.01.2017), WO2017/005411 (12.01.2017)

Declaration

The submitted thesis was supervised by Prof. Dr.-Ing. Kai-Olaf Hinrichsen and Dr. Kerstin Wiesner-Fleischer.

Affirmation
Hereby, I affirm that I am the sole author of this thesis. To the best of my knowledge, I affirm that this thesis does not infringe upon anyone's copyright nor violate any proprietary rights. I affirm that any ideas, techniques, quotations, or any other material, are in accordance with standard referencing practices.

Moreover, I affirm that, so far, the thesis has not been forwarded to a third party nor is it published. I obeyed all study regulations of the Technische Universität München.

Remarks about the internet
Throughout the work, the internet was used for research and verification. Many of the keywords provided herein, references and other information can be verified on the internet. However, no sources are given, because all statements made in this work are fully covered by the cited literature sources.

Munich, December 8, 2019

Nayra Sofia Romero Cuéllar